THE TRANSIENT RECEPTOR POTENTIAL VANILLOID-1 CHANNEL AND NEURONAL SURVIVAL IN DEGENERATIVE DISEASE

By

Nicholas J. Ward

Dissertation

Submitted to the Faculty of the

Graduate School of Vanderbilt University

in partial fulfillment of the requirements

for the degree of

DOCTOR OF PHILOSOPHY

in

Neuroscience

August, 2014

Nashville, Tennessee

Approved:

Professor David J. Calkins

Professor Bruce D. Carter

Professor Rebecca M. Sappington

Professor Kevin L. Schey

ACKNOWLEDGMENTS

I would like to thank my advisor, Dr. David Calkins, for his commitment to my training as a scientist. It has been a pleasure working with a mentor who is so passionate about research and pursuing interesting scientific questions. Looking back upon my training, his energy and enthusiasm influenced so many of my successes here at Vanderbilt. Agreeing to mentor a doctoral student is not a small commitment, and I appreciate that he invested his time and efforts into my development as a scientist. In addition to Dr. Calkins, I received excellent advice and guidance from the members of my thesis committee. I am thankful to Bruce Carter, who headed my committee and allowed me to pursue a teaching apprenticeship under his guidance. Since joining the Neuroscience Training Program, I have admired his kind nature and dedication to helping students grow as scientists. Dr. Rebecca Sappington was instrumental in my early training by teaching me many lab techniques during my rotation project in her lab. As I progressed through my project, I benefitted tremendously from her expertise in glaucoma and the visual system. At each of my committee meetings, Dr. Kevin Schey asked questions that showed a thoughtful consideration of my project and its aims. I appreciated that he would push me to think of my project in a way that reached beyond simply discussing data to understanding what that data meant in the context of disease pathology and treatment.

Throughout my time in the lab, I have relied upon the help and encouragement of the fantastic research team that Dr. Calkins has assembled. Dr. Wendi Lambert worked directly with me on many of the experiments presented here, and I am indebted to her for her patience and helpfulness at all stages of my research. Dr. Carl Weitlauf also worked with me on these experiments, and his willingness to provide me with filled ganglion cells made Chapter 4 of this dissertation possible. Wendi and Carl served in many capacities—they helped me brainstorm,

troubleshoot, and think critically about my data—and their efforts deserve special recognition. Brian Carlson handled many aspects of animal care throughout my project and worked with Wendi on the incredible number of microbead injections involved in all parts of this dissertation. Karen Ho has been an excellent colleague and fellow graduate student, and it has been exciting to work on projects with and alongside her. Ann Gearon and Erin Eckard, both previous members of the Calkins lab, aided in tissue preparation that was critical for gathering data that appears in Chapter 2. Tina Tian, Tracey Hong, and Kelsey Karas composed a skilled team of both past and present undergraduates who helped me with many aspects of image analysis and quantification. I am so proud to have been a part of this supportive and caring team of researchers.

My research was made possible by a combination of funding from Dr. Calkins and the Vanderbilt Vision Research Center (VVRC) Training Grant, which is managed by Dr. Jeff Schall. My training in both vision and neuroscience research was a collaborative effort that spanned three groups: the VVRC, the Vanderbilt Eye Institute (VEI), and the Neuroscience Training Program of the Vanderbilt Brain Institute (VBI). I am especially thankful to the Neuroscience Training Program's leadership, especially Drs. Mark Wallace and Doug McMahon for their efforts in creating a strong program for all VBI trainees. Between the VVRC, VEI, and VBI, there are many administrative assistants who helped me. I am grateful for the tireless efforts of Gale Newton (VVRC), Vanessa Alderson (VEI), Roz Johnson (VBI), Shirin Pulous (VBI), Beth Sims (VBI), and Mary Michael-Woolman (VBI). My research was additionally aided by Marie Rodriguez from the VVRC histology core as well as by the Cell Imaging Shared Resource. Both of these core resources enabled me to gather much of the data found in Chapters 2 and 3.

I would not have pursued a doctoral degree had it not been for the significant efforts and guidance of many people. When I was a freshman at St. Ignatius High School in Cleveland, Ohio, Mrs. Jo Ann Lane first opened my eyes to the incredible world of biology, a course that she taught with great enthusiasm. This excitement took hold in me, and I majored in biology at University of Notre Dame, where Dr. Michelle Whaley mentored me in pursuing research opportunities with Drs. David Hyde and Joseph O'Tousa. I am grateful for their willingness to teach me how to think scientifically, a skill I relied upon throughout graduate school. I have had many teachers and mentors throughout my life, and this sequence began with my father and mother, Robert and Rosemary Ward. As a physics teacher and librarian, respectively, they valued learning and encouraged my scientific pursuits. They have always been my inspiration to follow my interests, and I have looked to them for support and advice countless times throughout the years. None of this would have been possible without their love and support.

TABLE OF CONTENTS

LIST OF FIGURES

CHAPTER 1

INTRODUCTION[1]

The visual system and degenerative diseases of the central nervous system

One particular difficulty of studying components of the mammalian central nervous system (CNS) *in vivo* is the relative inaccessibility of the neural tissue. The CNS consists of the brain and spinal cord, which work together to process and integrate information from the environment and to exert control over an organism's interactions with that environment. The brain is encased in a protective cavity formed by the bony neurocranium, while the spinal cord is housed within a protective bony structure known as the vertebral column. Such protective structures help minimize trauma to the vertebrate CNS; however, these same structures are a hindrance to experimental manipulation and imaging of the CNS *in vivo* (London et al., 2013). To circumvent these hindrances, many neuroscientists have turned to studying the retina, a comparatively accessible CNS structure found within the eye (Ames and Nesbett, 1981; Nowak, 1987).

The retina, a neural tissue that lines the posterior portion of the eye, is the first component of the visual system that encodes incident light from the environment into a neural signal that can be interpreted by the brain. As vertebrates develop embryonically, the retina and optic nerve form as an outgrowth of the brain's diencephalon, and are therefore considered part of the CNS.

[1] Portions of this chapter were published as a co-authored review: Ho KW, Ward NJ, Calkins DJ. TRPV1: a stress response protein in the central nervous system (2012) Amer J Neurodegener Dis 1:1-14.

Both the retina and optic nerve each partially house a unique type of neuron known as the retinal ganglion cell (RGC). Like other neurons of the CNS, the RGC neurons are specialized to serve a particular purpose, that is, to convey visual information from the retina to regions of the brain critical for vision. Although very specialized for the visual system, these neurons are known to exhibit similarities to other CNS neurons, as they respond similarly to injury and exhibit a diminished potential for axonal regeneration subsequent to injury (Crish and Calkins, 2011; London et al., 2013).

Indeed, links between brain pathologies and degeneration of RGCs have been established in several diseases. In Alzheimer's disease (AD), accumulations of β-amyloid (Aβ) and phosphorylated tau are associated with the degeneration of multiple brain regions (Wenk, 2003). Similarly, these accumulations exist in the retinas of both AD patients (Koronyo-Hamaoui et al., 2011) and transgenic mouse models of the disease (Ning et al., 2008; Gasparini et al., 2011). In humans, AD patients exhibit reduced RGC numbers and degeneration of the optic nerve (Hinton et al., 1986; Sadun and Bassi, 1990). In multiple sclerosis (MS), a demyelinating disease, many patients are diagnosed with optic neuritis, in which RGC degeneration and demyelination is observed (Ghezzi et al., 1999). Therefore, it appears that RGCs may be adversely affected by AD and MS in much the same manner as other CNS neuronal populations.

Using this knowledge that RGCs can be affected by disease and injury in a similar fashion to other CNS neurons, it is reasonable to believe that studies of RGC degeneration could likewise inform research related to all CNS degenerative diseases. This document will present studies related to one such disease, glaucoma, which results in the degeneration of RGCs. Taking advantage of the accessibility of the retina, these studies examine how the cation channel transient receptor potential vanilloid-1 (TRPV1) influences RGC survival in response to

neuronal stressors in glaucoma. By understanding how TRPV1 influences survival in RGCs, we will be able to better determine how the channel may influence neurodegeneration throughout the CNS.

Glaucoma pathogenesis

Clinical presentation of glaucoma

Glaucoma is a family of optic neuropathies that causes progressive visual loss due to dysfunction and death of RGCs. It is the most common cause of irreversible blindness worldwide, and it is estimated that nearly 80 million people will be affected by this disease by the year 2020 (Quigley and Broman, 2006). Age and sensitivity to intraocular pressure (IOP) are the two main risk factors for developing glaucoma, and of these two, IOP is the only modifiable risk factor.

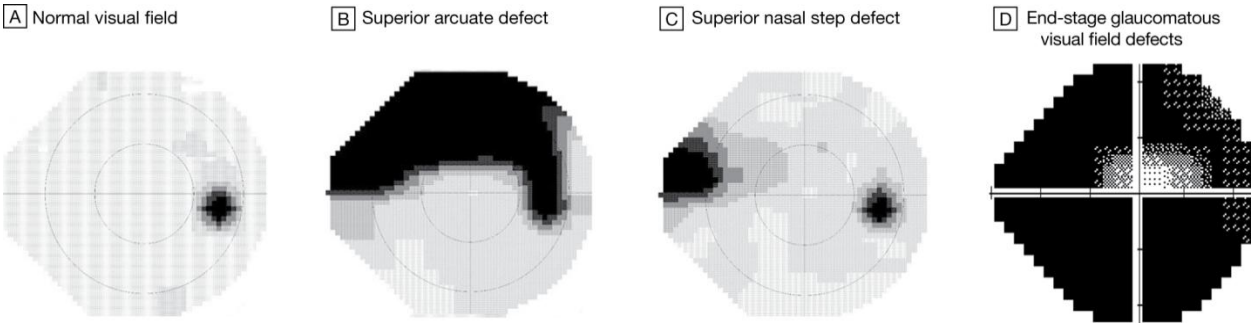

Figure 1.1. Visual field defects in human glaucoma patients. Visual field maps were collected using standard automated perimetry on right eyes of patients. Each map is from the perspective of the patient, so the left side of each map is located nasally and the right side is located temporally. Darker areas represent reduction in sensitivity, and the natural blindspot can be observed in patients with normal visual field, as in ***A***. Glaucoma typically affects peripheral vision first as in ***B*** and ***C***. Late-stage patients who have very progressed visual field deficits retain vision only in their central visual field, as in ***D***.

Figure from Hollands et al. (2013), and used in accordance with Copyright Clearance Center's RightsLink service.

In the clinic, glaucoma is typically defined by a number of characteristics. Primary among these are deficits in the visual field and thinning of the retinal nerve fiber layer (RNFL). Visual field loss can be assessed by perimetry, in which the examiner maps the patient's field of vision. Scotomas, or areas of visual field loss, are a hallmark of glaucoma (Figure 1.1). Although a variety of visual field defects are possible, the most common alterations to the visual field in glaucoma are arcuate scotoma (Levin, 2001). This scotoma commonly forms an arc that starts temporally near the region of the optic disc, curves around into the superior or inferior field, and ceases toward the nasal end of the horizontal axis (Figure 1.1B). Many patients do not notice the scotoma formation until it is well-progressed, as peripheral vision is affected much earlier than central vision (Figure 1.1D). The structural correlate of these visual field losses can be observed in the clinic by thinning of the RNFL, the retinal layer composed of RGC axons traversing toward the optic disc. Thinning of the RNFL is caused by loss of RGC axons, and can be associated with an increased "cupping" at the optic disc as observed in clinical ophthalmoscopic exams (Figure 1.2).

While outcome measures of glaucoma (e.g., visual field defects, RNFL thinning) are specific in nature, the etiology of this family of diseases is complex. To address this, cases of glaucoma that exhibit elevated IOP are typically grouped into one of two types: open angle and closed angle (Hollands et al., 2013). The "angle" referred to by each of these names is the iridocorneal angle formed by the iris and the cornea (Figure 1.3). The integrity of this angle is crucial for the proper drainage of aqueous humor, which both nourishes avascular eye tissue and maintains IOP. Aqueous humor is continuously produced in the posterior chamber of the eye, and it must flow through the pupil, into the anterior chamber of the eye, and finally exit at the angle via the trabecular meshwork (Figure 1.3). The proper balance of aqueous humor

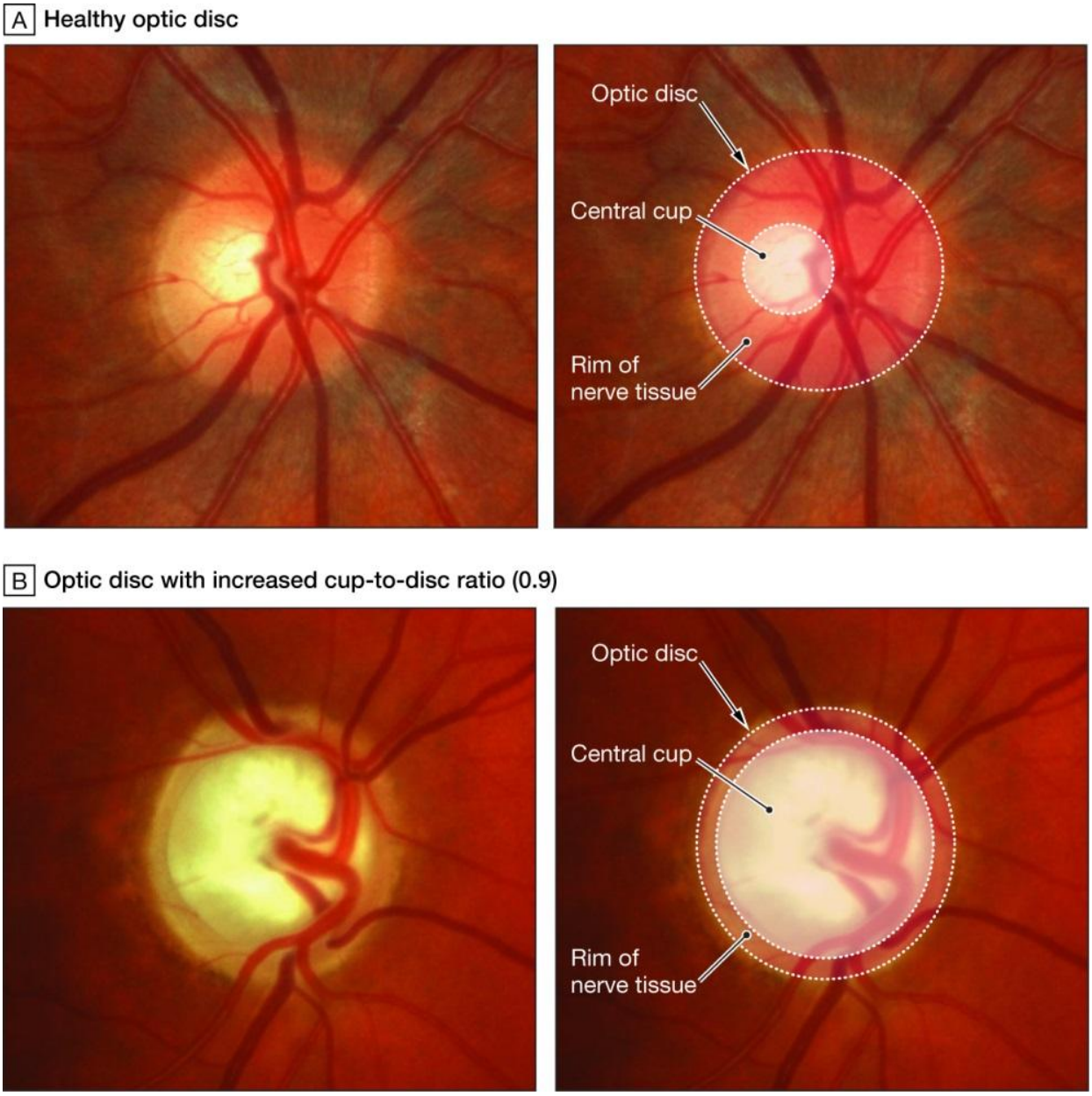

Figure 1.2. Optic disc cupping in human glaucoma patients. The optic disc, where RGC axons leave the eye to form the optic nerve, is the anatomical location of the eye's blind spot. ***A,*** A healthy optic nerve typically exhibits a slightly cupped shape (inner circle, central cup) where the RGC axons come together while leaving the retina. ***B,*** As glaucoma progresses, loss of RGC axons results in a thinning of the retinal nerve fiber layer that contributes to the shape of the central cup. When these axons are lost, the size of the central cup increases. When examining the eye, clinicians often speak of glaucoma patients exhibiting a high cup-to-disc ratio, meaning that the size of the central cup is large with respect to the size of the entire optic disc structure.

Figure from Hollands et al. (2013) and used in accordance with Copyright Clearance Center's RightsLink service.

production and drainage maintains IOP within the eye, thus any blockage or defects that exist in structures at the angle may disturb regulation of IOP.

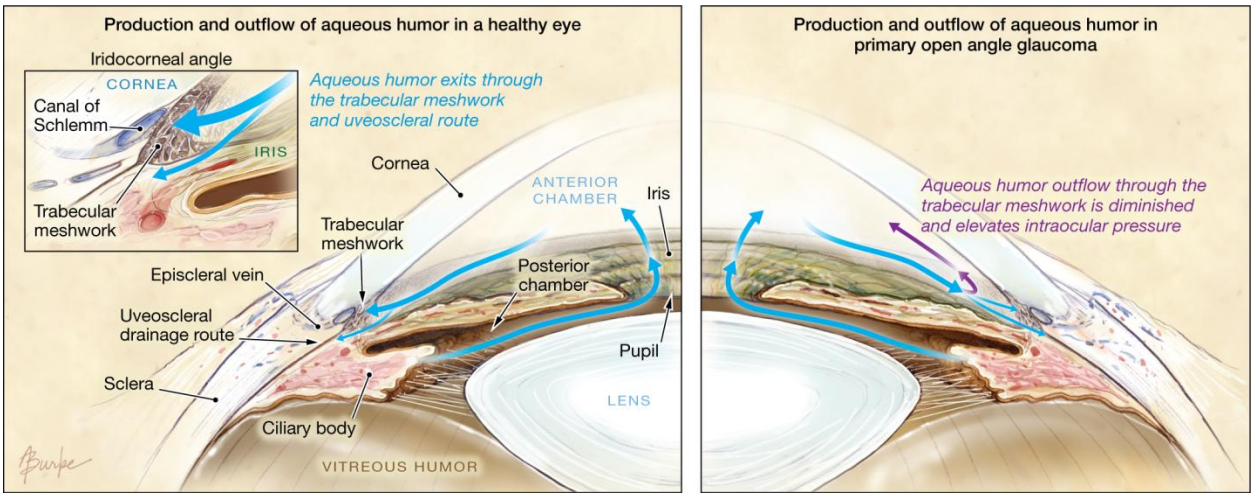

Figure 1.3. Production and outflow of aqueous humor in the eye. Aqueous humor is continually produced by the ciliary body to nourishes avascular eye tissue as well as to maintain intraocular pressure (IOP). This fluid enters the anterior chamber through the pupil and subsequently leaves the anterior segment of the eye through drainage structures at the iridocorneal angle (***see inset, left***). When the eye is healthy (***left panel***), production of aqueous humor and outflow of aqueous humor are in a proper balance that maintains IOP in what is generally considered to be a normal range ($\leq$ 21 mmHg). In primary open angle glaucoma (***right panel***), outflow of aqueous humor through the trabecular meshwork is diminished or obstructed in some way. The resulting build-up of aqueous humor in the anterior eye results in an increase in IOP because the correct balance of aqueous production and outflow has been disturbed.

Figure from Hollands et al. (2013) and used in accordance with Copyright Clearance Center's RightsLink service.

Closed angle glaucoma (CAG) arises from the iris pressing against the cornea, thereby closing the angle and preventing proper aqueous outflow (Nongpiur et al., 2011). Patients with CAG typically exhibit abnormally high IOP, which can create ocular pain (Salmon, 1999). Conversely, open angle glaucoma (OAG) is not painful and patients exhibit no angle closure. OAG involves the degradation and obstruction of the trabecular meshwork, leading to a decrease in outflow facility at the angle (Quigley, 1993). Decreased aqueous outflow, in turn, results in an

increase in IOP (Figure 1.3). Both CAG and OAG are associated with increases in IOP, thus measurement of IOP by tonometry is often a component of eye exams. Although ocular hypertension is associated with glaucoma, some patients exhibit disease progression despite never developing an elevated IOP, a condition deemed normotensive glaucoma (Heijl et al., 2002; Iester et al., 2012). Although these patients exhibit what is considered a normal IOP in the clinic, this does not mean that these patients progress solely due to IOP-independent mechanisms. In support of this idea, it has been determined that patients with normotensive glaucoma often benefit from IOP-lowering regimens (Heijl et al., 2002). It is therefore important to understand that glaucoma is not necessarily a disease related exclusively to IOP elevations, but rather to IOP sensitivity (Crish and Calkins, 2011).

RGCs and their susceptibility to glaucomatous neurodegeneration

All glaucomatous pathology ultimately converges upon the dysfunction and degeneration of RGCs. In humans, there are approximately 1.5 million RGCs, which possess the unique task of gathering information from other cells in the retina and conveying that information along their lengthy axons to distal brain regions (Campbell et al., 2013). To examine the implications of RGC death, it is critical to first understand the important role these neurons play within the context of the entire visual projection system.

Within the retina, visual information is first encoded when photons of light activate rod and cone photoreceptor cells in the outer retina (Figure 1.4). Photoreceptors release glutamate to activate bipolar cells, which in turn release glutamate to activate RGCs. Feed-forward signaling across the retina is most simply achieved at the two excitatory synapses between these three

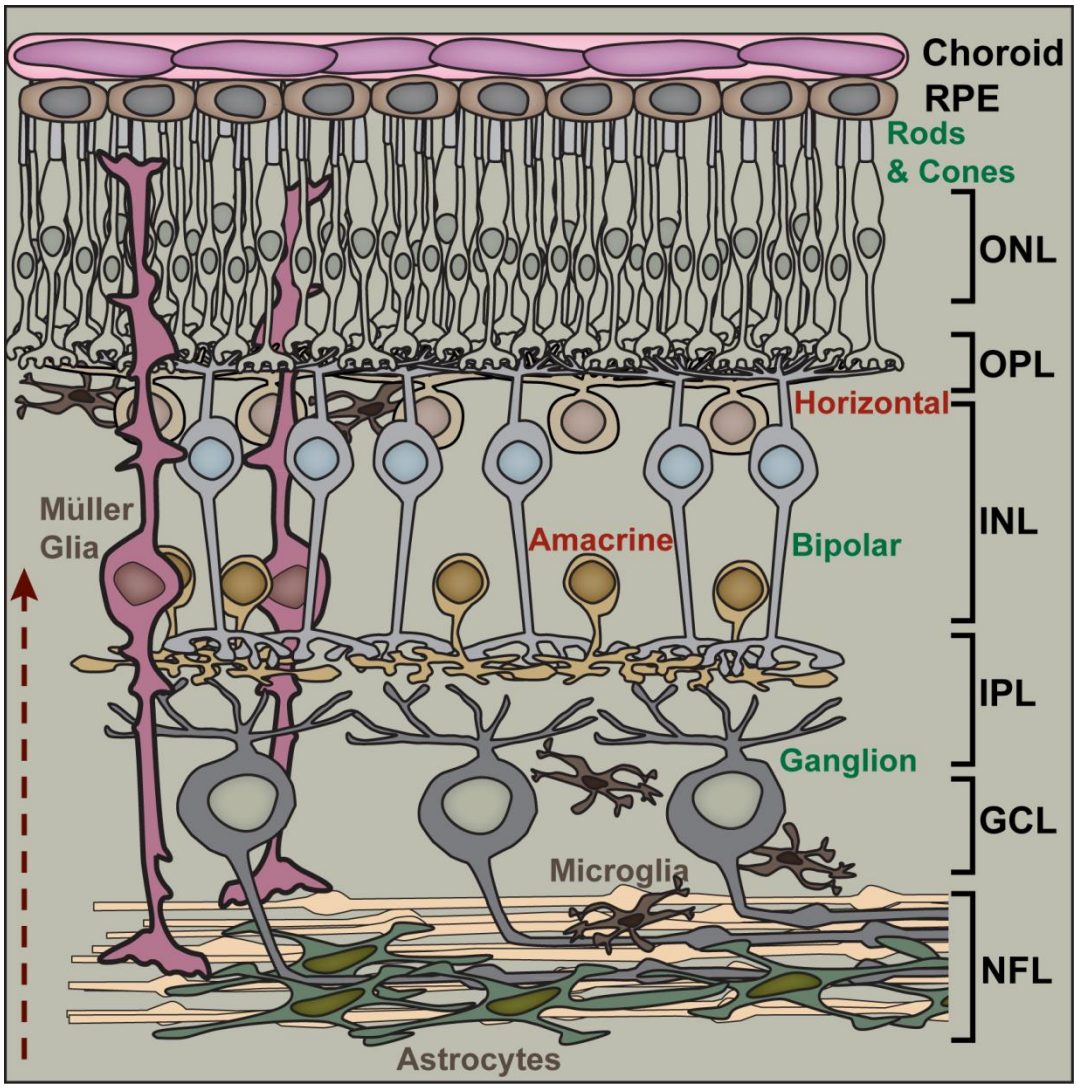

Figure 1.4. Retinal circuitry and layers. Traveling in the direction of the arrow (bottom, left), light reaches the rod and cone photoreceptors (with cell bodies in the outer nuclear layer, ONL) and is transduced into a neural signal. Transmission of visual information proceeds from photoreceptors to bipolar cells (with cell bodies in the inner nuclear layer, INL), and then from bipolar cells to ganglion cells (with cell bodies in the ganglion cell layer, GCL). This information is passed from one cell to another at excitatory synapses found in the outer plexiform layer (OPL) and inner plexiform layer (INL). Activity at these synapses are modulated by horizontal cells (at the OPL) and amacrine cells (at the IPL). As the ganglion cells course through the nerve fiber layer (NFL) toward the optic disc, they interact directly with astrocytes. In addition to astrocytes, other glial cells, such as microglia and Müller glia influence proper function within the retina as well as the overall health of the neuronal cells.

Figure from Calkins (2012) and used in accordance with Copyright Clearance Center's RightsLink service.

classes of neurons. Feed-forward retinal signaling is regulated by two sets of interneurons: horizontal cells in the outer retina and amacrine cells in the inner retina. Horizontal cells are GABAergic and modulate activity at synapses between photoreceptors and bipolar cells, while amacrine cells are mostly GABAergic and glycinergic and modulate synaptic activity between bipolar cells and RGCs (Wassle and Boycott, 1991; Oesch et al., 2011). Health and activity of all retinal cell types are additionally influenced by three retinal glial cells: astrocytes, microglia, and Müller glia.

Visual information that has been processed through the feed-forward pathway is then carried away from the retina along RGC axons. These axons exit the retina at the optic disc, at which point they bundle together to form the optic nerve. RGC axons terminate at several targets in the brain, particularly the lateral geniculate nucleus (LGN) in the thalamus and the superior colliculus (SC) in the midbrain. In primates, RGCs project primarily to the LGN, while only ~10% of RGCs project to the superior colliculus (Bunt et al., 1975; Perry et al., 1984; Liu et al., 2011). In contrast, rodent RGCs project primarily to the superior colliculus, with only ~30% of RGCs projecting to the LGN (Dreher et al., 1985). Unlike in primates, where half of RGCs cross to contralateral structures and the other half project ipsilaterally, the large majority of rodent RGCs project to contralateral brain structures, with only 3-10% of RGCs projecting ipsilaterally (Drager and Olsen, 1980; Jeffery, 1984; Kondo et al., 1993; Liu et al., 2011).

In glaucoma, it is known that dysfunction and death of RGCs results in progressive blindness, but less is known about why RGCs are the cells primarily affected in glaucoma. It has long been posited that pressure contributes to biomechanical stress on RGC axons as they leave the retina at the optic nerve head, and that this may contribute to damage (Burgoyne et al., 2005); however, it is likely that components intrinsic to RGCs make them particularly susceptible to

degeneration as well. More recent hypotheses suggest that a confluence of factors may determine the primary degeneration of RGCs in glaucoma (Calkins, 2012). These factors may include: (1) the relative thinness of RGC axons, (2) the presence of an energetically-demanding unmyelinated portion of the RGC axon, (3) a diminishment of transport of mitochondria along axons, and (4) a pressure-related reduction in ATP along the optic nerve.

Degenerative progression in glaucoma

Although the etiology of glaucoma is complex and not fully explained by current research, much more is known about the pathophysiological changes that occur in glaucoma due to disease modeling in animals. It is understood that during the course of glaucoma, RGCs exhibit signs of dysfunction preceding obvious structural degeneration and loss of neurons in the retina (Crish et al., 2010). It has also been determined that diminished visual function occurs prior to wide-scale loss of RGC somas in the retina (Harwerth et al., 2002). Developing knowledge of disease progression will therefore allow for targeted therapeutic interventions before dramatic vision loss occurs.

Thus far, deficits in anterograde axonal transport along the optic nerve are one of the earliest detectable signs of RGC dysfunction in animal models. Axonal transport is a method by which neurons are able to move cargo—organelles, lipids, synaptic vesicles, and proteins—from the cell body out toward synaptic terminals (anterograde transport) or from the terminals toward the cell body (retrograde transport). Cargo is transported along cytoskeletal tracks via motor proteins known as kinesin and dynein, which move in an anterograde and retrograde direction, respectively (Roy et al., 2005). Healthy axonal transport is critical to neurons because, among other functions, they depend on it to redistribute mitochondria to energetically demanding

regions of the neuron (Hollenbeck and Saxton, 2005) and to shuttle neurotrophic factors, which can influence cell survival (DiStefano et al., 1992).

The temporal progression of axonal transport deficits has perhaps been characterized best in studies using the DBA/2 mouse. In the DBA/2 mouse, which exhibits progressive glaucoma as animals age, significant RGC soma death begins at approximately 18 months, though some studies suggest it may begin earlier (Reichstein et al., 2007; Buckingham et al., 2008). However, when evaluating deficits in anterograde axonal transport, the earliest deficits are observed in 3-month-old DBA/2 mice (Crish et al., 2010). This indicates that one of the earliest known deficits exist far in advance of the final stage of RGC degeneration—caspase-dependent apoptotic cell death (Garcia-Valenzuela et al., 1995; Kerrigan et al., 1997). In fact, anterograde transport is almost completely lost by 11 to 12 months in DBA/2 mice, again prior to significant RGC death in the retina (Buckingham et al., 2008; Crish et al., 2010). Retrograde transport is affected later than anterograde transport, as studies in DBA/2 mice indicate deficits are first observed at 6-8 months (Buckingham et al., 2008).

In addition to disruptions in axonal transport, degeneration of axons in the optic nerve occurs prior to RGC soma loss in the retina as well. Axon density within the optic nerve was reduced starting at 13 months in the DBA/2 mouse, and this reduction in density is accompanied by disrupted axon fascicles and enlarged astrocytic processes (Buckingham et al., 2008). In a meta-analysis of studies using RGC soma counts in the retina and RGC axon counts in the optic nerve, it was apparent that reduction of axons was 2-3 times greater than reductions in RGC soma counts, even across different cumulative exposures to IOP (Calkins, 2012).

Although RGC death in the retina stands as the final stage of glaucomatous progression, disease-relevant alterations are not simply confined to the RGC axon alone. In 12-month-old

DBA/2 mice with observed optic nerve pathology, certain RGCs exhibited a reduction in dendritic branching as well as abnormal dendritic arbors when compared to controls (Jakobs et al., 2005). Likewise, one study found less PSD-95 present at synaptic sites in the inner plexiform layer of the retina in 10.5-month-old DBA/2 mice, likely indicating of dendritic retraction or pruning (Stevens et al., 2007). This assertion was strengthened by the presence of a concomitant upregulation of C1q protein, which may help target dendrites for pruning by microglia (Stevens et al., 2007). It is not yet clear how early dendritic changes occur, but these results indicate that it may happen alongside the development of pathology in the optic nerve.

Although dendritic pruning and synaptic elimination may occur at intermediate stages of disease progression, it appears that RGC axon terminals persist at target sites in the brain. In the DBA/2 mouse, immunolabeled presynaptic terminals from RGC axons persist within the SC for up to 18-22 months (Crish et al., 2010). This matches well with data suggesting that retrograde axonal transport, which exhibits deficits later than anterograde transport, persists up to 18 months in DBA/2 mice (Buckingham et al., 2008). This knowledge of structural persistence at distal brain sites is encouraging, especially when paired with the idea that therapeutics could focus on rescuing dysfunctional neurons before cellular structures degenerate.

While the DBA/2 mouse model of glaucoma has been highly informative in establishing a progression of degeneration, this model is not without its limitations. The DBA/2 has two mutations that result in a pigmentary form of glaucoma. These mutations in the *Gpnmb* and *Tyrp1* genes cause iris pigment dispersion and iris stromal atrophy, respectively (Anderson et al., 2002). The dispersion and atrophy entail sloughing off of iris pigment and cell debris into the ocular drainage structures, which obstructs aqueous outflow and gradually elevates IOP. In these mice, IOP elevation and disease progression are variable—the majority of mice have elevated

IOP by 5 to 6 months of age, but some present with elevated pressure by 3 months, and still others never show any pressure elevation (Inman et al., 2006). In addition, the level of IOP elevation also varies in these mice, ranging anywhere from 2.5 to 8 mmHg depending on the age and sex of the mouse (Inman et al., 2006). Finally, variables such as colony of origin (DBA/2J versus DBA/2NCrl versus DBA/2NTac), diet, along with other environmental factors all influence the natural history of disease in DBA/2 mice (McKinnon et al., 2009).

In consideration of the limitations of the DBA/2, we and other investigators have developed methods to induce ocular hypertension (elevated IOP) acutely. These models include laser photocoagulation of episcleral veins (WoldeMussie et al., 2001), episcleral vein occlusion (Garcia-Valenzuela et al., 1995), sclerosis of episcleral veins by injection of hypertonic saline (Morrison et al., 1997), and microbead occlusion of aqueous humor drainage (Sappington et al., 2010). In these models, IOP is typically elevated in one eye, leaving the other to serve as an internal control. We use the microbead model as it provides a reliable and robust (25 to 35%) increase in IOP, it is reproducible across cohorts, and IOP elevation can be sustained for multiple weeks in mice. The microbead model is also effective in inducing optic nerve pathology, as axon counts are reduced by approximately 20% following 4 weeks of elevated IOP. This model does not exhibit issues such as ocular ischemia and neovascularization, both of which can confound interpretation of data (Goldblum and Mittag, 2002; Pang and Clark, 2007). Ultimately, what makes this model so useful is that it produces IOP elevation that is more in line with pressure elevation seen in human disease (~38% elevation for moderate cases), whereas other models use 50-100% elevations that may not be a proper physiological representation of elevations seen in untreated human glaucoma (Sommer et al., 1991; Sappington et al., 2010).

Neurodegeneration in glaucoma

Within the CNS, neurodegenerative diseases such as Alzheimer's disease (AD), amyotrophic lateral sclerosis (ALS), Parkinson's disease (PD), and Huntington's disease (HD) exhibit diverse etiologies and a wide range of clinical presentations. Nevertheless, the underlying neurodegenerative cellular mechanisms often exhibit remarkable similarities (Crish and Calkins, 2011; London et al., 2013). In this section, we will first cover features that are common to most neurodegenerative diseases, such as dysregulation of Ca^{2+}, excitotoxicity, mitochondrial dysfunction, and disruption of axonal transport. Following that, we will examine how glaucoma shares common characteristics and cellular mechanisms with other neurodegenerative diseases.

Ca^{2+} homeostasis is dysregulated in neurodegeneration

Ca^{2+} is an important intracellular messenger that regulates a variety of important neuronal functions like neurotransmitter release, neuronal responses to the binding of neurotransmitter, potentiation and depression of synaptic activity, and gene transcription (Berridge, 1998; Berridge et al., 2000; Gleichmann and Mattson, 2011). While essential to many cellular processes, this cation functions under tight regulation by the cell; situations in which Ca^{2+} exceeds its typical spatial and temporal limits can result in irreversible damage. Across a number of neurodegenerative diseases, dysregulation of Ca^{2+} homeostasis is a common feature that underlies pathogenesis (Marambaud et al., 2009).

Two parts of the machinery that regulates the levels of intracellular Ca^{2+} are membranous ionotropic glutamate receptors known as NMDA and Ca^{2+}-permeable AMPA receptors (Figure 1.5). When these receptors are activated in an excessive manner, Ca^{2+} entry into the cell becomes

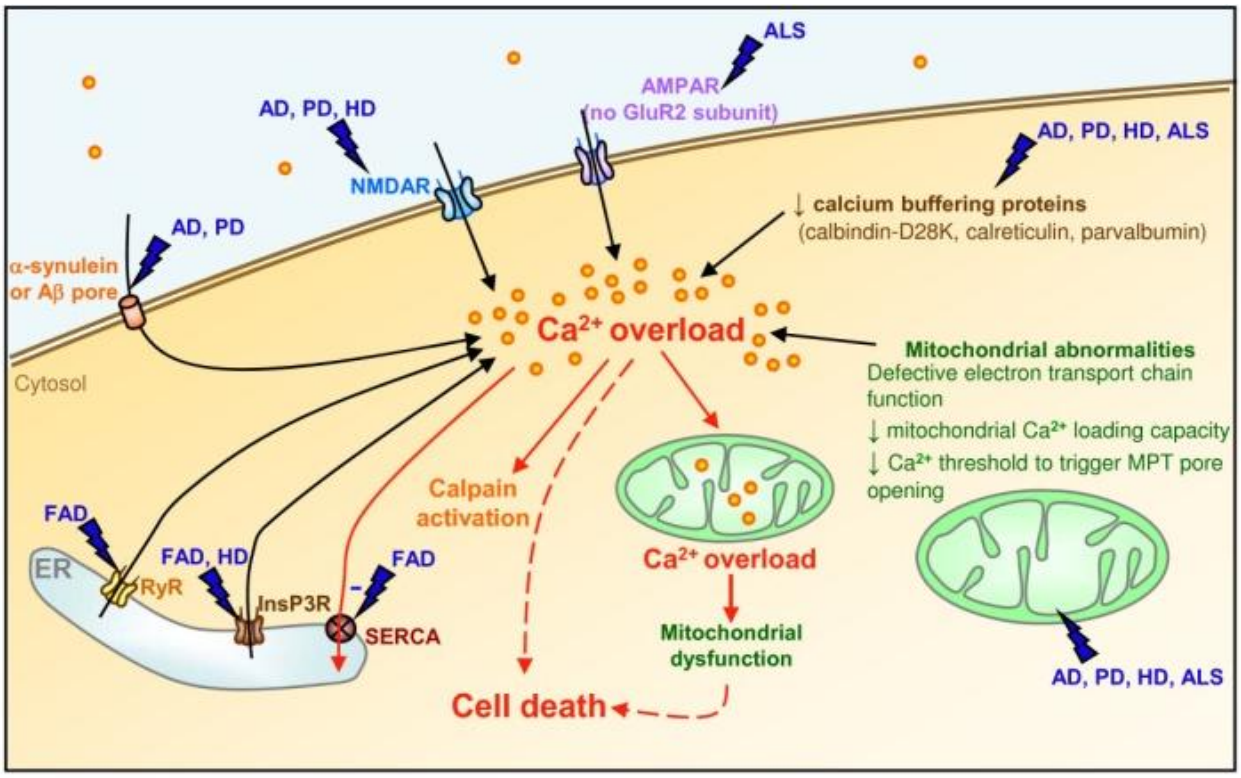

Figure 1.5. Dysregulation of Ca^{2+} in neurodegenerative disease. Many pathways converge upon Ca^{2+} overload as a damaging agent in neurodegenerative disease. Disease-relevant stressors such as excitotoxicity and decreased expression of Ca^{2+} buffering proteins contribute to an overload of Ca^{2+} within neurons. This excessive Ca^{2+} overloads the buffering potential of mitochondria and also activates damaging Ca^{2+}-activated proteases known as calpains. As mitochondria dysfunction, they are prone to release cytochrome *c*, inducing mitochondrially-mediated apoptosis of the affected neuron.

neurotoxic, a phenomenon known as excitotoxicity (Arundine and Tymianski, 2003). The propensity for certain neurons to experience excitotoxicity can be influenced by the type of receptors those cells express. For instance, not all AMPA receptors can flux Ca^{2+}, and this is dictated by the GluR2 subunit; if a GluR2 subunit is present in the AMPA receptor, it cannot flux Ca^{2+}. This is particularly relevant in ALS, as AMPA receptors in the affected spinal motoneurons appear to all lack GluR2 subunits, which may contribute to Ca^{2+}-mediated excitotoxicity

(Carriedo et al., 1996; Williams et al., 1997; Takuma et al., 1999). Additionally, protein aggregates that form in some neurodegenerative disease may influence the activity of NMDA receptors, pushing them toward a more excitotoxic activity profile (Sun et al., 2001; Shankar et al., 2007). For example, in AD aggregates of Aβ may directly associate with NMDA receptor subunits, causing an increase in channel activity and a resulting increase in Ca^{2+} flux into the cell (Shankar et al., 2007).

Multiple stressors can cause dysregulation of Ca^{2+} in neurodegenerative diseases. In AD, altered cleavage of amyloid precursor protein generates Aβ, which is toxic to neurons (Mattson, 2004). Formation of Aβ oligomers is associated with the production of reactive oxygen species (ROS), which results in membrane-associated oxidative stress (MAOS). MAOS involves lipid peroxidation, which disrupts the function of both Na^{+}/K^{+}- and Ca^{2+}-ATPases as well as transporters of glutamate and glucose (Mattson, 1998). This results in depolarization of the membrane and influx of Ca^{2+} through NMDA receptors and voltage-dependent Ca^{2+} channels (Mattson, 2007). Aside from AD, there is evidence for MAOS occurring in degenerating neurons in PD (Yoritaka et al., 1996) and ALS (Smith et al., 1998) as well.

Due to the dynamic nature of Ca^{2+} entry and activity within cells, it is important that neurons are able to buffer any excess intracellular Ca^{2+}. Specific proteins called Ca^{2+} buffering proteins are critical for this buffering process. Degenerative pathology has been associated with changes related to various Ca^{2+} buffering proteins, including calbindin-D28K, calmodulin, and parvalbumin (Figure 1.5). A common feature of motoneurons affected earliest in ALS is that they do not express calbindin-D28K or parvalbumin, which may render them susceptible to aberrant Ca^{2+} (Alexianu et al., 1994). Additionally, calbindin-D28K and calmodulin protein and mRNA levels are known to be reduced in several cortical regions in AD, showing that the ability

to buffer Ca^{2+} declines in areas susceptible to degeneration (McLachlan et al., 1987; Ichimiya et al., 1988).

In addition to being buffered by proteins, intracellular Ca^{2+} concentrations can be reduced via uptake of Ca^{2+} by mitochondria. However, when levels of Ca^{2+} within mitochondria become too high, mitochondrial dysfunction occurs (Figure 1.5), which may involve opening of the mitochondrial permeability transition (MPT) pore (Hunter and Haworth, 1979; Brustovetsky et al., 2002). Opening of the MPT pore allows Ca^{2+} to leave mitochondria again, which causes intracellular Ca^{2+} to elevate once again. Prolonged opening of MPT can result in other deleterious effects: disruption of the electron transport chain, reduced ATP production, increased production of reactive oxygen species, and release of cytochrome *c* from mitochondria (Buki et al., 2000; Luetjens et al., 2000; Stavrovskaya and Kristal, 2005). Cytochrome *c* release can cause activation of caspase-dependent cellular apoptosis, thus opening of the MPT can have dire consequences for neurons (Green and Reed, 1998). Studies in HD determined that mutant huntingtin protein could directly induce MPT pore opening due to a lowered tolerance of the Ca^{2+} load within mitochondria (Panov et al., 2002; Panov et al., 2003; Choo et al., 2004). This type of interaction also seems to occur in AD, in which Aβ accumulation in mitochondria may also aid in mediating Ca^{2+}-induced MPT opening (Reddy and Beal, 2008).

As intracellular Ca^{2+} increases to non-homeostatic concentrations within neurons, degenerative cascades are activated. Ca^{2+} can directly activate proteases known as calpains, which cleave cytoskeletal proteins, components of synapses, receptors, and enzymes involved in metabolism (Chan and Mattson, 1999; Lu et al., 2000; Vosler et al., 2008). Calpain activation due to dysregulated Ca^{2+} can therefore promote mechanisms that cause disruptive changes to neurons. Calpain-mediated cleavage of Bax is a feature of PD, and this cleavage promotes

release of cytochrome *c* from mitochondria, which pushes the neurons toward death (Choi et al., 2001). Calpains can also activate abnormal phosphorylation activity of several varieties of kinases, which in turn phosphorylate neurofilaments and tau protein, ultimately resulting in dysfunctional axon transport (Shea et al., 2004; Goni-Oliver et al., 2007; Morfini et al., 2009b).

Axonal transport disruption in neurodegenerative diseases

Disruption of neuronal function in neurodegenerative disease often includes development of deficits in axonal transport. The axon is therefore a challenging feature for neurons, as important cellular components necessary for axonal function must be transported from their location of synthesis in the cell body (Morfini et al., 2009b). In neurodegenerative diseases, there is evidence for abnormal phosphorylation of motor proteins, which leads to dysfunction of axonal transport. In HD, polyglutamine expansion of the huntintin protein (polyQ-Htt) is associated with neurodegeneration in the striatum and cerebral cortex (Sieradzan and Mann, 2001). PolyQ-Htt was determined to causes deficits in axonal transport by activating a neuron-specific kinase called JNK3, which phosphorylates kinesin protein (Morfini et al., 2009a). Similarly, kinase activity in AD is altered (Pigino et al., 2001; Wang et al., 2007), and one of these kinases—casein kinase 2 is activated and disrupts axonal transport via increased phosphorylation of kinesin-1 light chain (Pigino et al., 2009). This deregulated phosphorylation results in the uncoupling of kinesin-1 from its cargo, and thus disrupting transport along the axon.

Phosphorylation of motor proteins is not the only way that axonal transport can be disrupted in neurodegeneration. Excessive phosphorylation of neurofilaments can also be detrimental to axonal transport. Neurofilaments are cytoskeletal elements that are longitudinally

oriented in the axon. Neurofilaments were first named according to their molecular mass—light (NF-L), medium (NF-M), and heavy (NF-H)—however, a fourth subunit named α-internexin has since been discovered (Julien and Mushynski, 1998; Yuan et al., 2006). Of these four subunits, both NF-M and NF-H have long C-terminal regions commonly known as their side arms, which can be extensively phosphorylated (Julien and Mushynski, 1998). Increasing side arm phosphorylation decreases the affinity of NFs for kinesin (Yabe et al., 1999), and increases their affinity for dynein (Motil et al., 2006); therefore, these NFs are not anterogradely transported along the axon, where they are needed. Instead, increased affinity for dynein causes them to be transported retrogradely and accumulate at the cell soma. Additionally, the phosphorylated neurofilaments (pNFs) tend to bundle together, which considerably slows down anterograde transport by kinesin (Shea and Chan, 2008). Elevated or mislocated pNF and hyper-pNF have been reported in many neurodegenerative diseases, including ALS (Sobue et al., 1990), MS (Petzold et al., 2008), AD (Stokin et al., 2005), and glaucoma (Soto et al., 2008).

Degenerative cellular mechanisms in glaucoma

Although direct evidence for excitotoxicity in models of glaucoma is relatively scarce (Carter-Dawson et al., 2002; Levkovitch-Verbin et al., 2002; Casson, 2006), NMDA antagonists MK-801 (Chaudhary et al., 1998) and memantine (Hare et al., 2004a; Hare et al., 2004b) both exhibited a neuroprotective effect in models of glaucoma. Of these two drugs, memantine was tested for use with human patients in a set of clinical trials, which were deemed unsuccessful (Osborne, 2009). It has been hypothesized that glaucoma may be mediated in part by insufficient blood supply, potentially due to increased IOP or other risk factors that could reduce ocular blood flow (Flammer et al., 2002). Based on this hypothesis, RGC death may in part be due to

excitotoxic damage downstream of ischemia-reperfusion injury (Osborne et al., 1999; Flammer et al., 2002). One study used a rat model of retinal ischemia/refusion induced by non-physiologically high IOP (120 mmHg for 45 minutes) to demonstrate that intraocular administration of Coenzyme Q10 (CoQ10) afforded neuroprotection to RGCs by preventing mitochondrial permeability transition pore formation (Nucci et al., 2007a). While these mechanisms may be protective, it is difficult to assess whether or not these mechanisms are relevant to human glaucoma as it presents in the clinic, especially given the use of non-physiological IOP elevations. Presently, it is poorly understood how much of a role excitotoxic Ca^{2+} entry plays a role in glaucomatous degeneration.

Ca^{2+} binding proteins may be relevant in some initial responses to elevated pressure, as RGC-associated expression of Ca^{2+} buffering proteins parvalbumin and calbindin-D28K were transiently upregulated following pressure elevation in rats (Wang et al., 2005). The authors indicated that this upregulation was prior to loss of RGCs in the retina—it is possible that RGCs may use these buffering proteins to address the presence of aberrant Ca^{2+}. Excessive intracellular Ca^{2+} can activate calpains, and this activation has been observed in a rat model of glaucoma (Huang et al., 2010). In other neurodegenerative diseases (Vosler et al., 2008), calpains activate cyclin dependent kinase 5 (Lee et al., 2000), glycogen synthase kinase 3(Goni-Oliver et al., 2007), and c-Jun N-terminal kinases/JNK (Tan et al., 2006; Morfini et al., 2009b). Overactive phosphorylation of neurofilaments and the microtubule associated protein tau by kinases results in axonal transport deficits (Shea et al., 2004; Morfini et al., 2009b), which are a hallmark of glaucoma (Anderson and Hendrickson, 1974; Crish et al., 2010; Howell et al., 2012). In DBA/2 mice, somatic and somatodendritic accumulations of phosphorylated neurofilaments were associated with RGCs exhibiting failure of axonal transport (Soto et al., 2008). The kinases

associated with this excessive phosphorylation activity can affect motor protein activity as well: glycogen synthase kinase 3 phosphorylates kinesin, resulting in its dissociation from cargo, and JNK phosphorylates kinesin, inhibiting its ability to bind microtubules (Morfini et al., 2009b). Early changes in kinase activity in glaucoma may therefore influence onset and progression of axonal dysfunction (Crish and Calkins, 2011).

Dysregulated Ca^{2+} is also known to influence the development of oxidative stress through mechanisms such as increased neuronal metabolic rate and activation of ROS-producing enzymes (Abramov et al., 2007; Zundorf et al., 2009; Crish and Calkins, 2011). DBA/2 mice exhibit lipid peroxidation and upregulated oxidative stress-related proteins during pathogenesis, so a group of studies was focused on addressing the relative contribution of oxidative stress to glaucoma pathogenesis (Inman et al., 2013). In these studies, dietary supplementation with antioxidant α-lipoic acid reduced measures of oxidative stress, increased expression of antioxidant proteins, and increased protection of RGCs (Inman et al., 2013). This protection afforded by α-lipoic acid supplementation therefore indicates that oxidative stress contributes to the degenerative outcome of RGCs during the course of glaucoma.

Protective responses of the retina and RGCs

Although neurodegenerative cellular signaling drives neurons toward cell death, there is evidence for intrinsic protective mechanisms that slow this progression. In a study of both experimental glaucoma and optic nerve transection, upregulation of both proapoptotic and prosurvival genes occurred simultaneously in the retina (Levkovitch-Verbin et al., 2006). In this study, proapoptotic gene *Gadd45a* was significantly upregulated 1 week after IOP elevation and remained upregulated for 2 months, whereas upregulation of prosurvival gene *Iap-1* returned to

baseline prior to *Gadd45a*. RGCs exposed to elevated pressure *in vitro* exhibited upregulation of apoptotic genes, but these cells likewise showed a protective response through upregulation of the prosurvival *Bcl-2* gene (Sappington et al., 2006). These studies indicate that both RGCs and the retina as a whole have protective responses to counter the stresses of the degenerative milieu of glaucoma.

As in other neurodegenerative conditions, oxidative stress is a detrimental feature of glaucoma (Lin and Beal, 2006; Tezel, 2006). The retina combats oxidative stress associated with IOP elevation by reducing the formation of damaging reactive oxygen species (ROS). In the DBA/2 mouse, ceruloplasmin protein is upregulated in order to reduce iron-mediated mechanisms of ROS formation (Steele et al., 2006). This increase was observed in 5-month-old animals, suggesting that this protein is involved in an early response to glaucomatous stressors. In addition to ceruloplasmin, increases in other antioxidant proteins are elevated in the retina or aqueous humor in monkeys and humans with glaucoma (Farkas et al., 2004; Ferreira et al., 2004; Ghanem et al., 2010).

Many of these studies examining protective responses examine the retina as a whole tissue; however, this makes it difficult to determine if RGCs have intrinsic mechanisms for responding to glaucomatous stress and damage. Driving synaptic activity, even in injured or degenerating neurons, has been demonstrated to help neurons survive (Corredor and Goldberg, 2009). For example, after optic nerve axotomy in rats, stimulating retinal neurons using a trans-corneal electrode increased RGC survival *in vivo* (Morimoto et al., 2005). It is important to consider, then, if RGCs make any attempt to bolster their synaptic connections in an effort to survive degenerative stressors. Evidence from manganese-enhanced MRI of DBA/2 mice indicated that very little difference was seen in cationic activity in the DBA inner retina when

comparing between ages associated with axonopathy and those considered pre-axonopathy (Calkins et al., 2008). This may support the idea that despite degenerative progression, RGCs make an effort to maintain their synaptic activity in the inner retina as part of an effort to survive.

Ca^{2+}-mediated plasticity and a role for TRPV1 in neuronal survival

Role of Ca^{2+} in homeostatic synaptic plasticity

In cases of injury and disease, CNS neurons undergo plasticity that involves rewiring of neural circuitry (Moore et al., 2000; Kaas et al., 2008). Reductions in synaptic connectivity as well as dendritic retraction and abnormalities are common features of neurodegenerative diseases and injury (Posmantur et al., 1996; Lin and Koleske, 2010; Furutani and Kibayashi, 2012). However, it has been hypothesized that neurons may actually take an active role in maintaining synaptic activity following injury in order to recover and preserve function (Lee, 2012). In models of neuronal insult and injury (Liu et al., 2006; Spaethling et al., 2008), Ca^{2+}-permeable AMPA receptors were upregulated in neurons and their synaptic sites. Increased localization of Ca^{2+}-permeable AMPA receptors to postsynaptic specializations of neurons is often involved in potentiating activity at synapses (Malenka and Bear, 2004). It is not yet understood whether this increase in receptors contributes further to Ca^{2+}-related pathology or instead helps bolster neuronal activity and connectivity (Liu et al., 2006; Lee, 2012). It is known that many neurons exhibit homeostatic synaptic plasticity, meaning they are able to monitor their activity and in turn modify the strength of a synapse by trafficking glutamatergic receptors to or from that synapse (Ibata et al., 2008; Turrigiano, 2008; Lee, 2012). Altogether, these homeostatic

mechanisms would be useful when healthy neuronal function is compromised, especially given that maintaining activity is critical for neuronal survival (Corredor and Goldberg, 2009).

In terms of understanding neuronal responses to injury, cultures of mechanically lesioned leech nerve cord are used to better understand regenerative neurite outgrowth following CNS injury. One group demonstrated that endocannabinoids, a group of neuromodulatory lipids, were involved in neurite outgrowth following damage; however, they could not identify leech orthologs for the cannabinoid receptors CB1 and CB2 (Meriaux et al., 2011). Endocannabinoids, however, are also known to activate the TRPV1 receptor (Ross, 2003). TRPV1 is a polymodal cation channel with a high preference for fluxing Ca^{2+}, and it can be activated by heat, pH, and vanilloid compounds like capsaicin (Ho et al., 2012). Meriaux et al. (2011) confirmed that leeches possessed orthologs to the TRPV family of proteins, and then tested how neurite outgrowth was modulated by two agonists (arvanil and capsaicin) and one antagonist (capsazepine) of mammalian TRPV1. Both agonists accelerated neurite outgrowth and the antagonist halted all outgrowth. Intriguingly, this study showed that, subsequent to CNS injury in the leech, a TRPV1-like protein modulates neurite outgrowth.

Potential for TRPV1 to influence RGC survival in vivo

Immunolabeling for TRPV1 in primary cultures of RGCs reveals that this protein is expressed throughout the RGC, including all neurites (Sappington et al., 2009). In the DBA/2 mouse, TRPV1 exhibits an interesting expression pattern: at older ages and higher IOP, TRPV1 expression is especially localized to the inner plexiform layer, the layer of the retina into which RGC dendrites project (Sappington et al., 2009). This is interesting because Ca^{2+}-permeable AMPA receptors exhibit localization to synaptic sites following neuronal insult and injury (Liu

et al., 2006). TRPV1 is also permeable to Ca^{2+}, so if it localizes to RGC dendrites, it could exert beneficial or deterimental effects depending on its function. Previous studies *in vitro* indicated that Ca^{2+} influx into cultured RGCs exposed to pressure is partly mediated by TRPV1 (Sappington et al., 2009). *In vitro*, this is detrimental and causes apoptosis, especially given the acute nature of the stressor used. *In vivo*, this Ca^{2+} entry may be important, especially if TRPV1 is upregulated in RGC dendrites, where it could help modulate homeostatic synaptic interactions in response to stress (Lee, 2012). If this actually occurs, it would not be the first example of TRPV1 affording RGCs protection from damage, as has previously been demonstrated in models of NMDA-induced neuronal injury and ischemia-reperfusion injury (Nucci et al., 2007b; Sakamoto et al., 2014).

TRPV1 modulates CNS function

The TRP channel family

The transient receptor potential (TRP) family is a diverse group of channels that regulates cation entry and contributes to a vast variety of physiological conditions. In mammals, there are 28 TRPs, divided into 6 subfamilies based on homology: canonical (TRPC1-7), vanilloid (TRPV1-6), melastatin (TRPM1-8), ankyrin (TRPA1), polycystin (TRPP1-3) and mucolipin (TRPML1-3). All six subfamilies share a common structure of six transmembrane domains with a hydrophobic pore located between the fifth and sixth domains. Situated in the plasma membrane, TRP channels serve as polymodal integrators due to their activation by a variety of stimuli including temperature, osmolality, mechanical force, chemoattractants and ischemia.

One subfamily of the TRP channels is the vanilloid family, named for their responsiveness to various ligands that possess vanillyl moieties. Within the TRPV family, TRPV1 is the best studied particularly due to its role in nociception. Although first identified as the receptor for capsaicin, TRPV1 can also be activated endogenously by voltage, noxious heat (>42°C), pH and lipoxygenase products. Endocannabinoids, including anandamide and *N*-arachidonoyl dopamine, can activate both TRPV1 and cannabinoid receptors, indicating the importance of cross-talk mechanisms. TRPV1 nonselectively gates cations; however, channel activation results in a 10-fold higher preference for Ca^{2+} (Chung et al., 2008). Functional TRPV1 preferentially forms a homotetramer but can also oligermerize with other TRP family subunits including TRPV3 and TRPA1 (Smith et al., 2002; Moiseenkova-Bell et al., 2008; Staruschenko et al., 2010).

The structure of TRPV1

Structural analysis of TRPV1 indicates a compact transmembrane region and a large basket-like intracellular domain (Moiseenkova-Bell et al., 2008). The intracellular N-terminal tail contains numerous phosphorylation sites and ankyrin repeats that serve as binding sites for calmodulin and ATP (Lishko et al., 2007). The intracellular C-terminal tail contains a TRP domain as well as binding sites for both calmodulin and PIP2, an endogenous TRPV1 inhibitor (Numazaki et al., 2003; Garcia-Sanz et al., 2004; Ufret-Vincenty et al., 2011). Agonist activation is also mediated intracellularly, as lipophilic capsaicin readily crosses the membrane to bind several sites on TRPV1 (Figure 1.6). The cation selectivity filter for TRPV1 is believed to lie in the pore domain formed by transmembrane regions 5 and 6. This selectivity is dynamic, not static, and can vary depending on stimulus duration or agonist concentration. Activation can alter

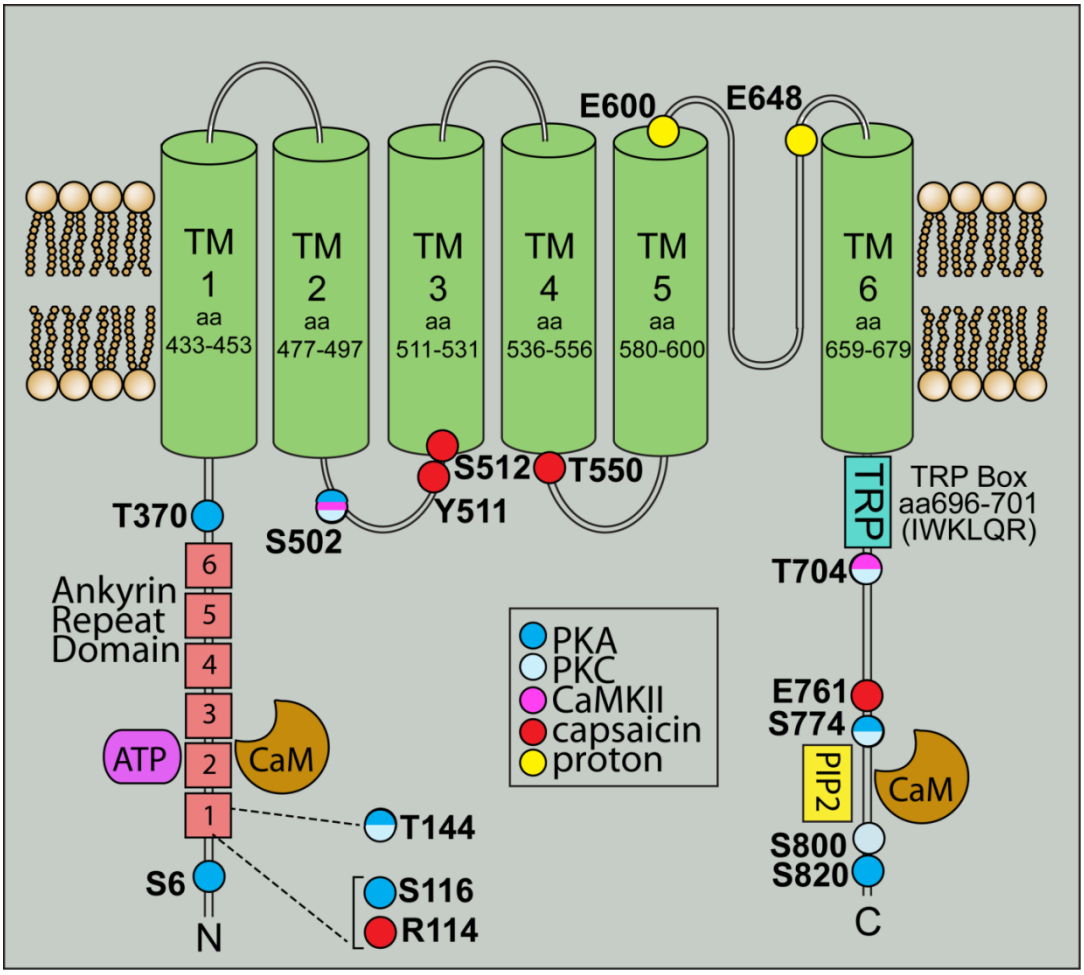

Figure 1.6. TRPV1 is a member of the transient receptor potential family. TRPV1 consists of six transmembrane domains with a pore region between the fifth and sixth domain, and long intracellular N- and C- terminal tails. Within the N-terminal tail, six ankyrin repeat domains allow binding of calmodulin and ATP to modulate TRPV1 activation. The C-terminus contains a TRP domain as well as binding sites for PIP2 and calmodulin. Throughout TRPV1 are multiple phosphorylation sites for PKA, PKC and CaMKII, in addition to putative sites for capsaicin and proton binding.

the Ca^{2+} permeability and pore diameter of TRPV1 to allow influx of larger cations (Chung et al., 2008). The method of channel stimulation can also have a significant effect on Ca^{2+} permeability—activation by protons produces a smaller Ca^{2+} current than activation by capsaicin (Samways et al., 2008).

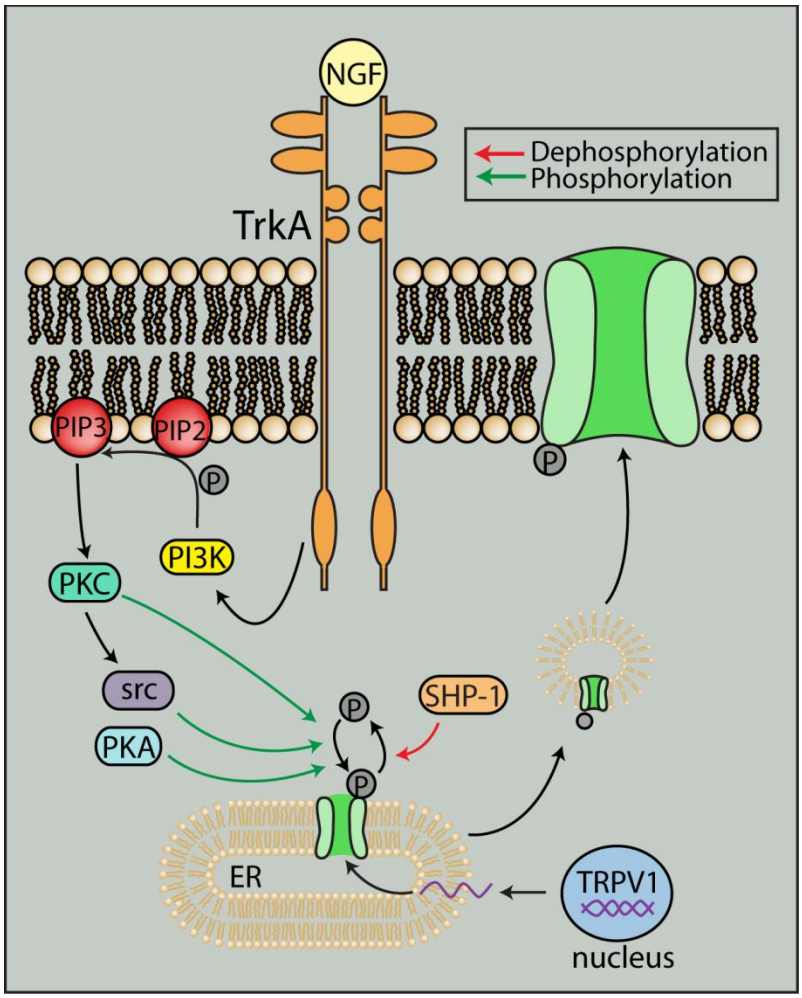

Figure 1.7. Interaction with other signaling pathways can traffic TRPV1 to the plasma membrane. TrkA stimulation by NGF can cause src-mediated phosphorylation of TRPV1 to traffic TRPV1 from the endoplasmic reticulum to the plasma membrane. Translocation of TRPV1 to the membrane can also be increased through PKA- and PKC-mediated phosphorylation. Dephosphorylation by SHP-1, however, can inhibit translocation.

Figure from Ho et al. (2012) and used in accordance with the Creative Commons Attribution Noncommercial License.

Regulation of TRPV1

In addition to membrane expression, TRPV1 is also found in the endoplasmic reticulum where it mobilizes Ca^{2+} from intracellular stores (Liu et al., 2003; Marshall et al., 2003). Activation of signaling pathways can translocate TRPV1 from intracellular compartments to the membrane usually via phosphorylation. For example, PKC activation can lead to membrane insertion of TRPV1 via SNARE-mediated exocytosis (Morenilla-Palao et al., 2004). Furthermore, nerve growth factor activation of the tyrosine kinase src can phosphorylate TRPV1 to increase membrane localization (Figure 1.7).

Phosphorylation is also important in modulating the channel, allowing for rapid responses to external stimuli or environmental changes. Generally, phosphorylation sensitizes while dephosphorylation desensitizes the channel. PKC phosphorylation reverses desensitization of TRPV1 from prolonged capsaicin treatment and increases the sensitivity of TRPV1 to agonists (Mandadi et al., 2006; Varga et al., 2006). PKA can also reduce desensitization by direct phosphorylation of TRPV1 (Bhave et al., 2002). In addition, PKC or PKA activation through stimulation of multiple receptors including the protease-activated receptor PAR2, bradykinin B1 and B2, purinergic P2 receptors, chemokine receptor CCL3, and endothelin receptors have all been shown to increase sensitivity of the channel (Figure 1.8). On the other hand, dephosphorylation by calcineurin/PP2B and increases in intracellular Ca^{2+} can desensitize the channel (Koplas et al., 1997; Mohapatra and Nau, 2005).

TRPV1 in the CNS

Although it is expressed throughout the CNS, TRPV1 is most robust in the sensory neurons of the dorsal root ganglion (Sanchez et al., 2001). Using a combination of knockout

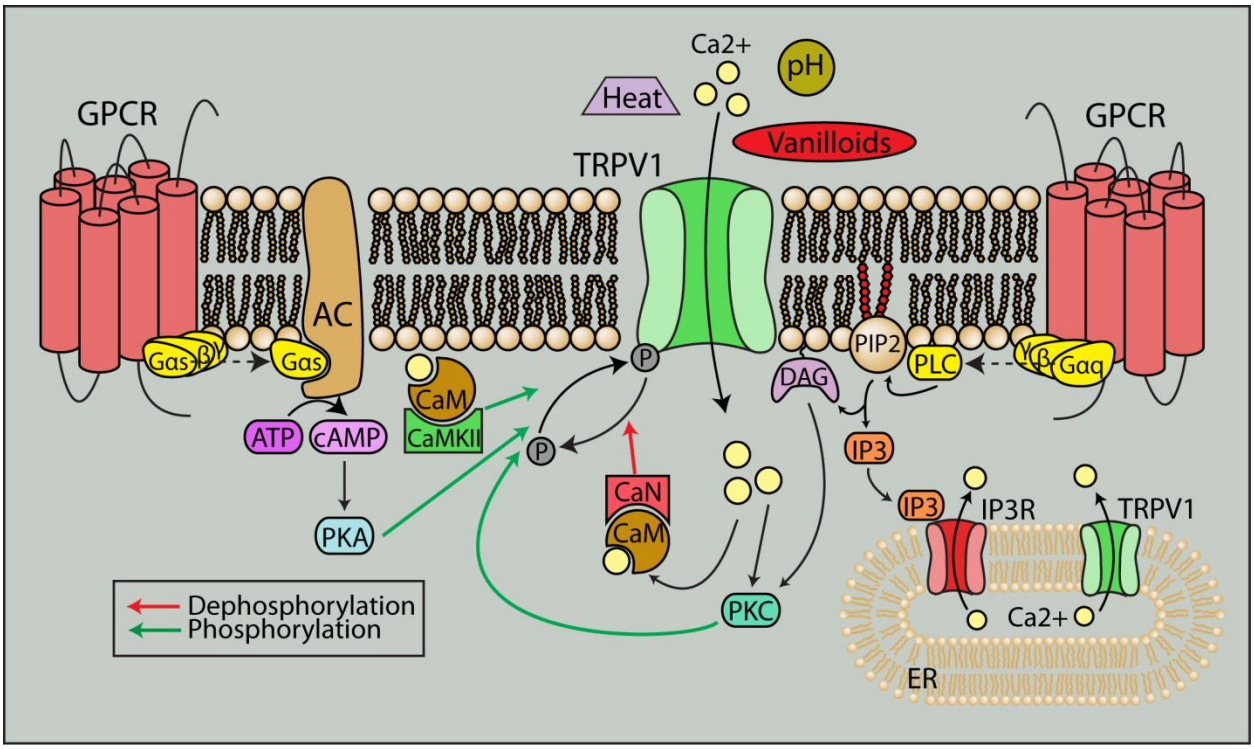

Figure 1.8. TRPV1 is a polymodal cation channel. TRPV1 can be activated by a variety of noxious stimuli such as heat, pH and pressure, and its interaction with other receptors including G protein-coupled receptors (GPCRs) contributes to its polymodal nature. GPCR activation can directly lead to recruitment of PKC and PKA, through phospholipase C and adenylyl cyclase respectively, to phosphorylate TRPV1 and sensitize the channel. Elevations in intracellular Ca^{2+} from TRPV1 and GPCR stimulation can activate calcineurin and CaMKII via calmodulin to further modulate TRPV1 activity.

Figure from Ho et al. (2012) and used in accordance with the Creative Commons Attribution Noncommercial License.

mice, radioligand binding and immunocytochemistry, TRPV1 expression within the CNS has been documented. These studies localize TRPV1 mainly to the hippocampus and cortex with additional expression in hypothalamus, olfactory nuclei, dentate gyrus, locus coeruleus, superior colliculus and spinal cord (Roberts et al., 2004; Toth et al., 2005). These observations of widespread TRPV1 expression, however, are contested by a TRPV1 reporter mouse that indicates limited expression in the CNS outside of nociceptors in the sensory ganglia. CNS

expression was restricted to the posterior caudal hypothalamus, the rostral midbrain, the periaqueductal grey and the hippocampus (Cavanaugh et al., 2011). Although there is discrepancy regarding the exact distribution of TRPV1, it can be appreciated that CNS expression of TRPV1 indicates a broader function of the channel beyond sensory transmission.

Subcellularly, TRPV1 expression has been found in cell bodies and synapses, predominantly on the post-synaptic dendritic spines of neurons and also in synaptic vesicles (Toth et al., 2005; Goswami et al., 2010; Puente et al., 2011; Puente et al., 2014). TRPV1 is also highly expressed in the cell bodies and neurites of both sensory neurons and neurons differentiated by induction with retinoic acid (Puntambekar et al., 2005; El Andaloussi-Lilja et al., 2009). Retinal ganglion cells also exhibit TRPV1 expression in somas and in discrete pockets in axons (Sappington et al., 2009). In addition to neurons, TRPV1 protein has also been found in glia including astrocytes and microglia (Doly et al., 2004; Sappington and Calkins, 2008).

TRPV1 in neuronal function

As a cation channel that preferentially fluxes Ca2+, TRPV1 is also involved in neurite outgrowth and growth cone dynamics. Growth cones are incredibly dynamic and undergo rapid directional changes in response to a chemical gradient. Localized elevations in Ca^{2+} at the growth cone can induce extension and turning by activating CaMKII for attraction and calcineurin for repulsion (Zheng, 2000; Wen et al., 2004). Neurite outgrowth is also believed to be Ca^{2+} dependent. By interacting with microtubule kinase MARK2, CaMKI is able to induce neurite outgrowth under conditions of increased intracellular Ca^{2+} (Uboha et al., 2007). In retinoic acid-induced differentiation of neuroblastoma cells into neurons, TRPV1 is upregulated in both cell bodies and developing neurites (El Andaloussi-Lilja et al., 2009). Activation of

TRPV1 can also induce the formation of varicosities along neurites and retraction of growth cones through microtubule disassembly in a dorsal root ganglia cell line (Goswami et al., 2007).

In addition to growth cones and neurites, TRPV1 also localizes to synapses, and emerging studies indicate the channel can modulate synaptic transmission. In a DRG cell line, TRPV1 colocalizes with synaptic proteins at filopodia tips, where activation results in vesicle fusion. This activity suggests that TRPV1 modulates neurotransmitter release (Goswami et al., 2010). For example, capsaicin can activate a subset of neurons in the solitary tract to induce an inward current and an increase in spontaneous activity to facilitate glutamate release (Doyle et al., 2002; Peters et al., 2010). Furthermore, in DRG and spinal cord co-cultures as well as slices from substantia nigra and hypothalamus, capsaicin increases presynaptic Ca^{2+} to enhance presynaptic activity and glutamate release (Sasamura et al., 1998; Marinelli et al., 2003; Medvedeva et al., 2008). In addition to glutamate release, TRPV1 has also been implicated in dopamine release at the nucleus accumbens and in enhancing the firing of dopaminergic neurons (Marinelli et al., 2005). In the peripheral nervous system, capsaicin-induced Ca^{2+} increases lead to the release of neuropeptides substance P and calcitonin-gene related peptide (Gazzieri et al., 2007; Huang et al., 2008).

TRPV1 in synaptic transmission and plasticity

By altering synaptic Ca^{2+} levels and neurotransmitter release, TRPV1 can modulate synaptic transmission. In spinal cord slices from rats injected with Freund's complete adjuvant, the TRPV1 antagonist, SB-366791 decreases the frequency but not amplitude of spontaneous and miniature excitatory post-synaptic currents (EPSCs) (Lappin et al., 2006). In striatal medium spiny neurons and sensory neurons, TRPV1 enhances the frequency of glutamatergic EPSCs that

were potentiated by PKC-mediated decrease in desensitization (Sikand and Premkumar, 2007; Musella et al., 2009). TRPV1-mediated increases in EPSC frequencies have also been observed in the substantia gelatinosa, periaqueductal gray, medial preoptic nucleus, substantia nigra and locus coeruleus (Marinelli et al., 2003; Karlsson et al., 2005; Xing and Li, 2007; Jiang et al., 2009).

By modulating synaptic transmission, TRPV1 can influence synaptic plasticity and survival. In hippocampal neurons, TRPV1 activation by capsaicin or 12-(S)-HPETE is necessary to cause long-term depression (LTD) by high frequency stimulation. This effect was notably absent in TRPV1-null mice (Gibson et al., 2008). As a result of this finding, the authors propose a model in which glutamate induces post-synaptic release of 12-(S)-HPETE into the synaptic cleft to activate presynaptic TRPV1 channels. Activated TRPV1 subsequently decreases pre-synaptic glutamate release through a Ca^{2+}-dependent pathway (Figure 1.9). Another study found that in the dentate gyrus and in the medium spiny neurons of the nucleus accumbens, post-synaptic activation of TRPV1 by anandamide leads to LTD through Ca^{2+}-mediated endocytosis of AMPA receptors (Chavez et al., 2010; Grueter et al., 2010). In the developing superior colliculus, TRPV1 antagonist iodoresiniferatoxin (I-RTX) blocks the induction of tetanus-induced LTD, while an agonist, resiniferatoxin (RTX), reduces the amplitude of field excitatory postsynaptic potentials (Maione et al., 2009). In TRPV1-null mice, there was a reduction in long-term potentiation (LTP) compared to wild type mice in the CA1 region of the hippocampus (Marsch et al., 2007). These previous studies indicate that TRPV1 facilitates LTD; however, another study found that capsaicin and RTX amplified LTP and suppressed LTD in the CA1 region of the hippocampus (Li et al., 2008).

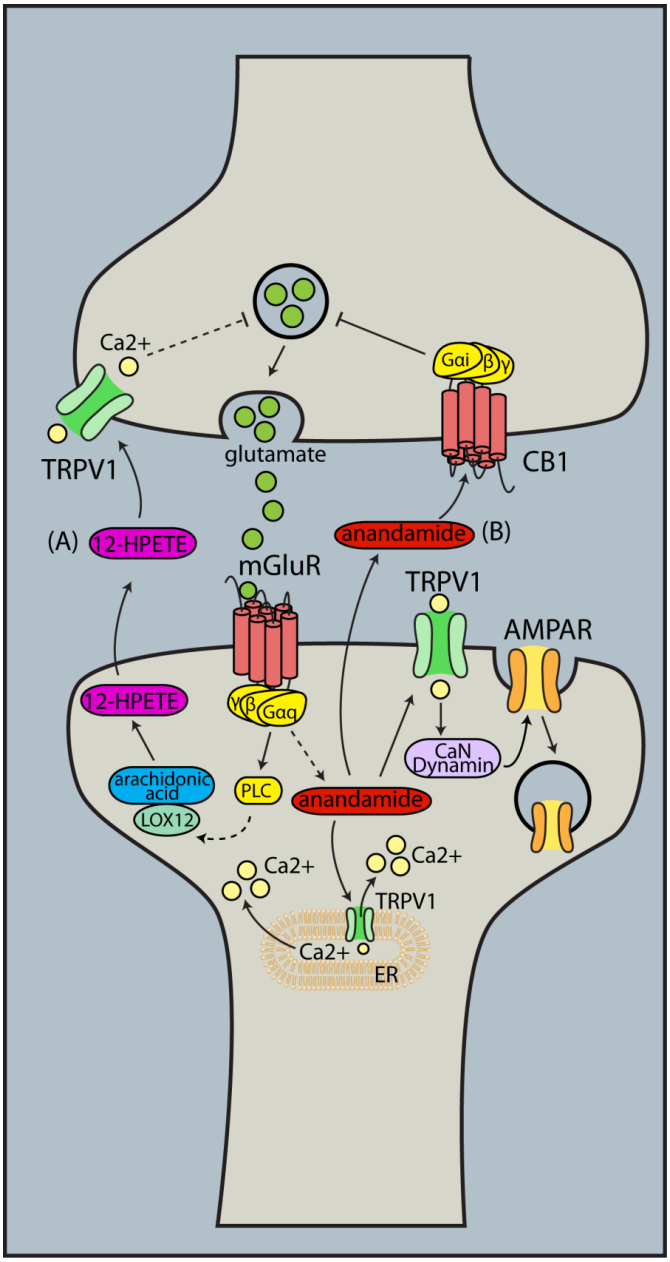

Figure 1.9. TRPV1 contributes to synaptic plasticity. As a calcium cation channel, TRPV1 has been implicated in synaptic plasticity, especially in facilitating long term depression. (A) Activation of mGluR by glutamate triggers the synthesis and release of 12-(S) HPETE into the extracellular milieu. 12-(S)HPETE activates pre-synaptic TRPV1, and through a Ca^{2+}-mediated pathway, glutamate release is blocked. (B) mGluR activation can also lead to production and release of anandamide. Anandamide binds postsynaptic TRPV1 to cause endocytosis of AMPA receptors, or to pre-synaptic cannabinoid receptors to inhibit glutamate release.

Figure from Ho et al. (2012) and used in accordance with the Creative Commons Attribution Noncommercial License.

TRPV1 in neurodegeneration

Associated with increases in intracellular Ca^{2+}, overactivation of TRPV1 can be toxic to cells. Capsaicin leads to elevated levels of intracellular Ca^{2+} and subsequent mitochondrial damage and apoptosis in both cultured cortical microglia and mesencephalic neuronal cultures (Kim et al., 2005; Kim et al., 2006). Capsaicin can also induce apoptosis of cultured retinal ganglion cells in a dose-dependent manner (Sappington et al., 2009). Likewise, intranigral injections of capsaicin lead to death of dopaminergic neurons through Ca^{2+}-mediated mitochondrial damage. This damage can be reduced by coinjections of capsazepine (Kim et al., 2005). Moreover, capsaicin triggers apoptosis in cortical neurons through ERK phosphorylation, activation of caspases and production of reactive oxygen species (Shirakawa et al., 2008). TRPV1 has also been found in gliomas, where its activation by capsaicin leads to cell death through Ca^{2+}-induced mitochondrial damage and p38 activation (Amantini et al., 2007). The association between TRPV1 and cell death is further supported by the ability of I-RTX to block pressure-induced apoptosis of cultured retinal ganglion cells (Sappington et al., 2009).

Because TRPV1 can initiate Ca^{2+}-dependent apoptosis of neuronal and glial cell types, TRPV1 has been implicated in neurodegeneration. Intriguingly, TRPV1 appears to modulate aspects of neurodegeneration, and can even influence neuroprotective mechanisms. In a gerbil model of global transient ischemia, capsaicin and the CB1 receptor antagonist rimonabant can both improve locomotor activity, memory and the number of neurons in the CA1 hippocampus. This effect is diminished with capsazepine pre-treatment, suggesting that TPRV1 is neuroprotective during ischemia (Pegorini et al., 2005; Pegorini et al., 2006). Capsaicin has also exhibited a neuroprotective function in ouabain-mediated excitotoxicity (Veldhuis et al., 2003).

This protection may be mediated by rapid agonist-induced desensitization of TRPV1, as TRPV1 antagonism by capsazepine was also neuroprotective and could reduce brain damage.

TRPV1 has also been implicated in Huntington's disease (HD), a genetic neurodegenerative disorder characterized by cell death in the basal ganglia. HD arises from the expansion of the polyglutamine tract in the huntingtin protein, causing gain-of-function. The symptoms of HD include motor defects as well as cognitive and psychiatric problems. In a 3-nitropropionic acid-induced model of Huntington's disease, the endocannabinoid ligand AM404 is able to reduce hyperkinesia (Lastres-Becker et al., 2003). This phenomenon can be reversed by capsazepine, but not by the CB1 antagonist SR141716A, suggesting that TRPV1 activation can reduce locomotion. Capsaicin itself is antihyperkinetic and can restore dopamine and GABA transmission in the basal ganglia (Lastres-Becker et al., 2003). Furthermore, intraperitoneal injections of capsaicin into rats reduce ambulation and stereotypic behavior and increase inactivity time during open field testing (Di Marzo et al., 2001). These studies indicate that drugs targeting TRPV1 might be beneficial to patients diagnosed with HD. The ability of TRPV1 to modulate behavior related to degenerative disease as well as its ability to influence neuronal survival, indicate that TRPV1 is a particularly interesting channel to study in the context of neurodegenerative diseases.

TRPV1 in glaucomatous neurodegeneration

TRPV1 activity is known to modulate aspects of neurodegeneration, and can influence survival of many different subsets of neurons. Based on previous *in vitro* and *in vivo* studies of the effects of TRPV1 activity on RGC survival, it is likely that TRPV1 influences neurodegenerative progression in glaucoma. Studies using *in vitro* cultures of RGCs indicated

that TRPV1 antagonism reduced pressure-induced RGC death (Sappington et al., 2009). This study suggests that TRPV1 activation may be deleterious during disease progression. However, in an ischemia-reperfusion injury model using extreme intraocular pressure elevation, RGC survival was increased, in part, by TRPV1 activation. In this *in vivo* model, both CB1 and TRPV1 protein levels were upregulated. Treatment with a stable anandamide analogue reduced RGC loss, an effect that was diminished with CB1 and TRPV1 antagonists (Nucci et al., 2007b). This suggests that endocannabinoid binding to CB1 or TRPV1 is neuroprotective, and that TRPV1 activity may be needed for survival mechanisms. Both of these studies indicate the importance of TRPV1 activity in modulation of disease progression; therefore, we made it our focus to understand how TRPV1 modulates RGC degenerative processes in an *in vivo* model of glaucoma.

Specific Aims of Dissertation

The ***objective*** of this project is to examine how the cation channel TRPV1 (transient receptor potential vanilloid-1) modulates degenerative processes in RGCs during glaucoma. Our ***central hypothesis*** is that TRPV1 functions as a stress response protein that counteracts IOP-related RGC dysfunction by enhancing excitatory activity at neuronal synapses. This hypothesis draws on the knowledge that retention of synapses requires maintenance of synaptic activity. Having previously implicated TRPV1 as a modulator of RGC survival *in vitro* (Sappington et al., 2009), we are now prepared to address the function of this channel in a model of glaucomatous degeneration that results in reproducible and sustained elevation of IOP, the microbead occlusion model (Sappington et al., 2010). This modeling will allow us to directly assess TRPV1 function within the context of degenerative influences. To test our central hypothesis, we have developed these specific aims:

Aim 1. Determine influence of TRPV1 on RGC degenerative outcomes. *Our working hypothesis is that TRPV1 helps RGCs survive exposure to IOP-related stress*. We will therefore examine whether TRPV1 knockout exacerbates RGC degenerative outcomes with microbead-induced IOP elevations. We will **(1)** assess RGC dysfunction by examining axonal transport to the superior colliculus, and **(2)** quantify any changes in axon survival in the optic nerve. Within the retina, we will **(3)** quantify RGC soma survival and look for markers of dysfunction, such as accumulation of phosphorylated neurofilaments.

Aim 2. Determine compartmental nature of TRPV1 response in RGCs. *Based on results in DBA/2 mice, our working hypothesis is that TRPV1 responds to elevated IOP by translocating to RGC dendrites*. We will use microbead-induced IOP elevation to **(1)** determine changes in *Trpv1* mRNA over time using whole retina. Within the retina we will **(2)** determine if TRPV1 levels change in dendritic, somatic, and axonal RGC compartments, and we will **(3)** look for increased localization of TRPV1 near synaptic structures.

Aim 3. Establish relevance of TRPV1 in survival of RGC dendrites. *Our working hypothesis is that TRPV1 helps boost activity at RGC dendrites to counter their degenerative retraction*. We will compare RGCs from C57 and *Trpv1*-/- mice to see if TRPV1 affects dendritic morphology in response to microbead-induced IOP elevations.

CHAPTER 2

ABSENCE OF TRPV1 ACCELERATES STRESS-INDUCED AXONOPATHY IN THE OPTIC PROJECTION[2]

Introduction

Onset and progression of neurodegeneration in disease and injury involves integration of both protective and destructive intra- and extracellular signals (Schwartz and Yoles, 2000; Qu et al., 2010). Determining how relevant stressors mediate production of these signals is critical to understand disease progression and identify molecular targets for therapeutic intervention. The transient receptor potential (TRP) family of cation-selective ion channels mediates a variety of neuronal responses to both physiologic and pathogenic stimuli (Lin and Corey, 2005; Ho et al., 2012; Vennekens et al., 2012). The diversity of TRP channels arises in part from the broad spectrum of ligand-based, membrane-bound and biophysical mechanisms through which they are activated. The capsaicin-sensitive vanilloid-1 channel TRPV1 exemplifies this diversity, contributing to tactile sensitivity, diabetic sensory neuropathy, pressure-induced pain, injury monitoring and visceral distension (Mutai and Heller, 2003; Hwang et al., 2004; Rong et al., 2004; Scotland et al., 2004; Jones et al., 2005; Ma et al., 2005; Liedtke, 2006; Plant et al., 2006; Daly et al., 2007; Pingle et al., 2007). Like other TRP channels, TRPV1 activation is associated with a robust Ca^{2+} conductance that supports many Ca^{2+}-dependent intracellular cascades linked to both normal signaling and stress-related processes (Agopyan et al., 2004; Aarts and Tymianski, 2005; Reilly et al., 2005; Kim et al., 2006; Miller, 2006).

[2] Portions of this chapter were published as Ward NJ, Ho KW, Lambert WS, Weitlauf C, Calkins DJ (2014) Absence of transient receptor potential vanilloid-1 accelerates stress-induced axonopathy in the optic projection. J Neurosci 34:3161-3170.

In the optic projection, retinal ganglion cells (RGCs) and their axons express TRPV1 and other TRP channels, which upon activation increase intracellular Ca^{2+} and modulate survival of RGCs challenged by different disease-relevant stressors such as ischemic insult and pressure (Nucci et al., 2007b; Maione et al., 2009; Sappington et al., 2009; Wang et al., 2010; Ryskamp et al., 2011; Leonelli et al., 2013). TRPV1 also contributes to retinal glial cell signaling and may modulate RGC survival indirectly through inflammatory cytokine pathways (Sappington and Calkins, 2008). These results all have bearing on RGC survival in glaucoma, the most common optic neuropathy and leading cause of irreversible blindness worldwide (Quigley and Broman, 2006). Glaucoma involves sensitivity to intraocular pressure (IOP), a potent stressor that induces early RGC axonal dysfunction with subsequent optic nerve degeneration and later loss of RGC bodies in the retina (Calkins, 2012; Howell et al., 2012). We have presented evidence that TRPV1 in RGCs contributes to transducing stress typically associated with glaucoma (Sappington et al., 2009). In this chapter, I tested how genetic knock-out of *Trpv1* (-/-) influences progression of RGC degeneration with exposure to elevated IOP in an inducible model.

Trpv1-/- mice are viable, but demonstrate phenotypic alterations when compared to their C57BL/6 counterparts. These mice exhibit reductions in nociception, thermal hypersensitivity after inflammation, and responses to vanilloid stimulation (Caterina et al., 2000; Davis et al., 2000). *Trpv1*-/- mice additionally demonstrate alterations in neuronal function in the central nervous system (Ho et al., 2012). Several studies have also used *Trpv1*-/- mice to demonstrate the importance of TRPV1 in synaptic plasticity, particularly in long-term potentiation (Marsch et al., 2007; Li et al., 2008) and long-term depression (Gibson et al., 2008; Maione et al., 2009; Chavez et al., 2010; Grueter et al., 2010).

The alterations observed in *Trpv1*-/- mice indicate that TRPV1 influences neuronal physiology and synaptic function. By examining *Trpv1*-/- mice in our inducible model of glaucoma, we are able to examine how this channel functions in response to degenerative stressors *in vivo*. This model elevates IOP by using microbeads to occlude aqueous humor outflow from the anterior segment of the eye. To examine the effect *Trpv1*-/- has on degenerative progression, we compared *Trpv1*-/- and C57BL/6 mice based on their responses to microbead injections. We examined outcome measures that have been previously used with this model, including quantification of deficits in axonal transport, decreased density of axons in the optic nerve, and loss of RGC somas in the retina (Crish et al., 2010; Sappington et al., 2010; Dapper et al., 2013). Accelerated pathology in *Trpv1*-/- microbead animals compared to C57BL/6 controls indicates that TRPV1 contributes to an intrinsic stress response present in RGCs.

Materials and Methods

Animals, tissue harvesting, and tissue preparation

All rodent experiments were conducted following protocols approved by the Vanderbilt University Medical Center Institutional Animal Care and Use Committee. C57BL/6 (C57) mice were obtained from Charles River (Wilmington, MA) and B6.129X1-*Trpv1*^{tm1Jul}/J (*Trpv1*-/-) mice were obtained from Jackson Laboratories (Bar Harbor, ME). All mice were maintained in a 12-h light/dark cycle with standard rodent chow available *ad libitum* as previously described (Crish et al., 2010).

Trpv1-/- mouse

For all *Trpv1*-/- mouse experiments, B6.129X1-*Trpv1*^{tm1Jul}/J mice were obtained from Jackson Laboratories (Bar Harbor, ME). This knockout is a germ-line mutation that was created by deletion of an exon encoding part of the fifth and all of the sixth transmembrane domains of the TRPV1 channel, including the pore-loop region between the two. This *Trpv1*-/- strain is maintained at Jackson and was created by Julius and colleagues using methods described elsewhere (Caterina et al., 2000). Briefly, mouse-specific *Trpv1* primers were used to produce a 129/SVJ mouse genomic DNA clone of part of the *Trpv1* gene. A 10-kb subfragment of this clone was produced by *Hin*dIII digestion and was used as a targeting vector for transfection of JM1 embryonic stem (ES) cells (Qiu et al., 1995).

ES cells were electroporated by Julius and colleagues with the targeting vector DNA, and screened via ganciclovir/geneticin double selection for homologous recombination at the *Trpv1* locus (Caterina et al., 2000). One of these clones was used for injection of C57 mouse blastocysts, which were subsequently implanted into pseudopregnant Black/Swiss female mice.

Male offspring with chimeric coats were mated with C57 females, and the resulting *Trpv1*+/- males were backcrossed to C57 females for multiple (≥4) generations. *Trpv1*+/- offspring were then intercrossed to generate *Trpv1*-/- mice on a C57 genetic background.

Southern blot analysis of genomic DNA from *Trpv1*+/+, *Trpv1*+/-, *Trpv1*-/- mice confirmed proper targeting and disruption of the *Trpv1* gene (Caterina et al., 2000). Northern blot analysis of *Trpv1* mRNA expression in dorsal root ganglia (DRG) indicated the presence of *Trpv1* transcript in *Trpv1*+/+ and *Trpv1*+/-, but not *Trpv1*-/- mice (Caterina et al., 2000). Additionally, no protein gene product is detected in DRG (JAX® Mice Database; http://jaxmice.jax.org/strain/003770.html). Loss of TRPV1 immunoreactivity in *Trpv1*-/- mice was verified in the supraoptic and paraventricular nuclei (Sharif Naeini et al., 2006) using a C-terminal antibody to TRPV1 (Neuromics), and in the lumbar spinal cord using antisera (from David Julius, UCSF) raised against the C-terminus of TRPV1 (Tominaga et al., 1998; Caterina et al., 2000). Specificity of the mouse-specific C-terminal TRPV1 antibody from Neuromics was demonstrated in both Western blots and immunolabeled tissue from mouse retina (Sappington et al., 2009). Western blots demonstrated full-length TRPV1 at 90 to 113 kDa depending on glycosylation state, and 198 kDa for TRPV1 dimers (Sappington et al., 2009).

Trpv1-/- and C57 mouse genotyping

Trpv1-/- mice were created on a C57BL/6 (C57) background, so C57 mice are used as controls (Caterina et al., 2000; Ciura and Bourque, 2006; Treesukosol et al., 2007). All mice used in *Trpv1*-/- experiments were genotyped to verify *Trpv1* gene knockout. 3mm x 3mm ear clippings were collected from all mice used in *Trpv1*-/- experiments, and tissue was placed in microcentrifuge tubes on dry ice. DNA was extracted using the DNeasy Blood and Tissue Kit

(Qiagen, MD) following the Bench Protocol: Animal Tissues (Spin Column) protocol. Concentration of DNA was determined using a NanoDrop 8000 (Thermo Scientific, Wilmington, DE) and DNA was stored at 4ºC prior to running PCR reactions.

Each PCR reaction was 25 µl in volume and contained the following: 2.5 µl 10X PCR Buffer (Invitrogen), 0.75 µl 50 mM $MgCl_2$ (Invitrogen), 0.5 µl 10 mM dNTP mix (Promega, Madison, WI), 0.5 µl of each primer (10 µM working stocks; Integrated DNA Technologies), 0.1µl Platinum Taq polymerase (Invitrogen), 40 ng of extracted template DNA, and the correct amount of DNase/RNAse free water to increase the total reaction volume up to 25 µl. I determined the volume of DNA to add by dividing 40 ng by the sample's concentration as determined by the NanoDrop. For detection of *Trpv1* gene truncation in *Trpv1*-/- mice, two forward primers were used to produce wild-type (Jackson Laboratory, oIMR1561; 5' CCT GCT CAA CAT GCT CAT TG 3') and knockout (Jackson Laboratory, oIMR0297; 5' CAC GAG ACT AGT GAG ACG TG 3') gene products, both of which used a shared reverse primer (Jackson Laboratory, oIMR1562; 5' TCC TCA TGC ACT TCA GGA AA 3'). With this primer combination, wild-type animals yield a product size of 984 bp and *Trpv1*-/- animals yield a product size of 600 bp. Positive control detection of *Gapdh* gene products used forward (5' TTG GCA TTG TGG AAG GGC TC 3') and reverse (5' TGC TGT TGA AGT CGC AGG AGA C 3') primers to detect a 363 bp product. All tubes were lightly centrifuged prior to running PCR reactions.

PCR reactions were carried out using a Mastercycler gradient thermocycler (Eppendorf AG, Hamburg, Germany) using the following cycling steps:

Step 1: Denaturing: 94ºC for 3 minutes

Step 2: Denaturing: 94ºC for 30 seconds

Step 3: Annealing: 65ºC for 1 minute

Step 4: Extension: 72ºC for 1 minute

Step 5: Repeat steps 2-4 40 times

Step 6: Extension: 72ºC for 2 minutes

Step 7: Finish, holding reactions at 4ºC

PCR products from these cycling steps were used as template DNA for a second round of PCR using the same steps. A second round of PCR was necessary because the first round did not yield enough product to detect bands on an agarose gel. These reactions all used 2.7 µl of first round PCR product, and the reactions were set up the same, only adjusting the amount of DNase/RNAse free water added to produce a final volume of 25 µl per reaction.

Second round PCR products and a 100 bp DNA ladder (New England BioLabs) were separately mixed with 6X loading dye (Fermentas) and separated at 100 V for 45 minutes on a 1.5% agarose gel (1.5 g agarose in 100 ml 1X TAE) stained with ethidium bromide. Gels were digitally imaged on a Gel Doc XR+ (Bio-Rad, Hercules, CA) gel reader to confirm successful PCR reactions (*Gapdh* positive control) and to distinguish C57 and *Trpv1*-/- mice (984 bp and 600 bp reaction products, respectively).

Induction of ocular hypertension by microbead occlusion

Intraocular pressure (IOP) was acutely elevated in 4-month-old C57 and *Trpv1*-/- mice by microbead occlusion of aqueous flow as described previously (Sappington et al., 2010). Prior to injections, mice were anesthetized with isoflurane (Minrad Inc., Bethlehem, PA) and efficacy of anesthesia was evaluated by gentle pinching of the tail and paw. The eye was washed with a sterile saline solution and received application of 1% tropicamide ophthalmic drops (2-3 drops)

to dilate the iris. Local anesthetic drops containing 0.5% proparacaine were also applied to the eye. This solution is used to maintain eye moisture and provide pre- and post-operative analgesia. Drops of antibiotic tobramycin ophthalmic solution (0.3%, Akorn) were also applied prior to the injection to counter infection.

For microbead injection into the anterior chamber, a standard microinjection setup (World Precision Instruments) consisting of a microsyringe pump and micromanipulator was used. This setup included a borosilicate microneedle (pulled to a final diameter of 100µm) attached to a syringe filled with mineral oil. The needle tip was sterilized with 100% EtOH before drawing the solution to be injected into the microneedle. We unilaterally injected 1.0µl of PBS containing inert polystyrene microbeads (15µm diameter; 1 x 10^6 microbeads/ml solution; Life Technologies, Carlsbad, CA) into the anterior chamber of the eye (Figure 2.1). We injected the contralateral eye with an equivalent volume of PBS containing no microbeads for an internal control. Following the procedure, additional numbing drops containing 0.5% proparacaine were applied to both eyes.

IOP was measured in anesthetized (2.5% isoflurane) mice at least twice weekly using TonoPen XL (Medtronic Solan, Jacksonville, FL) rebound tonometry as previously described (Inman et al., 2006; Sappington et al., 2010). An IOP measurement was determined as the mean of at least 20 readings. To avoid corneal irritation, hydrating eye drops were administered to each eye following IOP measurements. IOPs were measured for 2 days prior to microbead procedures to calculate an average baseline value (day 0) for each eye of every animal.

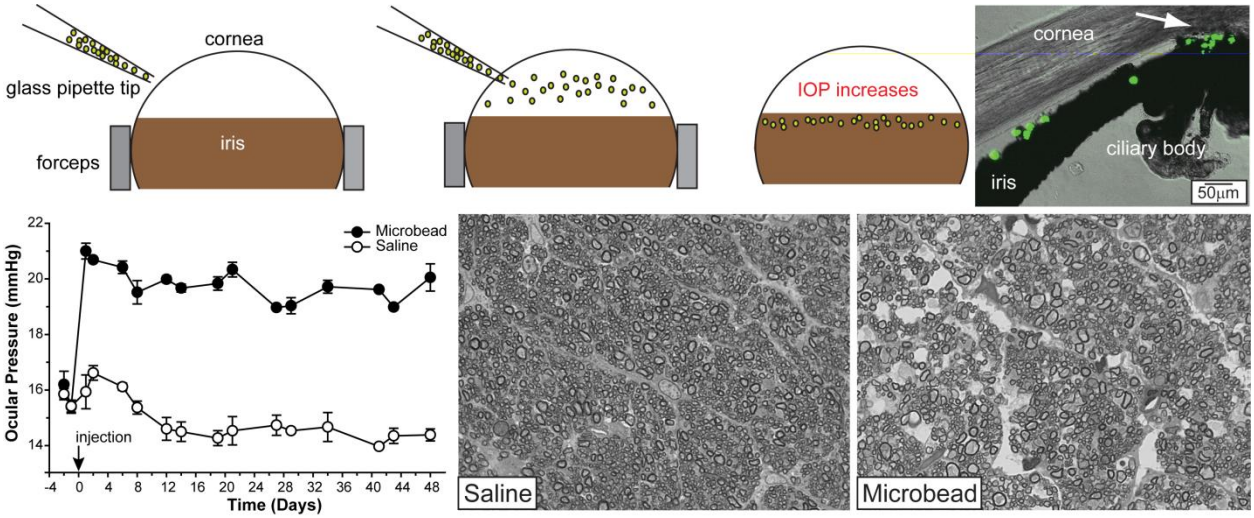

Figure 2.1. Elevation of intraocular pressure by microbead occlusion of aqueous outflow. Occluding aqueous outflow in rodents is an *in vivo* method for modeling pressure-related glaucomatous stressors. Polystyrene microbeads are injected into the anterior chamber of the eye using a glass micropipette (top left). Beads accumulate and settle at the irido-corneal angle (top right; arrow), impeding outflow of aqueous humor through drainage structures. Decreased outflow of aqueous humor results in an increased intraocular pressure in microbead-injected eyes when compared to eyes injected with an equivalent volume of saline (bottom left). Elevated pressure causes pathology seen as early as 3 weeks, such as RGC axon loss (bottom right).

Figure modified from Sappington et al. (2010), and used in accordance with fair use standards as specified by the publisher.

Anterograde tracing of retinocollicular and retinogeniculate tracts

To establish an example of healthy anterograde transport from the retina to LGN and SC, we conducted tract tracing in a C57 mouse not previously injected with microbeads. Forty-eight hours prior to sacrifice, the mouse was anesthetized with 2.5% isoflurane before injections of tracer. Using a Hamilton syringe and 33 gauge, 0.375-inch needle, we injected 0.5 mg cholera toxin subunit B (CTB; Molecular Probes, CA) in 1 µl of sterile water into each eye (Figure 2.2). To highlight eye-specific projection systems, the injected CTB was conjugated either to Alexa Fluor-488 (green; left eye) or Alexa Fluor-594 (red; right eye). In addition to this naïve mouse, we also conducted tracing in microbead-injected animals. These mice were anesthetized and

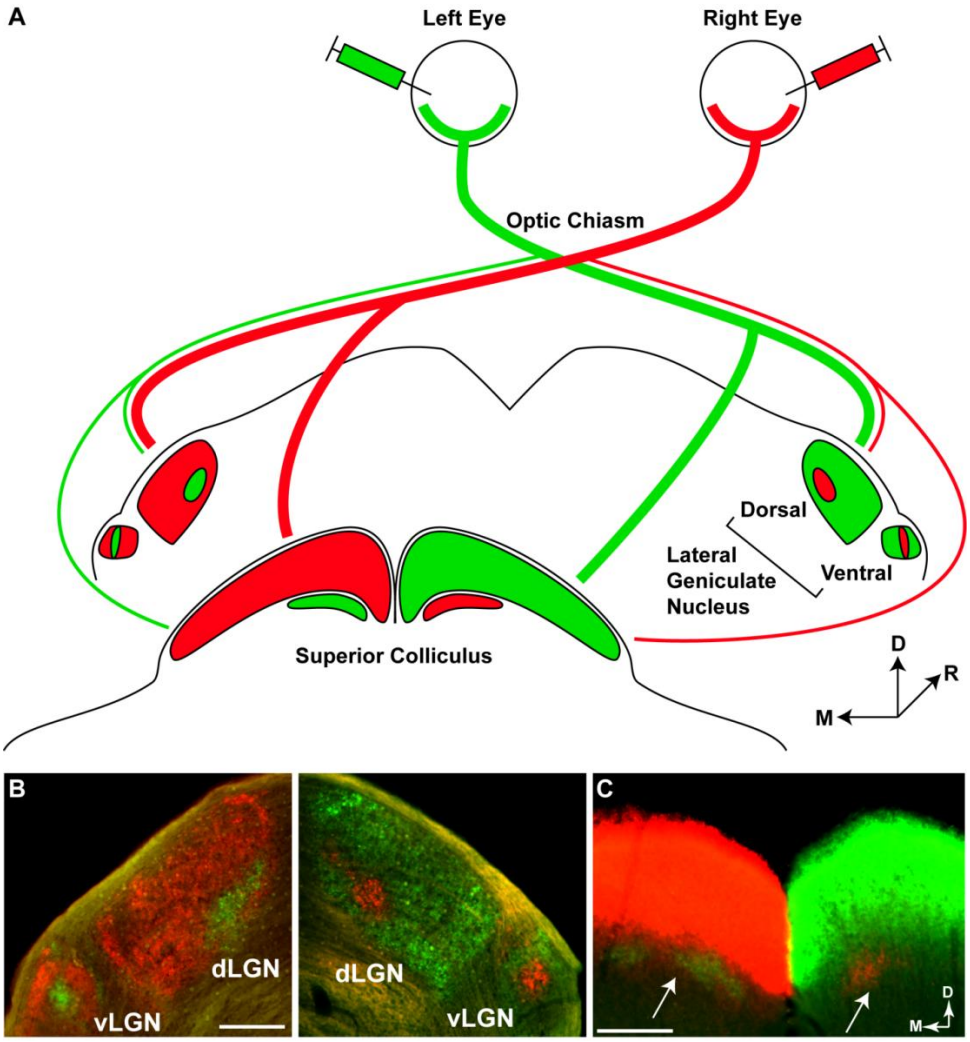

Figure 2.2. Anterograde tracing of the mouse retinogeniculate and retinocollicular tracts. ***A,*** Schematic representing eye-specific ipsilateral and contralateral RGC axon projections from the retina to the dorsal and ventral lateral geniculate nuclei (d/vLGN) and superior colliculi (SC). Fluorescently-labeled CTB tracers (red and green fluorophores) injected into mouse eyes are anterogradely transported to both thalamic (d/vLGN) and midbrain (SC) structures. At the optic chiasm, RGC axons either cross the midline or project to structures on the same side as their eye of origin. Rodents exhibit extensive decussation at the optic chiasm, with only a small percent of axons projecting to ipsilateral brain structures. Contralateral projection systems are represented by thick lines while ipsilateral projection systems are represented by thin lines. ***B,*** dLGN and vLGN from the same C57 brain show dominant contralateral with smaller ipsilateral projections. ***C,*** Coronal section shows both SC near the rostral pole following bilateral intravitreal injection of cholera toxin B (CTB) into left (green CTB) and right (red CTB) eyes of C57 mouse. Fluorescent signal for dominant contralateral projection is over-exposed purposely to reveal sparser ipsilateral projection (arrows) for each eye. Medial (M), rostral (R), and dorsal (D) orientations indicated. Scale = 200 µm in all images.

injected with CTB in the same manner as the naïve animal, with the only difference being that these animals were given bilateral injections of Alexa Fluor-488.

Animals were transcardially perfused with phosphate buffered saline (PBS) followed by 4% paraformaldehyde (PFA) in PBS and tissue was harvested. Brains were cryoprotected overnight in 30% sucrose/PBS and 50 µm coronal sections were taken through the midbrain and thalamus on a freezing sliding microtome. Alternating sections of brain containing superior colliculus and lateral geniculate nucleus were photographed using a Nikon Ti Eclipse microscope (Nikon Instruments Inc., Melville, NY) and intensity of CTB label in collicular sections was quantified using ImagePro (Media Cybernetics, Bethesda, MD) as previously described (Crish et al., 2010; Lambert et al., 2011). Fluorescent signal was normalized to background and intensity calculations from alternating sections were combined to reconstruct CTB signal intensity across a retinotopic map of the colliculus (Figure 2.3). We determined percentage of intact transport for each map, defined as percent of map area with intensity ≥70% maximum CTB signal.

Preparation of optic nerves

Following transcardial perfusion with 4% PFA, optic nerves were removed from C57 and *Trpv1*-/- mice. A 3 mm section of optic nerve proximal to the globe was isolated, post-fixed for 1 hour in 4% PFA, and prepared for embedding and semi-thin cross-sectioning. Optic nerves were placed in 12-well culture plates containing 0.1 M cacodylate buffer (CB) in a fume hood. Using a transfer pipette, nerves were moved from CB to 2% osmium for 45 minutes of incubation on ice. Nerves were then moved from 2% osmium to a well of fresh CB, and then immediately into another well of fresh CB. Nerves were then moved to a new culture plate of CB to remove the nerves from the fume hood. All containers and transfer pipettes that came in contact with

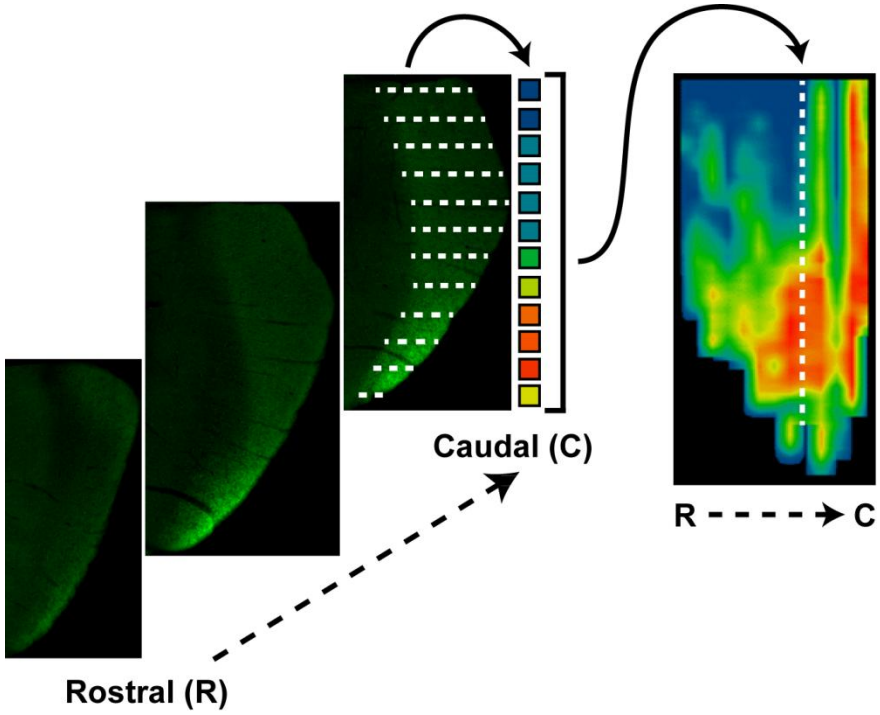

Figure 2.3. Creating a retinotopic map of fluorescent CTB transported to the SC. Serial sections of SC (left) with fluorescent CTB (green) transported along RGC axons projecting from the retina. Serial sections are oriented with the midline at top and organized in a rostral to caudal fashion. Average pixel intensity is measured across each row of pixels (horizontal dotted lines) and is represented colorimetrically (bracketed boxes; "warm" colors represent intact transport while "cool" colors represent transport deficits). Column of pixels generated for each section are lined up rostral to caudal to reconstruct a retinotopic heat map of transport across the entire SC.

osmium were kept in a fume hood and disposed of properly. The nerves were washed 3 times for 5 minutes each in CB at room temperature.

Nerves were dehydrated using a series of EtOH solutions of increasing percentage. Nerves were incubated with shaking for 30 minutes in each solution: 50%, 70%, 95%, 100% EtOH. Nerves were moved to a second batch of 100% EtOH to incubate for 15 minutes with shaking. Nerves were moved to a glass scintillation vial containing a 1:1 mixture of propylene oxide/EtOH. This vial was sealed and nerves were incubated for 30 minutes while shaking. Using a transfer pipetted fitted with a 20 µl-200 µl pipette tip, the 1:1 mixture of propylene oxide/EtOH was carefully removed and replaced with 100% propylene oxide. Nerves were

incubated in this solution for 1 hour with shaking. This solution was removed and replaced with a 1:1 mixture of propylene oxide/epon. Nerves were incubated in this solution overnight at 4ºC with shaking. This solution was removed and replaced with fresh 1:1 propylene oxide/epon. Nerves were incubated for at least 4 hours at room temperature with shaking. Nerves were removed from glass vials and transferred to a new culture plate containing 100% epon. These nerves were incubated overnight at room temperature in a vacuum containing Drierite dessicant. All propylene oxide solutions were discarded properly and all vials that came in contact with the solutions were stored in the fume hood until all solution was evaporated.

Nerves were placed in new 100% solutions of epon to incubate for 6 hours at room temperature in a vacuum. Nerves then were moved to new 100% epon to incubate overnight at room temperature in a vacuum. This 6-hour and overnight incubation was repeated once more, with the last incubation occurring in a flat mold in a vacuum. This flat mold was then placed within a 60ºC oven for 3 days in a tip box containing Drierite. Molds were trimmed with a razor blade such that the nerve was located in the center of a double pyramid shape of dried epon. Using an ultramicrotome with a diamond knife, 1-2 µm cross-sections of optic nerve were cut and collected on a slide using distilled water. Sections were dried onto the slide in a 60ºC oven until all water was evaporated, and were then left to cool to room temperature.

Slides were immersed for 28 minutes in 1% paraphenylenediamine (PPD) in a 1:1 mixture of methanol and 2-propanol. Slides were then washed in twice in fresh mixtures of 1:1 methanol/2-propanol with no PPD for 1 to 2 minutes each followed by a 1-minute wash in 100% EtOH. Sections were air dried before slides were placed in a humidified box with 1% Toluidine Blue placed drop-wise onto the slide until the sections were completely covered. The box was placed in a 60ºC oven for 20 minutes. Slides were rinsed with ddH_2O and allowed to air dry.

Slides were cover slipped using Permount mounting media and allowed to dry overnight prior to imaging.

Quantification of RGC axons

Photomicrographs of C57 and *Trpv1*-/- optic nerve cross-sections were acquired and assembled as a montage on a Nikon Ti Eclipse microscope (Nikon Instruments Inc., Melville, NY) using 100x oil-immersion and differential interference contrast optics. Images were contrast- and edge-enhanced using custom routines programmed for Image Pro (Media Cybernetics, Bethesda, MD). These routines screen out glia and identify myelin sheaths in order to detect and count RGC axons in the optic nerve (Figure 2.4). Using random sampling, these routines calculate average axon density for an optic nerve section. This density can be multiplied by nerve area to estimate the total number of axons in the nerve. Manual counts of a subset of these nerves were conducted to create a correction factor to adjust for undercounting by the routines.

Immunohistochemistry in retinal wholemount tissue

Retinal wholemount tissue was retrieved by dissecting perfused C57 and *Trpv1*-/- mouse eyes under a dissecting scope. Prior to dissection, the superior pole of the eye was identified using vasculature surrounding the optic nerve as a landmark. Using microdissection scissors, the eye was cut in a circular fashion above the ora serrata, and #5 forceps were used to separate the retina from the ora serrata. The retina was removed from the optic disc with a cut using microdissection scissors. To flatten the retina in preparation for imaging, four relief cuts were

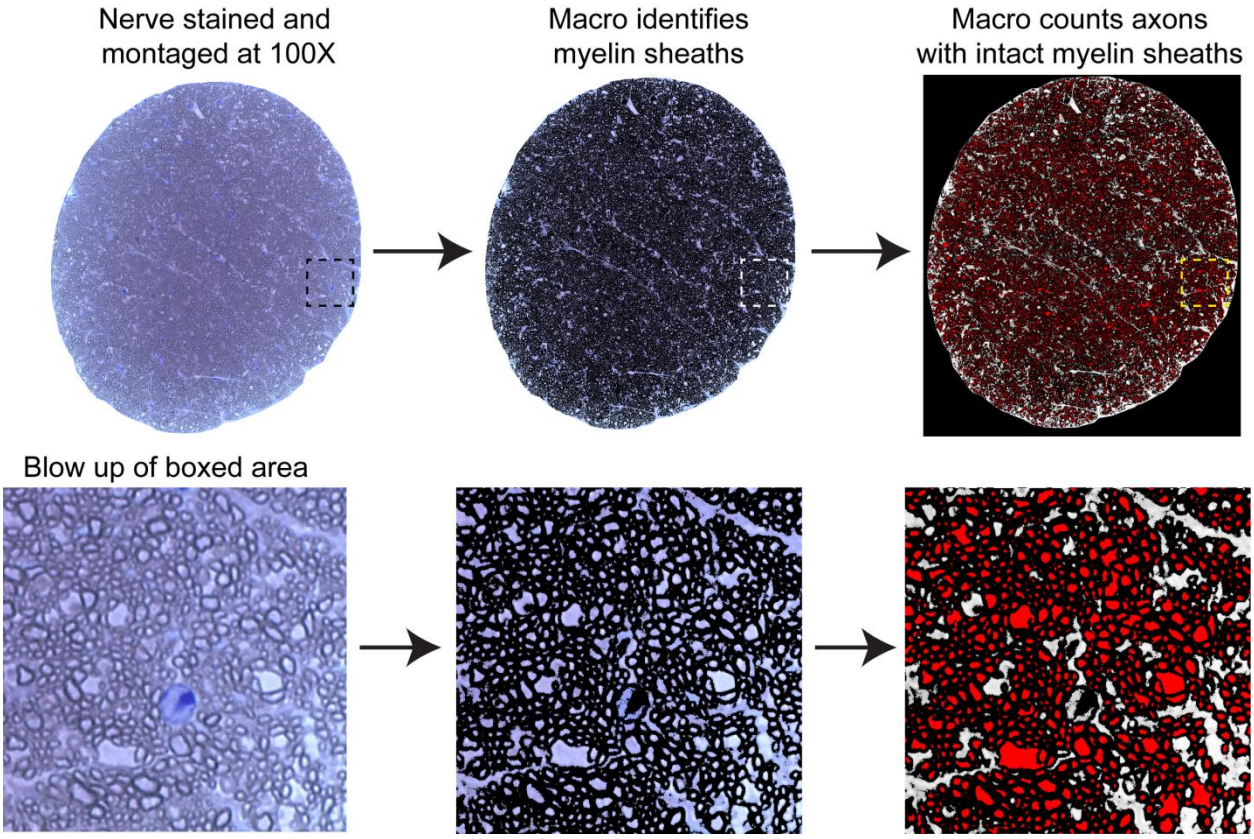

Figure 2.4. Quantification of axons in optic nerve sections. Sections of optic nerve are stained with p-phenylenediamine and imaged as a montage at 100X (left). Axons with intact myelin sheaths are identified and outlined by a computer program (middle) and counted (red; right).

made to create a cross shape in which each of the arms represented a retinal pole (i.e., superior, nasal, inferior, temporal; Lambert et al., 2011). A small incision was placed in the superior arm to distinguish it and additionally aid in identification of the other poles. To improve antibody penetration and imaging of the tissue, vitreous was manually removed using forceps.

Whole retinal tissue was immersed in increasing sucrose/PBS solutions ranging from 10% to 30%. Tissue was moved to higher concentrations of sucrose solution when tissue sank to the bottom of the solution. Once in 30% sucrose, retinas were incubated overnight at 4ºC. Following overnight incubation, the retinas were placed on glass microscope slides. These slides were placed on dry ice to allow the tissue to freeze through completely. The retinas were freeze-

thawed in this manner a total of three times. Retinas were washed three times in PBS for 5 minutes each. Tissue was blocked in a solution of 5% normal donkey serum plus 0.1% Triton-X 100 diluted in PBS. Retinas were incubated in blocking solution overnight at 4ºC.

Retinas were immunolabeled for phosphorylated neurofilaments used to identify RGCs and their axons. Tissue was placed in a primary antibody solution of SMI31 antibody (1:1000; Sternberger Monoclonal Incorporated, Baltimore, MD) against phosphorylated neurofilaments diluted in 3% normal donkey serum plus 0.1% Triton-X 100 in PBS. Retinas were incubated in primary antibody solution for 4 days at 4ºC on a shaker. Retinas were washed 3 times in PBS for 10 minutes each at room temperature. Tissue was then placed in a solution of donkey anti-mouse 488 secondary antibody (1:200, Jackson), 1% normal donkey serum, and 0.1% Triton-X 100 diluted in PBS. Tubes containing retinas were covered with foil and incubated overnight at 4ºC with shaking. Retinas were then washed three times in PBS for 10 minutes each. Each retina was mounted RGC side up on a slide under a dissecting microscope using aqueous mounting media (Fluoro-mount). Slides were coverslipped and allowed to dry overnight in the dark at room temperature and were then sealed along the coverslip edges using Cytoseal.

RGC soma quantification

To identify RGCs, whole-mounted retinas were stained for phosphorylated neurofilaments (SMI31 antibody; Sternberger Monoclonal Incorporated, Baltimore, MD), which identify RGC cell bodies and axons. To assess RGC survival in the retina, 0.101 mm^2 were captured of C57 and *Trpv1*-/- retinas on an Olympus FV-1000 inverted confocal microscope. For each retina, images were captured along the midline of each retinal quadrant at 0.75, 1.5, 2.25,

and 3.0 mm from the optic disc following previously published methods (Lambert et al., 2011). SMI31-positive RGCs were counted for each image to calculate RGC density as cells per mm^2.

Mapping of CTB transport onto retinal quadrant and eccentricity coordinates

To determine whether transport deficits in the SC corresponded with areas of RGC soma loss in the retina, an overlay of SC transport maps onto coordinates of the SC retinotopic map was conducted as detailed previously (Lambert et al., 2011). These retinotopic maps follow the conventions of papers documenting electrophysiological characterization of the topography of visual projections to the SC (Siminoff et al., 1966; Drager and Hubel, 1976). Each topographic map indicates areas of SC receiving input from specific quadrants (superior, nasal, inferior, temporal) of the retina.

Statistical methods

Group averages were calculated and compared in SigmaPlot (version 11.1, SYSTAT) using two-sided *t*-tests for all data passing Shapiro-Wilk normality tests. For data that did not pass Shapiro-Wilk normality, non-parametric Mann-Whitney Rank Sum tests were used. Error as reported in text and on bar graphs represents mean ± SEM.

Results

Trpv1-/- mice exhibit a truncated *Trpv1* gene

To confirm that all mice used for *Trpv1*-/- studies were of the correct genotype, I conducted PCR to verify gene ablation in *Trpv1*-/- mice. Agarose gels indicate a shift in PCR products produced from the same set of primers (Figure 2.5). PCR products from C57 mice appeared as a band at the expected size of 984 bp. Products from *Trpv1*-/- mice appeared as a band at the expected size of 600 bp.

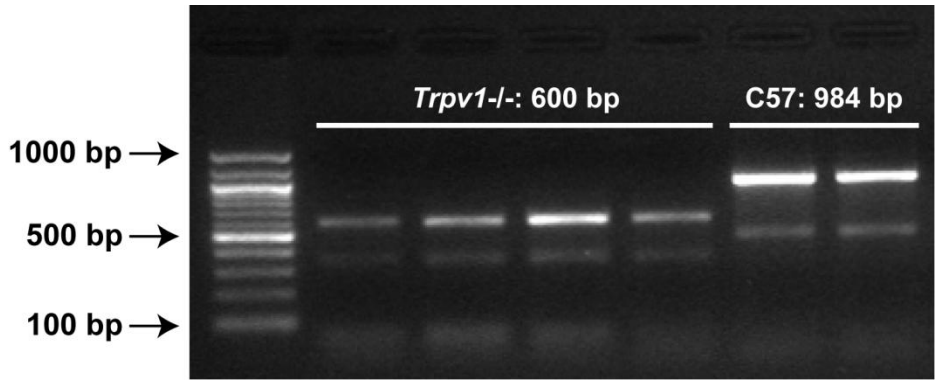

Figure 2.5. Confirmation of knockout in *Trpv1*-/- mice. Agarose gel showing PCR products from genotyping of several C57 and *Trpv1*-/- mice used in experiments. PCR reactions produced a 984 bp product for all C57 mice and a 600 bp product for all *Trpv1*-/- mice as expected. Correct genotype was verified for all animals involved in *Trpv1*-/- experiments.

Trpv1-/- accelerates axonopathy in the optic projection

We elevated intraocular pressure (IOP) in C57 and *Trpv1*-/- mice by microbead occlusion of aqueous fluid in the anterior chamber (Sappington et al., 2010; Chen et al., 2011). A single unilateral microbead injection elevated IOP by ~33% for just over 5 weeks (36 days), while IOP from saline-injected fellow eyes remained near baseline (~15 mmHg) for the duration of the experiment (Figure 2.6A). This elevation was significant in both C57 and *Trpv1*-/- mice ($p <$

0.001). *Trpv1*-/- had no significant effect on IOP for either control or experimental eyes compared to C57 mice ($p \geq 0.842$; Figure 2.6B).

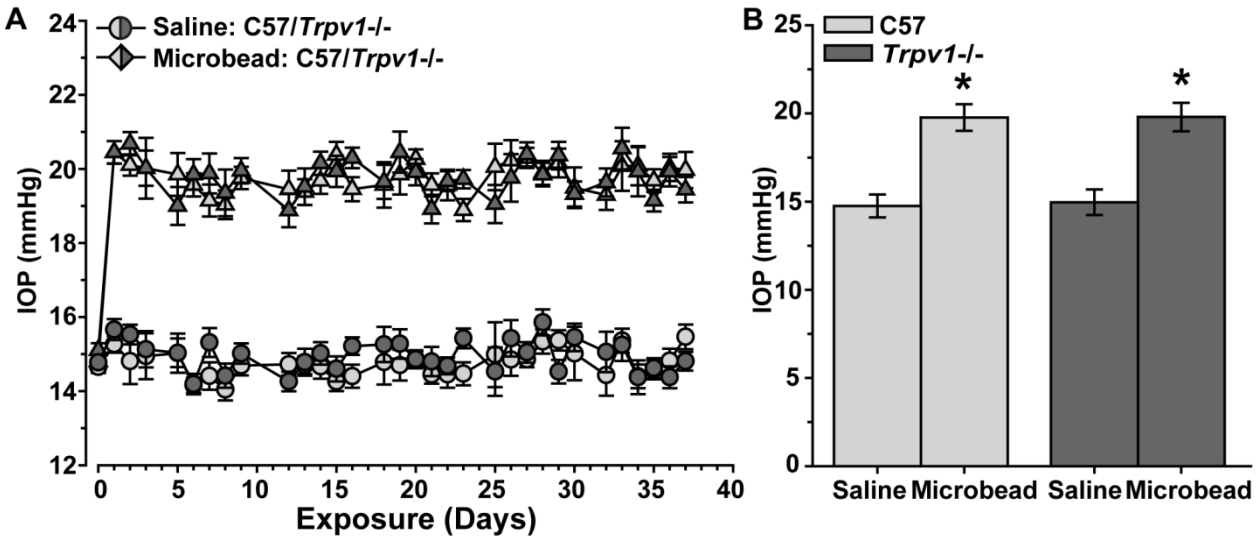

Figure 2.6. Microbead-induced elevations in mouse intraocular pressure. ***A,*** Daily mean intraocular pressure in mmHg (IOP; $n \geq 20$ measurements each day, mean ± SEM) for a 37 day period in cohorts of C57 vs. *Trpv1*-/- mice ($n = 10$ each) before (day 0) and following (days ≥ 1) a single unilateral injection of polystyrene microbeads (1.0 µl) into the anterior chamber. The fellow eye in each animal received an equivalent volume saline injection as internal control. ***B,*** Microbead eyes exhibited a significant increase in IOP following injection (mean ± SEM for days ≥ 1) compared to saline eyes in both C57 (19.77 ± 0.76 vs. 14.75 ± 0.65 mmHg) and *Trpv1*-/- (19.79 ± 0.80 vs. 14.96 ± 0.72 mmHg) mice (* $p < 0.001$). Between the two cohorts, IOP was similar for both saline-injected ($p = 0.842$) and microbead-injected ($p = 0.980$) eyes.

In naïve C57 mice, RGC axonal transport of cholera toxin B (CTB) injected intravitreally in both eyes (Figure 2.2A) reveals the dominant contralateral and lesser ipsilateral projections to the lateral geniculate nucleus (LGN; Figure 2.2B) and more distal superior colliculus (SC; Figure 2.2C). Following the period of IOP elevation, the LGN projection (Figure 2.7A) from saline-injected eyes in C57 and *Trpv1*-/- mice demonstrated intact CTB transport (Figure 2.7B), while the projection from the microbead-injected eyes demonstrated deficits in transport (Figure 2.7C). These deficits in CTB transport to the LGN in *Trpv1*-/- mice appeared more dramatic than those

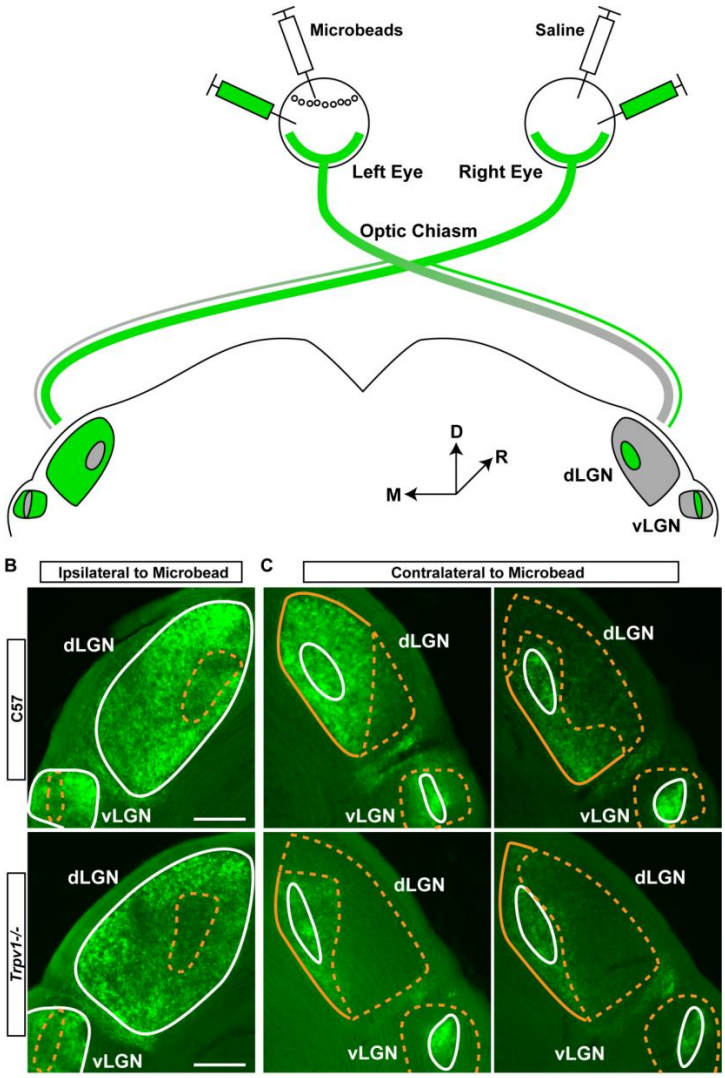

Figure 2.7. *Trpv1*-/- exacerbates microbead-induced transport deficits to the LGN. ***A***, Schematic illustrating unilateral elevation of IOP for 36 days by microbead occlusion followed by bilateral CTB tracing 48 hours before sacrifice. Deficits in transport (indicated by gray) are expected in large contralateral projections and small ipsilateral projections to both the dLGN and vLGN. Medial (M), dorsal (D), and rostral (R) orientations indicated. ***B,C***, Coronal sections through LGN from C57 (top row) and *Trpv1*-/- mice (bottom row) following bilateral intravitreal injections of CTB (green). In LGN ipsilateral to microbead eye ***B***, CTB signal from saline-injected eye remains intact (solid white outline), while signal from microbead-injected eye shows deficits embedded in both dLGN and vLGN (dashed yellow outline). Deficits appear worse in *Trpv1*-/- LGN. In LGNs contralateral to microbead eye ***C***, CTB signal from saline-injected eye is again intact (solid white outline). In the dLGN, CTB signal from microbead-injected eyes (yellow outlines) shows a range in deficits (dashed yellow). Once again, deficits appear worse in *Trpv1*-/- dLGN. The *Trpv1*-/- vLGN also appears to have less CTB signal. Scale = 200 µm in all images.

seen in C57. Similarly, while the SC projection (Figure 2.8A) from microbead-injected eyes in C57 and *Trpv1*-/- mice demonstrated transport deficits, CTB transport from the saline eye remained intact (Figure 2.8B).

Next we compared the spatial progression of transport deficits in the SC after microbead injection, since this distal-most target in the RGC projection demonstrates IOP-related transport deficits earliest (Crish et al., 2010). Following the period of microbead-induced IOP elevation, the SC of C57 mice demonstrated a partially intact retinotopic representation of axonal transport of CTB injected intravitreally (Figure 2.9A). Depletion of transport progressed in sectors extending from the peripheral edge of the map towards the representation of the optic disc, consistent with our previous studies using this model (Crish et al., 2010). While anterograde transport from saline-injected eyes was intact for both cohorts, the SC from microbead-injected eyes of *Trpv1*-/- mice often demonstrated a nearly complete retinotopic loss (Figure 2.9B). When quantified, each cohort exhibited a range in the magnitude of transport deficits with elevated IOP, as measured by the fraction of intact retinotopic map (Figure 2.10A). However, the range for *Trpv1*-/- mice was entirely below 50%, while most C57 SC were above this point (Figure 2.10A). Accordingly, deficits in *Trpv1*-/- SC were twice as severe as in C57, with average intact transport of about 25% of the retinotopic map compared to just over 50% for C57 (Figure 2.10B).

In models of glaucoma, outright degeneration of RGC axons in the optic nerve is subsequent to dysfunction in anterograde axonal transport to central structures like the SC and LGN (Calkins, 2012). We found that with elevated IOP, cross-sections of C57 optic nerve demonstrated early signs of pathological progression such as degenerating axon profiles and diminished axon density (Figure 2.11A). Nerves from *Trpv1*-/- mice exhibited accelerated

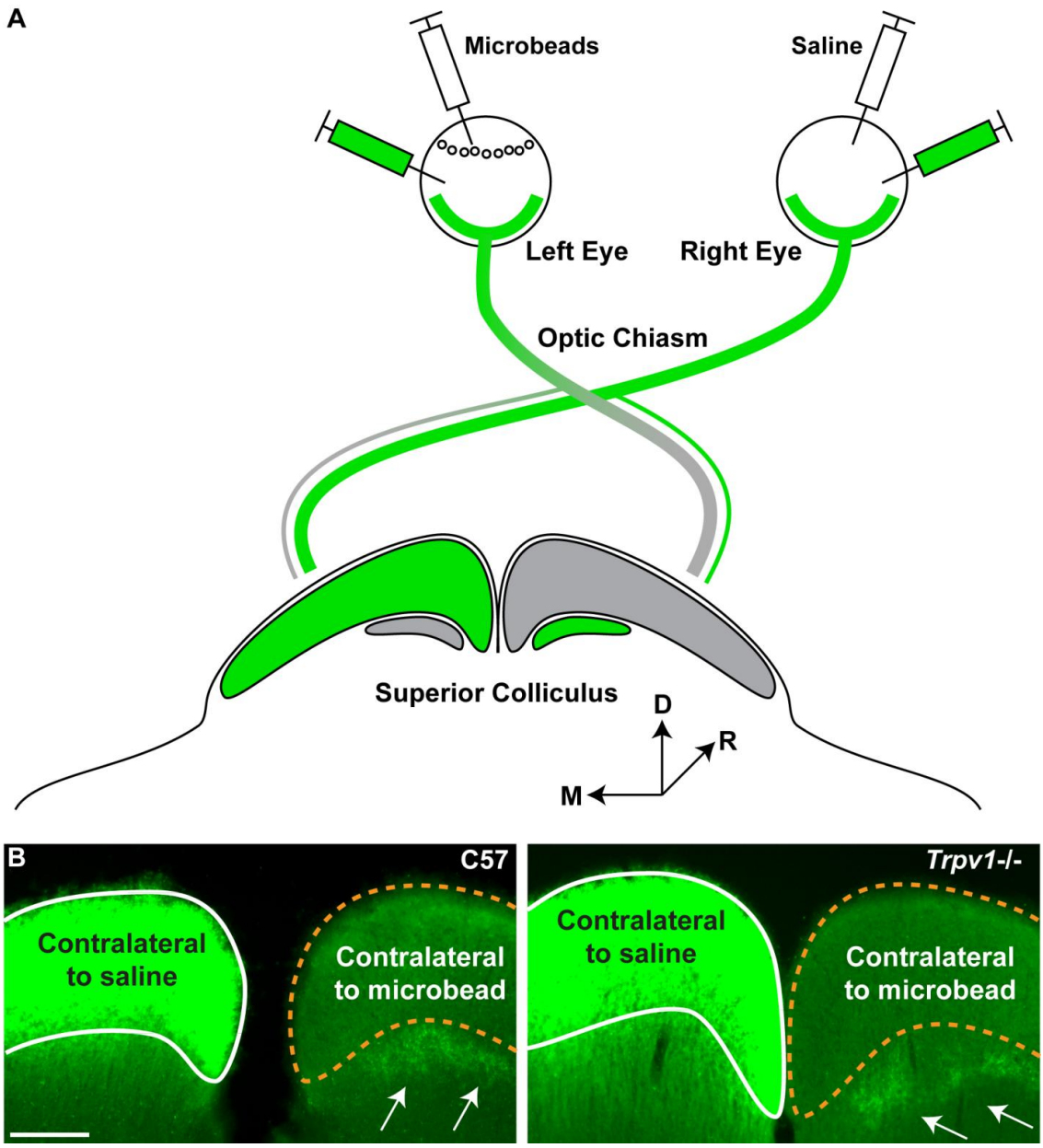

Figure 2.8. *Trpv1*-/- exacerbates microbead-induced transport deficits to the SC. ***A***, Schematic illustrating unilateral elevation of IOP for 36 days by microbead occlusion followed by bilateral CTB tracing 48 hours before sacrifice. Deficits in transport (indicated by gray) are expected in large contralateral projections and small ipsilateral projections to the SC. Medial (M), dorsal (D), and rostral (R) orientations indicated. ***B***, Coronal sections through rostral pole of C57 (left) and *Trpv1*-/- (right) SC show intact CTB signal (green) in the SC contralateral to saline injection (white outline). CTB signal in the SC contralateral to microbead injection (dashed yellow outline) is reduced following 5 weeks of elevated IOP. In SC contralateral to microbead-injection, CTB signal in ipsilateral projections (arrows) remain intact, as expected. Scale = 200 µm in all images.

pathology, with the most extreme samples from the cohort accented by a pronounced increase in degenerating profiles, severely reduced axon density, and overt hypertrophy of astrocyte processes (Figure 2.11B). Nerves from the saline eyes of the two cohorts appeared similar.

Using custom programmed routines, we determined average axon density from sections of optic nerve. Axon density in nerves from saline-injected C57 eyes ranged from 384,000-538,000 axons/mm^2 (Figure 2.12A), consistent with previous studies (Sappington et al., 2010). Microbead elevation shifted this range to 277,000-477,000 axons/mm^2. *Trpv1*-/- had no effect on axon density in the saline nerve (range of 356,000-521,000 axons/mm^2), but, like transport to the SC, exacerbated the reduction caused by elevated IOP. Nerves from *Trpv1*-/- microbead eyes had axon densities that ranged from 67,000-331,000 axons/mm^2 (Figure 2.12A). On average, elevated IOP reduced axon density in C57 optic nerves by 14% compared to saline nerves (p = 0.029; Figure 2.12B). *Trpv1*-/- microbead nerves exhibited a 47% decrease in density compared to their saline counterparts ($p < 0.001$; Figure 2.12B). This decrease in axon density was accompanied by a small decrease (about 14%) in cross-sectional nerve area only in *Trpv1*-/- mice (Figure 2.12C). Finally, we estimated the total number of axons in each nerve by multiplying axon density by nerve cross-sectional area. This yielded a range of 32,000-54,000 axons in nerves from saline eyes from both cohorts (not shown), again consistent with previous studies (Sappington et al., 2010). The corresponding mean was 41,659 axons for C57 (± 2700) and 42,990 for *Trpv1*-/- (± 1917; Figure 2.12D). On average, elevated IOP reduced the number of axons in C57 optic nerves by 17% compared to saline nerves (p = 0.04; Figure 2.12D). Again, the *Trpv1*-/- microbead nerves exhibited a far worse effect, with an average 53% loss of axons ($p < 0.001$; Figure 2.12D).

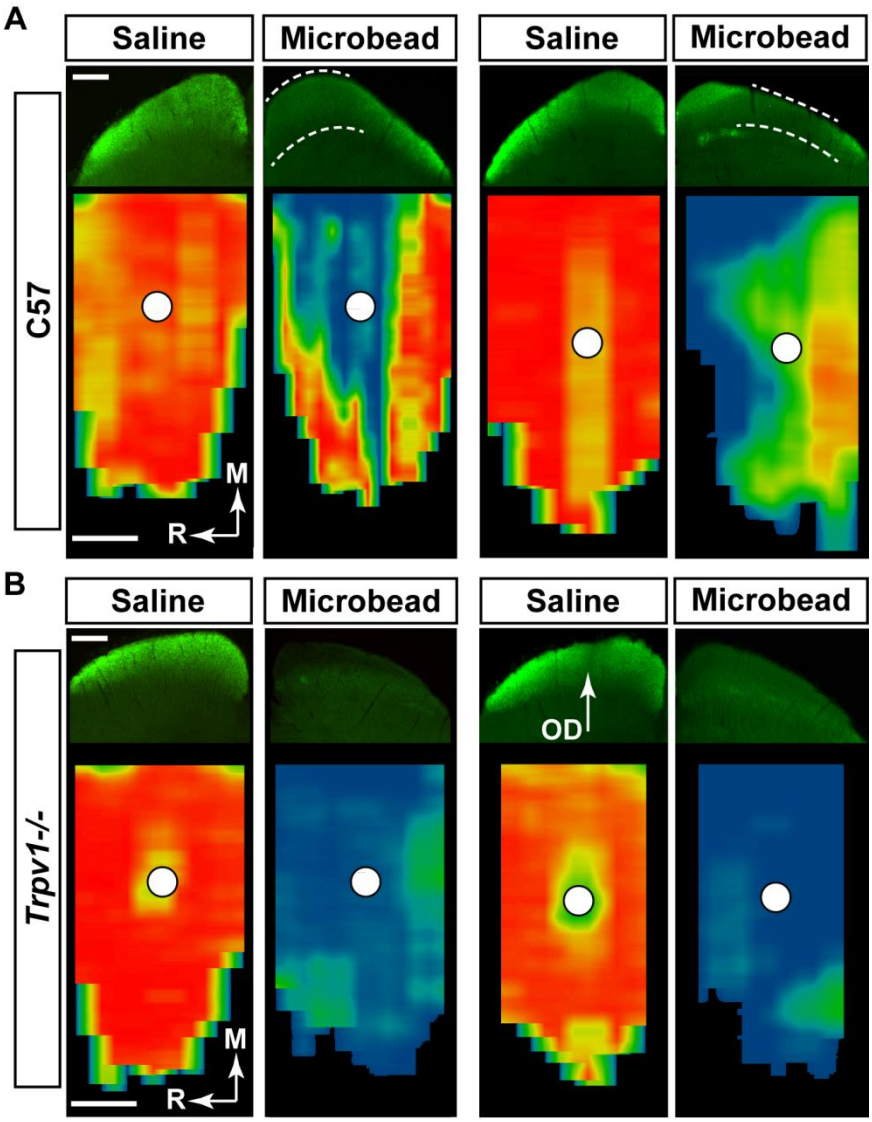

Figure 2.9. *Trpv1*-/- exacerbates deficits in anterograde axonal transport. ***A,*** Top row: coronal sections through superior colliculus (SC) following intravitreal injection of cholera toxin B (CTB; green) into saline- and microbead-injected eyes of C57 mice. Microbead-induced IOP elevation (see Figure 1) induced deficits in anterogradely transported CTB (dotted lines). Bottom row: retinotopic maps reconstructed from serial sections of SC with optic disc gap indicated (circles). Density of signal from transported CTB ranges from 0% (blue) to 50% (green) to 100% (red). Medial (M) and rostral (R) orientations indicated. ***B,*** Top row: sagittal SC sections from *Trpv1*-/- mice with microbead-induced IOP elevations show worse deficits in CTB transport compared to C57. Corresponding retinotopic maps (bottom row) demonstrate nearly complete loss of CTB transport. OD: optic disc representation (no RGCs). Scale = 500 µm for ***A***,***B***.

Trpv1-/- influences RGC survival in the retina

RGC somal degeneration in the retina follows optic nerve axonopathy in both chronic and inducible models of glaucoma, including the microbead model used here (Calkins, 2012). The five week duration of IOP elevation in our cohorts did not induce large-scale RGC body loss in either mouse strain (Figure 2.13A,B), though accumulation of phosphorylated neurofilaments—indicative of a deficit in anterograde transport—tended to be worse for the *Trpv1*-/- (Figure 2.13C). We have previously demonstrated in both chronic and inducible models that initial deficits in anterograde transport are not due to reduced uptake of CTB by RGCs (Crish et al., 2010; Lambert et al., 2011; Dapper et al., 2013). For example, in the *Trpv1*-/- mouse with 15% intact transport of CTB to the SC with IOP elevation (Figure 2.10A), the number of RGCs labeled by CTB uptake (3842 ± 271 mm^2) was the same as that labeled for phosphorylated neurofilaments (4123 ± 214 mm^2; $p = 0.423$). Similarly, RGC uptake of CTB is not affected by *Trpv1*-/- in either saline or microbead retina—nearly every RGC contains label (Figure 2.13B). We therefore cannot attribute the transport deficits we see in the colliculus to an apparent difference in CTB uptake between cohorts.

Moreover, when quantified across retinal quadrants, for most distances from the optic nerve head, neither cohort showed significant RGC body loss (Figure 2.14). At most locations, the ratio of RGC body density in the two eyes did not differ from unity, though there was a certain degree of variability. However, in microbead retinas from *Trpv1*-/- mice, accelerated loss was observed in the nasal quadrant; the most pronounced loss was nearest the optic disc with 40 ± 7% reduction compared to the saline eye ($p = 0.03$). At the same location, reduction in the C57 microbead retina was 24 ± 11%, which was not significant ($p = 0.20$). Thus, in both the optic projection and the retina, *Trpv1*-/- accelerates RGC degeneration associated with elevated IOP.

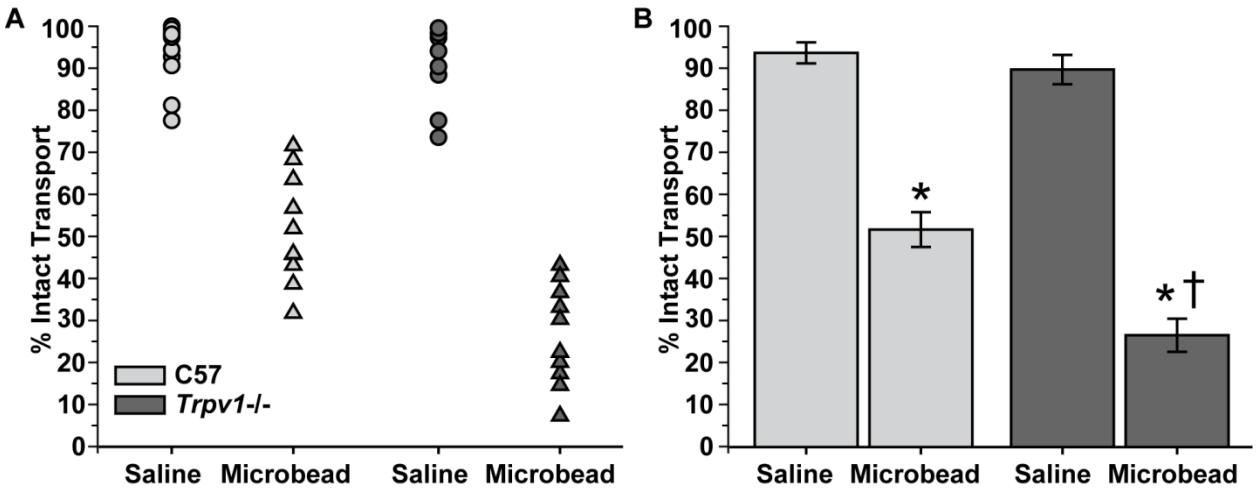

Figure 2.10. Quantification of anterograde transport in the superior colliculus. ***A,*** Fraction of the retinotopic map with intact RGC axonal transport (defined by ≥70% CTB signal) to individual C57 and *Trpv1*-/- saline (n = 10 and 8, respectively) and microbead (n = 10 and 10, respectively) superior colliculi. ***B,*** Transport of CTB from saline eyes was near 100% and similar for C57 (93.8 ± 2.5%) and *Trpv1*-/- (90 ± 3.5%) cohorts (mean ± SEM; $p = 0.46$). Intact transport in SC following IOP elevation was reduced in both cohorts compared to the saline eye (*, $p < 0.001$), but the decrease in *Trpv1*-/- (26.6 ± 4.0%) was twice as severe as in C57 (51.7 ± 4.1%; †, $p < 0.001$). Legend as in ***B***.

The results in Figure 2.14 also complement our previous work in which rats with elevated IOP for a similar duration exhibited reduced RGC density in the nasal quadrant (Lambert et al., 2011). Within the visual system, perception dictates that neuronal projections are precisely organized so that a continuous retinotopic representation of the space is retained (Chklovskii and Koulakov, 2004). In terms of RGCs, axons projecting from the retina onto the SC form a precise retinotopic map, which can be used to determine where in the retina deficits in transport originate. Taking advantage of this, we transformed our retinotopic maps (Figure 2.9) using retinal quadrant and eccentricity coordinates for rodents (Figure 2.15; Siminoff et al., 1966; Drager and Hubel, 1976). Deficits in axonal transport to the SC from microbead-injected eyes in C57 and *Trpv1*-/- mice tended to progress from or spread to the nasal quadrant of the retina (Figure 2.15). Interestingly, the nasal quadrant was where we observed a significant loss of RGC

bodies in *Trpv1*-/- retinas from microbead-injected eyes (Figure 2.14). This indicates that the retinotopic pattern of degeneration is conserved in this model.

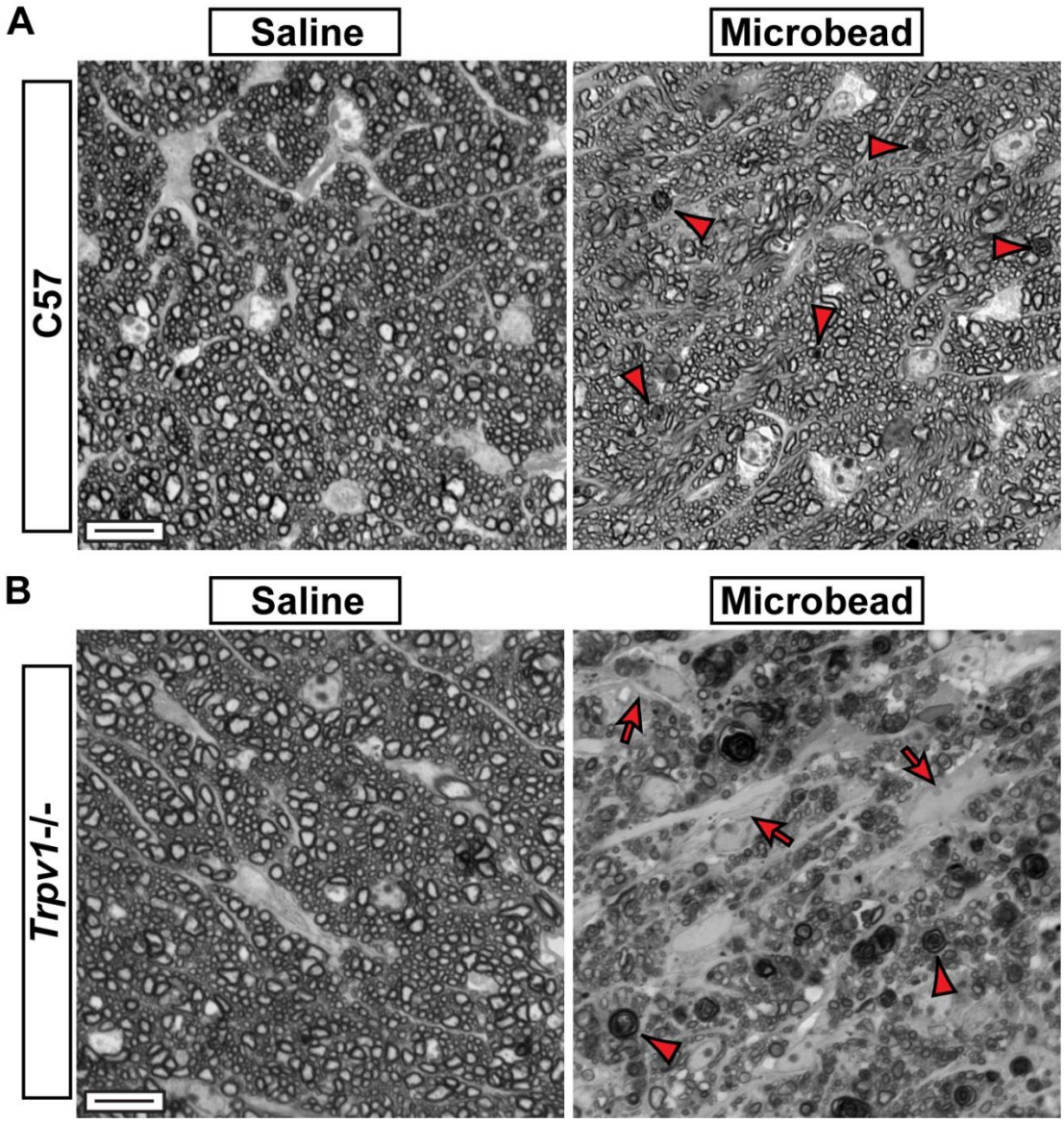

Figure 2.11. *Trpv1*-/- mice exhibit more severe optic nerve pathology following elevated IOP. ***A,*** Cross-sections of C57 optic nerve from saline and microbead eyes. Microbead-induced elevated IOP yielded a modest reduction in the packing density of intact axons and increased incidence of degenerating axonal profiles (red arrowheads). ***B,*** Cross-section through *Trpv1*-/- optic nerve from microbead eye shows severely diminished axon packing, overt gliosis (red arrows), and far more degenerating profiles compared to C57 nerves (red arrowheads). Saline eye nerves from the two cohorts appear similar. Scale = 10 µm for ***A***,***B***.

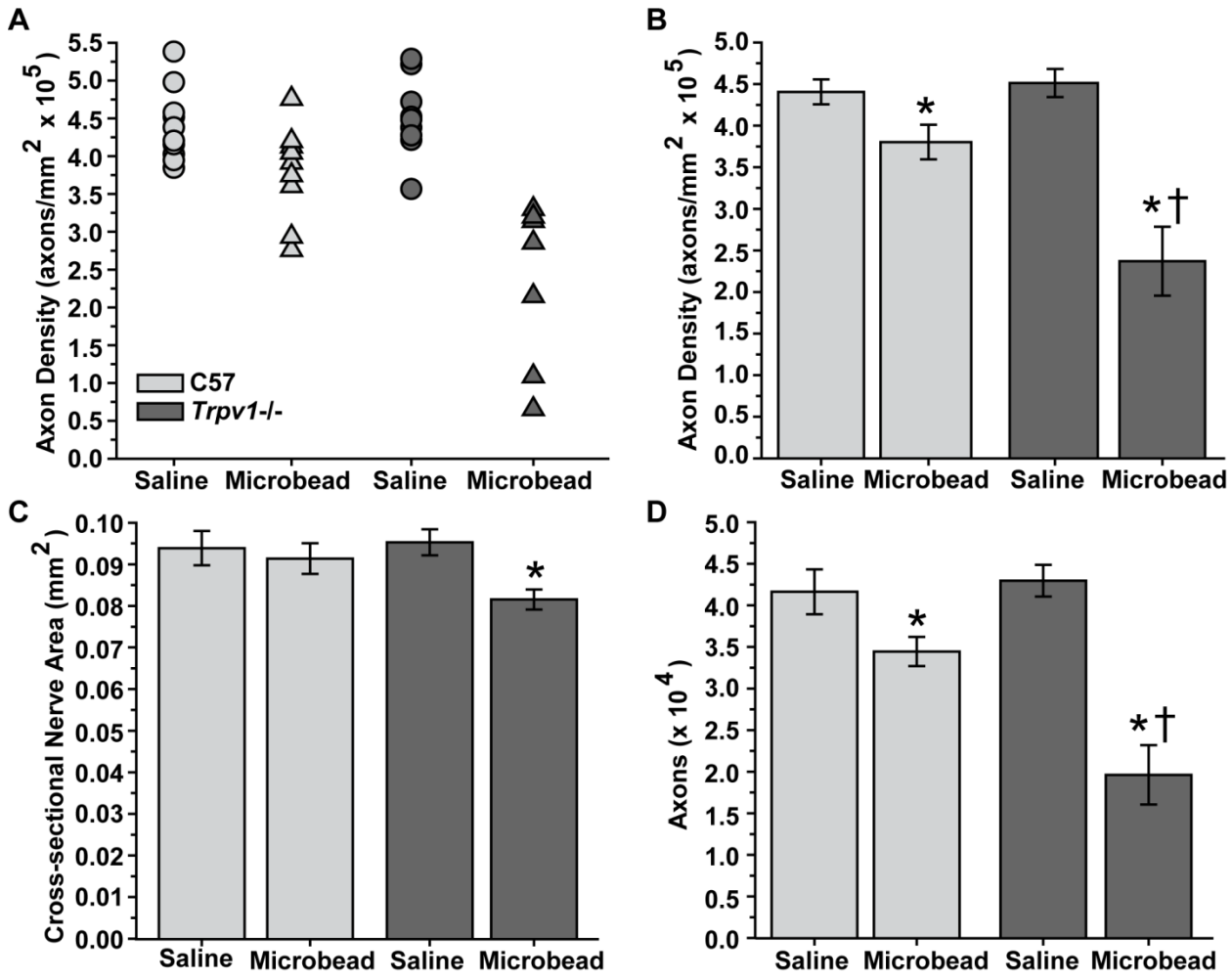

Figure 2.12. Quantification of axon loss in the optic nerve. ***A,*** Density of intact axons in cross-sections through individual C57 and *Trpv1*-/- saline (n = 10 and 9, respectively) and microbead (n = 9 and 7, respectively) optic nerves quantified from cross-sections as shown in Figure 4. ***B,*** Mean axon density (± SEM) in C57 and *Trpv1*-/- optic nerves. Diminished density from microbead-induced IOP elevation in *Trpv1*-/- nerves is more than twice that of C57 nerves (†, $p < 0.001$). An * indicates significance for microbead compared to corresponding saline nerve (*, $p = 0.001$ for C57; $p < 0.001$ for *Trpv1*-/-). ***C,*** Cross-sectional area (mean ± SEM) of *Trpv1*-/- optic nerves shrinks with elevated IOP compared to saline eye (*, $p = 0.005$). ***D,*** Number of axons (mean ± SEM) calculated as product of nerve area and axon density. *Trpv1*-/- nerves have nearly twice the loss compared to C57 nerves with elevated IOP (†, $p < 0.001$), though both groups have fewer axons compared to saline nerves (*, $p = 0.03$ for C57 and 0.04 for *Trpv1*-/-). Number of axons in saline nerves was similar in two cohorts ($p = 0.70$). Legend applies to ***A-D***.

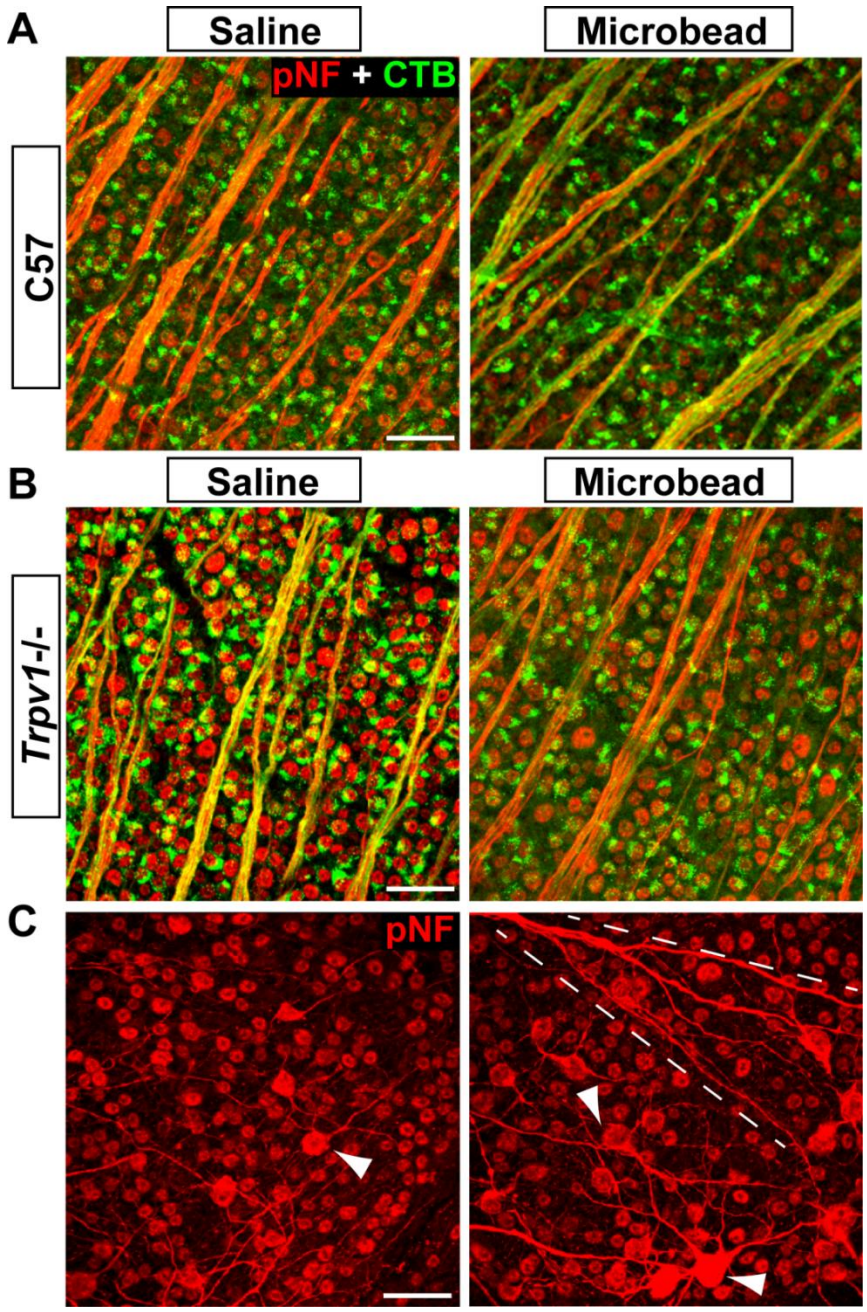

Figure 2.13. Progression to RGC body loss accelerated in *Trpv1*-/- mice. Confocal micrographs of C57 ***A,*** and *Trpv1*-/- ***B,*** retinas show RGCs labeled both by CTB uptake (red) and with antibodies against phosphorylated neurofilaments (green). In both cohorts, there is little apparent change in cell number with microbead-induced IOP elevations. Importantly, nearly every RGC is labeled by both markers, indicating intact RGC uptake of CTB. ***C,*** C57 (left) and *Trpv1*-/- (right) retinal peripheries show accumulation of phosphorylated neurofilaments in RGC dendritic arbors (arrowheads) with IOP elevation. Tendency is more robust in *Trpv1*-/- retina, with axonal accumulation as well (dashed lines). Scale = 20 µm for ***A-C***.

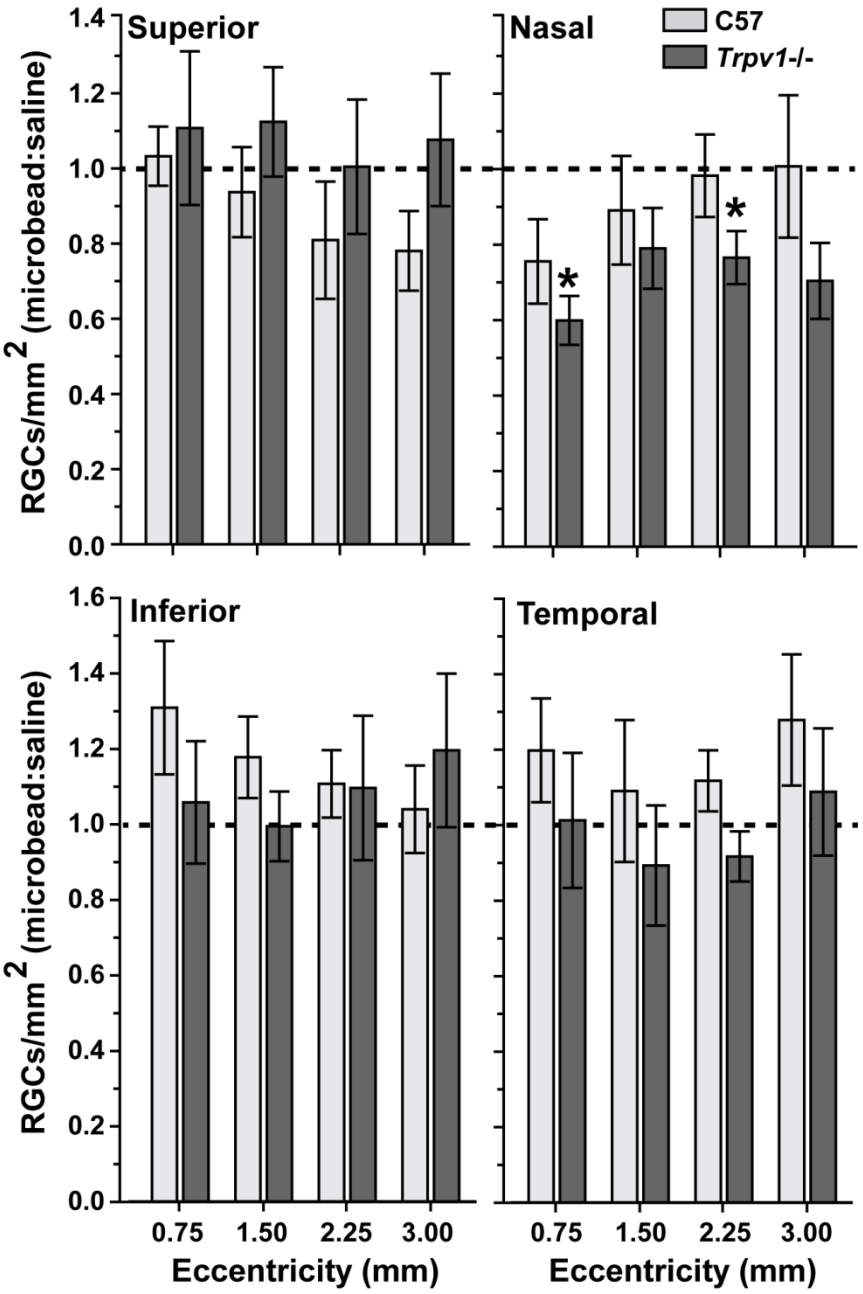

Figure 2.14. Quadrant-specific RGC body loss in *Trpv1*-/-. Density of RGC bodies (RGCs/mm^2) labeled for phosphorylated neurofilaments (cells/mm^2) expressed as the ratio of microbead to saline retina (means ± SEM) for increasing eccentricities from the optic disc. At each location, cells were scored as described above (see Methods) in images of 0.101 mm^2 in area (n = 5 retina each). For superior, inferior and temporal quadrants, neither cohort had significant RGC body loss at any eccentricity ($p \geq 0.08$). In the nasal quadrant, *Trpv1*-/- microbead retina showed moderate (20-40%) accelerated loss compared to saline at 0.75 and 2.25 mm eccentric (*, p = 0.03 and 0.05, respectively).

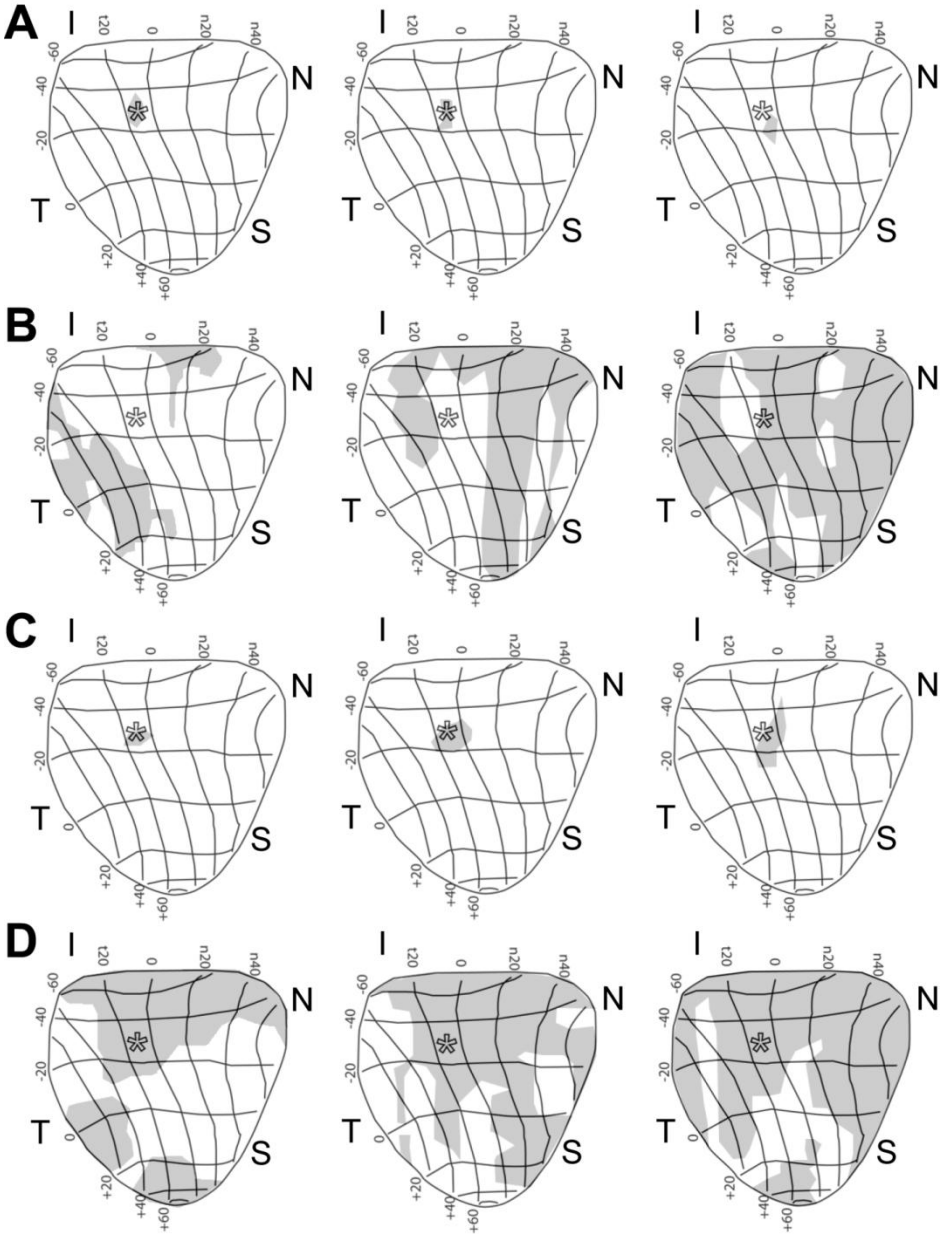

Figure 2.15. Microbead-induced anterograde transport deficits in SC are retinotopically sectorial. Reconstructed CTB transport maps transformed into retinal quadrant and eccentricity coordinates as specified by Siminoff et al. (1966) and Drager and Hubel (1976). Retinal quadrants are indicated by abbreviation: inferior (I), nasal (N), superior (S), and temporal (T). ***A,*** Maps of superior colliculi from C57 saline control eyes are complete (approximately 98%) with optic disc indicated (*). ***B,*** Transport deficits (shaded regions) in colliculi from C57 microbead-injected eyes with intact transport of 72%, 57%, and 32% (left to right, respectively). Deficits in nasal quadrant were moderate (middle) to severe (right). ***C,*** Maps of colliculi from *Trpv1*-/- saline control eyes are complete (95-99%). ***D,*** Transport deficits from *Trpv1*-/- microbead-injected eyes exhibited a spread to nasal quadrant in eyes with both moderate (42% intact, left) and severe (32% and 19% intact, middle and right, respectively) deficits.

Discussion

TRPV1 is known to influence neuronal physiology and synaptic function, as demonstrated by neurophysiological changes in *Trpv1*-/- mice (Marsch et al., 2007; Gibson et al., 2008; Li et al., 2008; Maione et al., 2009; Chavez et al., 2010; Grueter et al., 2010). Here, we show that with elevated pressure in the eye, the absence of functional TRPV1 accelerates neurodegeneration. An early characteristic of neurodegeneration in glaucoma is degradation of active transport from the retina to the colliculus, which occurs prior to outright axon degeneration in the optic nerve (Crish et al., 2010; Lambert et al., 2011; Dapper et al., 2013). After a five-week period of an equivalent elevation in IOP (33%; Figure 2.6), both deficits in anterograde transport to the colliculus (Figures 2.9 and 2.10) and degeneration of axons in the optic nerve (Figures 2.11 and 2.12) were about twice as severe in *Trpv1*-/- than in age-matched C57 mice. Similar to other neurodegenerative diseases, axonopathy is among the earliest pathogenic events in glaucoma, with RGC body loss in the retina following later (Whitmore et al., 2005; Calkins, 2012; Howell et al., 2012). This period is especially pronounced in models utilizing modest elevations in IOP, including the microbead model used here (Calkins, 2012; Dapper et al., 2013). Thus, while RGC body drop-out was hardly detectable in C57 retina, *Trpv1*-/- retina demonstrated significant loss in the nasal quadrant, especially in the region of normally highest RGC density near the optic nerve head (Figure 2.14). This extra susceptibility of the nasal quadrant (Figure 2.15), while not yet understood, is consistent with results from other rodent models (Lambert et al., 2011).

The nasal quadrant of the C57 mouse retina exhibits a high density of RGC somas across all eccentricities, whereas the temporal, superior, and inferior quadrants exhibit a gradient of somal density (Jeon et al., 1998). For all retinal quadrants except for the nasal quadrant, somal

density increases moving from the periphery (furthest from the optic disc) to the center (closest to the optic disc). Within the nasal quadrant, RGC density in the periphery is approximately equal to the density at more central eccentricities, so this region has an overall higher density of RGC somas (Jeon et al., 1998). Knowing this specific difference within the nasal quadrant may be useful for understanding why earliest pathological signs are present in this quadrant first. Perhaps this is due to local increases in extracellular factors that may accompany the earliest stages of RGC dysfunction and degeneration. It is known that mechanical strain, as is expected in glaucoma, causes RGCs to release ATP through pannexin channels, and that this extracellular ATP, in turn, acts on $P2X_7$ receptors that can cause pro-apoptotic Ca^{2+} influx into RGCs (Zhang et al., 2005b; Hu et al., 2010; Xia et al., 2012; Sugiyama et al., 2013). Essentially, stressed RGCs may release factors like ATP into the extracellular environment, and these factors may then act locally on $P2X_7$ receptors of nearby RGCs. If these cells are more densely packed, it is possible that factors released from a stressed RGC have a better chance of affecting nearby RGCs simply due to increased proximity. Areas of retinal tissue with higher RGC density, such as the nasal region, may therefore exhibit higher levels of apoptosis. This may explain why in *Trpv1*-/- mice we observe somal loss in the nasal quadrant before any of the other quadrants.

It is also important to consider trends from data that, though statistically non-significant, may be biologically relevant. In the nasal quadrant of C57 mice, RGC somal density exhibits near-significant reduction following pressure elevation (Figure 2.14). This reduction may be biologically relevant, as we see this trend in *Trpv1*-/- mice, which exhibit an accelerated pathology compared to C57 mice. Likewise, following pressure elevation in C57 mice, RGC density within the superior quadrant exhibited a non-significant decrease in the retinal periphery. These changes were not observed in the *Trpv1*-/- mice, possibly indicating a protective effect of

Trpv1-/- in this quadrant. It is likely that the effects of TRPV1-mediated Ca^{2+} entry are very dependent on the context and local milieu of the RGCs. For example, not only could activation of TRPV1 cause pro-apoptotic Ca^{2+} influx in RGCs (Sappington et al., 2009), but it could also activate glial NFκB signaling, which has been linked to induction of oxidative stress (Neufeld and Liu, 2003; Sappington and Calkins, 2008). If TRPV1 contributes to this type of signaling within the superior quadrant, then *Trpv1*-/- may be protective. This is not entirely unexpected, as it has been observed that different spatially-organized signaling microenvironments exist within glaucomatous retinas (Sims et al., 2012). Such microenvironments may exist for TRPV1-related signaling and relevant stressors, which may in part explain why we see differences in stress response and pathology when comparing between retinal quadrants. It is also possible that these soma counts are affected by our use of an antibody against phosphorylated neurofilaments to identify RGC somas. This antibody labels axons of RGCs in addition to their somas, and axonal labeling can sometimes obstruct the view of cell bodies, especially at eccentricities closer to the optic disc. Future studies could use a marker such as Brn3 protein, which only labels RGC somas and may provide a more accurate readout of somal density. Overall, there are many explanations that can be considered for these statistically non-significant results, but they do seem to indicate the importance of understanding TRPV1 signaling microenvironments within the retina.

We propose that TRPV1 plays an early, Ca^{2+}-dependent role in detecting stress associated with elevated pressure in glaucoma, in order to mediate a compensatory response to counter disease progression. In isolated RGC cultures exposed to elevated hydrostatic pressure *in vitro*, the pressure stressor is acute, and TRPV1 activation is sufficient to induce an apoptotic increase in intracellular Ca^{2+} (Sappington et al., 2009). In the intact system, the same activation by a *modest*, chronic stressor would seem to initiate protective cascades that may in part boost

RGC excitation. Thus, progression is accelerated with *Trpv1*-/-, in which the absence of TRPV1 abolishes an intrinsic physiological mechanism that enhances RGC excitatory signaling under conditions that stress the neuron, especially the axon. This model is consistent with other *in vivo* results in which pharmacological antagonism of TRPV1 ablated the protection afforded by an anandamide analogue on RGC survival with ischemic-reperfusion injury induced by acutely elevated IOP (Nucci et al., 2007b). Our hypothesis is also supported by recent work showing that the related TRPC6 channel is protective in a model of retinal ischemia/reperfusion injury (Wang et al., 2010).

We do not yet understand all possible mechanisms through which TRPV1 could counter neuronal stress, though both neuronal and glial mechanisms are likely (Ho et al., 2012). TRPV1 can be activated and/or sensitized either directly by mechanical stress or by endogenous ligands like endocannabinoids and growth factors (Straiker et al., 1999; Stamer et al., 2001; Zhang et al., 2005a). In addition to RGCs, TRPV1 is expressed in both astrocytes and microglia of the retina (Leonelli et al., 2009; Sappington et al., 2009). Activation in retinal microglia is coupled to release of interleukin-6, which is protective of isolated RGCs exposed to elevated pressure (Sappington et al., 2006; Sappington and Calkins, 2008). The endogenous cannabinoid anandamide is a ligand for both TRPV1 and the cannabinoid type 1 receptor and is known to protect against ischemic injury and excitotoxicity (Kim et al., 2007). TRPV1 and the anandamide precursor enzyme NAPE phospholipase D are expressed in the RGC projection to the colliculus (Maione et al., 2009), the primary target for RGCs in the rodent visual system. Thus, TRPV1 could help counter progression through axonal mechanisms outside of the retinal milieu.
With stress, neuronal TRPV1 is upregulated and undergoes translocation to the plasma membrane, where it increases post-synaptic neurite activity and survival (Zhang et al., 2005a;

Biggs et al., 2008; Goswami et al., 2010; Schumacher and Eilers, 2010). Once translocated, TRPV1-gated Ca^{2+} promotes spontaneous excitation and potentiates post-synaptic responses to glutamate (Marinelli et al., 2003; Xing and Li, 2007; Medvedeva et al., 2008; Jiang et al., 2009; Peters et al., 2010). Phosphorylation promotes sensitization, continued translocation, and increased depolarization (Van Buren et al., 2005). TRPV1 can become desensitized by dephosphorylation via the calmodulin-dependent protein phosphatase, calcineurin, or by re-internalization (Mohapatra and Nau, 2005). Together with these findings, our results suggest that TRPV1 could contribute to RGC survival in response to stress or injury by utilizing both extrinsic and intrinsic signaling mechanisms.

CHAPTER 3

ELEVATED PRESSURE INCREASES RETINAL TRPV1 AND ITS RELATION TO GANGLION CELL SYNAPSES[3]

Introduction

In the retina, TRPV1 has been linked to RGC survival *in vivo* in response to stressors such as transient ischemic insult induced by acutely elevated IOP (Nucci et al., 2007b) and NMDA-induced neuronal injury (Sakamoto et al., 2014). These studies and our data (Ward et al., 2014) demonstrate the relevance of TRPV1 in RGC survival; however, our understanding of how TRPV1 functions depends on our knowledge of how the protein responds to stressors. To appreciate how TRPV1 mediates its effects during injury, we must first determine where the channel is localized within the retina and how glaucomatous stress influences its expression and localization.

Previous studies have demonstrated expression of TRPV1 in both non-mammalian (Zimov and Yazulla, 2004, 2007) and mammalian (Sappington and Calkins, 2008; Leonelli et al., 2009; Sappington et al., 2009; Martinez-Garcia et al., 2013) retinal tissue. Immunolabeling for TRPV1 protein in the rabbit retina indicates TRPV1 is expressed across all nuclear and synaptic layers of the retina (Martinez-Garcia et al., 2013). TRPV1 expression in the rat retina appears more restricted than in the rabbit retina; however, expression is still widespread. Immunolabeling for TRPV1 protein and *in situ* hybridization of *Trpv1* mRNA in rat retinal tissue indicates that TRPV1 can be found in the nerve fiber, ganglion cell, inner plexiform, inner nuclear, and outer plexiform layers (Sappington et al., 2009). Additionally, TRPV1 has been localized to retinal

[3] Portions of this chapter were published as Ward NJ (2012) TRPV1 and the intrinsic neuronal response to stress. Vanderbilt Rev Neurosci 4:108-113.

glia (i.e., astrocytes, microglia, and Müller glia), which are found in several different retinal layers (Sappington and Calkins, 2008; Leonelli et al., 2009; Sappington et al., 2009). TRPV1 localization in C57 mice is similar to that of rats, and the protein is found in all retinal layers associated with each cellular compartment of the RGC—the cell body, dendrites, and axon (Sappington et al., 2009).

Localization studies of TRPV1 in the retinal plexiform layers that contain synapses indicates a potential synaptic function for the protein (Zimov and Yazulla, 2004; Leonelli et al., 2009; Sappington et al., 2009; Martinez-Garcia et al., 2013). Synaptic localization of TRPV1 in the retina is not a surprising idea, as TRPV1 protein was identified in synaptosomal fractions isolated from primary cultures of cortical neurons (Goswami et al., 2010). Primary cultures of RGCs exhibit expression of TRPV1 throughout their neurites, including node-like clusters of TRPV1 that may indicate synaptic specializations (Sappington et al., 2009). Likewise, previous studies within the CNS have localized TRPV1 to postsynaptic dendritic spines by using pre-embedding immunogold labeling imaged by high resolution electron microscopy (Puente et al., 2011; Puente et al., 2014). These studies indicate that in both the hippocampus and extended amygdala, TRPV1 exhibits perisynaptic and extrasynaptic localization. The number of TRPV1-associated immunoparticles was greatest in the perisynaptic membrane region immediately abutting the postsynaptic density, and gradually decreased as distance from the postsynaptic density increased. Localization of TRPV1 to the inner plexiform layer of the retina, where RGC receive synaptic input at postsynaptic dendritic sites, suggests that TRPV1 may affect dendritic or synaptic function in these neurons (Sappington et al., 2009; Martinez-Garcia et al., 2013).

Currently, TRPV1 has not been associated with synaptic structures in the retina. Here, we examine TRPV1 expression alongside PSD-95 and MAP2 proteins to better understand its

localization. PSD-95 is a scaffolding protein found in postsynaptic specializations on dendrites, and it associates with receptors and cytoskeletal elements at these synaptic structures (El-Husseini et al., 2000). Within the retina, PSD-95 has previously been used to identify postsynaptic specializations found on RGC dendrites (Stevens et al., 2007). We also examined MAP2 (microtubule associated protein 2), which is a component of microtubule structures in neuronal dendrites. Within the retina, MAP2 has previously been used to identify RGC dendritic structures within the inner plexiform layer of the retina (Okabe et al., 1989). The following studies aim to determine whether TRPV1 protein levels and localization within the retina are affected by elevated IOP. Additionally, we sought to examine how RGC dendrites and synapses respond to pressure, and if TRPV1 may be associated with these responses.

Materials and Methods

Induction of ocular hypertension by microbead occlusion

Intraocular pressure (IOP) was acutely elevated in 3-month-old C57 mice by microbead occlusion of aqueous flow as described previously (Sappington et al., 2010). All procedures and IOP measurement methods followed those described in Chapter 2 Methods. For qPCR studies, cohorts of mice were sacrificed by cervical dislocation at 1 week, 2 weeks, 3 weeks, and 5 weeks after microbead injection, and each cohort included 4 animals. For immunohistochemistry studies, cohorts of mice were sacrificed at 4 days, 1 week, 3 weeks, 5 weeks, or 7 weeks after microbead injection, and each cohort included between 3 and 5 animals.

Tissue preparation

For mice used in qPCR studies, fresh retinal tissue was dissected from both saline- and microbead-injected eyes and was stored at -80ºC prior to RNA extraction. For mice used in immunohistochemistry studies, all animals were transcardially perfused with phosphate buffered saline (PBS) followed by 4% paraformaldehyde (PFA) in PBS and tissue was harvested. Eyes were enucleated and submitted to the Vanderbilt Eye Institute Histology Core for sectioning. Eyes were processed, paraffin embedded, and the middle two-thirds of the eyes were cut into 6-10 µm thick sections.

Quantitative PCR

RNA was extracted from retinas of microbead-injected C57 mice as previously described (Hanna and Calkins, 2006; Crish et al., 2013). Tissue was incubated overnight in lysis buffer (10 mM Tris/HCl, pH 8.0; 0.1 mM EDTA, pH 8.0; 2% SDS, pH 7.3; and 500 µg/ml proteinase K

(Clontech Labs, Mountain View, CA)) before RNA extraction with Trizol (Invitrogen) and 10 µg glycogen used as an RNA carrier. RNA purity and concentration were determined with a NanoDrop 8000 spectrophotometer (Thermo Scientific, Wilmington, DE). Samples (1 µg) were treated with DNase (Invitrogen) and cDNA was synthesized (Applied Biosystems reagents, Foster City, CA). We performed qPCR as previously described (Crish et al., 2013) using an ABI PRISM 7300 Real-Time PCR System and FAM dye-labeled gene-specific probes for *Trpv1* (Applied Biosystems). ABI software (SDS v1.2) was used to automatically determine cycling conditions and threshold values. Using 18S rRNA as an endogenous control, relative *Trpv1* product quantities were measured at least in triplicate and determined using the $2^{\Delta\Delta Ct}$ analysis method (Livak and Schmittgen, 2001).

Immunolabeling of retinal paraffin sections

Paraffin sections were deparaffinized by incubation at 60ºC for 1 hour. Slides were rinsed in two separate washes of xylene for 10 min. Sections were rehydrated using an ethanol series comprised of 10 minute washes each in freshly-prepared 100% EtOH (twice), 95% EtOH, 70% EtOH, and ddH_2O. Tissue was washed in PBS for 5 min with shaking, excess PBS was removed by blotting with a Kimwipe, and boxes were traced around all sections with a hydrophobic PapPen to prevent solution runoff. Non-specific binding was blocked by incubating sections in 5% normal donkey serum (NDS) plus 0.1% Triton-X 100 diluted in PBS for 2 hours at room temperature.

Primary antibodies were diluted to recommended concentration in a solution of 3% NDS plus 0.1% Triton-X 100 diluted in PBS. Primary antibodies used in these studies were rabbit anti-TRPV1 (1:100, Neuromics), mouse anti-PSD-95 (1:200, Millipore), rabbit anti-MAP2

(1:200, Cell Signaling Technology), and goat anti-ChAT (1:100, Millipore). Blocking buffer was drained from sections, primary antibody solution was applied to tissue, and all slides were incubated for 3 days at 4ºC in a humidified chamber. For control experiments in which no primary antibody was used, this same solution was used but no antibody was included. Slides were drained of primary antibody solution and washed in PBS 3 times for 10 minutes at room temperature while shaking. Secondary antibodies were diluted 1:200 in a solution of 1% NDS plus 0.1% Triton-X 100 diluted in PBS. Secondary antibodies used in this study were raised in donkey and conjugated to Alexa-488 or Cy3 (Jackson Immunoresearch). Secondary antibody solution was applied to tissue sections and incubated for 2 hours at room temperature in the dark. Slides were drained of secondary antibody solution and washed in PBS 4 times for 10 minutes followed by ddH_2O for an additional 10 minutes. Slides were optionally counterstained for cell nuclei using 4',6–diamidino–2–phenylindole dihydrochloride (DAPI). DAPI diluted 1:100 in ddH_2O was applied to sections and incubated for 5 min at room temperature in the dark. Excess DAPI was drained and slides were washed 5 times in PBS for 5 min with shaking. Tissue was mounted using Fluoro-Mount aqueous mounting media, and slides were coverslipped and sealed using Cytoseal.

Imaging and quantification of immunohistochemistry

Following immunolabeling, vertical paraffin sections of retina were imaged using an Olympus FV-1000 inverted confocal microscope. For experiments in which intensity comparisons were made, microscope settings (e.g., laser intensity, pinhole size, exposure time) were kept consistent for all slides during the entirety of the imaging session. Using DAPI labeling as a reference point for all nuclear layers of the retina, ImageJ software (National

Institutes of Health, Bethesda, MD) was used to outline specific retinal layers. Fluorescent intensity of immunolabeled proteins was determined within outlined areas and averaged over the selected area of pixels. Using FluoView software (Olympus, Center Valley, PA), colocalization of TRPV1 and PSD-95 was examined by using Z-stacked micrographs through multiple optical planes of retinal tissue. To examine potential synaptic localization of TRPV1, studies were conducted specifically focusing on the inner plexiform layer.

Statistical methods

Group averages were calculated and compared in SigmaPlot (version 11.1, SYSTAT) using two-sided *t* tests for all data passing Shapiro-Wilk normality tests. For data that did not pass Shapiro-Wilk normality, non-parametric Mann-Whitney Rank Sum tests were used. For data presented as ratios, comparisons versus unity (hypothesized mean = 1) were conducted using one-sample *t*-tests. Error as reported in text and on bar graphs represents mean ± SEM.

Results

Regulation of *Trpv1* transcript levels following microbead-induced IOP elevation

To examine whether IOP elevation induces changes in *Trpv1* transcript levels, we injected C57 mouse eyes with microbeads to block aqueous fluid outflow (Sappington et al., 2010; Chen et al., 2011). Microbead injection was used to elevate IOP in these mice for 1, 2, 3, and 5 weeks (n = 4 animals per timepoint, Figure 3.1A). Post-injection IOPs averaged for all animals indicate an approximately 22% elevation in microbead-injected eyes compared to contralateral eyes injected with an equivalent volume of saline. Pressure elevation in microbead-injected eyes was significant when compared to saline-injected eyes ($p \leq 0.05$; Figure 3.1B).

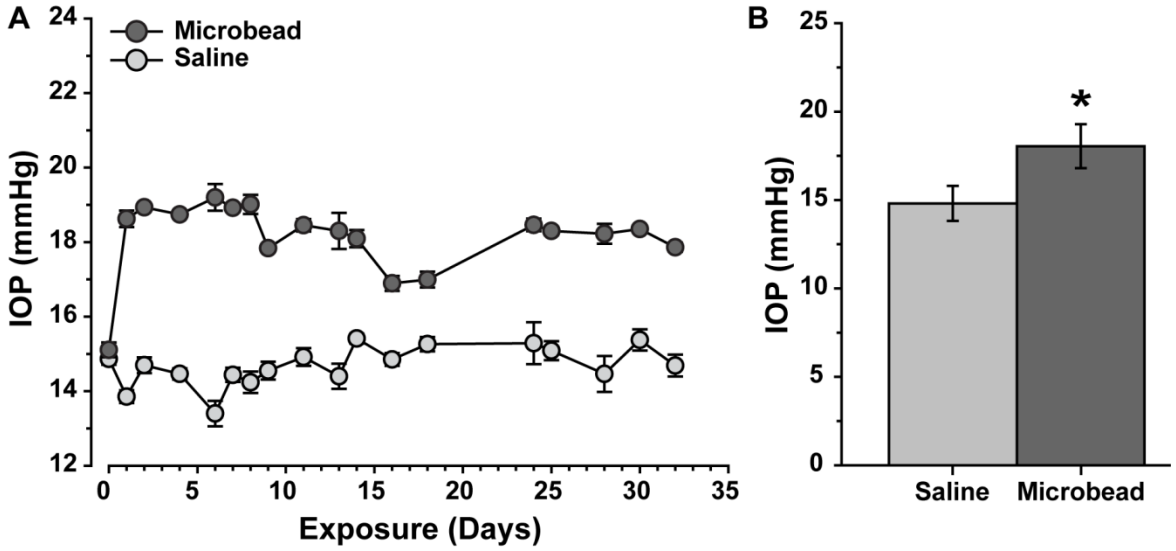

Figure 3.1. Microbead-induced IOP elevation for animals used in *Trpv1* transcript qPCR. ***A***, Measurements of IOP taken from C57 mice injected with microbeads. Baseline IOPs (Day 0) were measured prior to injection. Each animal received an injection of microbeads in one eye and an equivalent volume of saline in the contralateral eye. Each line represents IOPs of animals from cohorts sacrificed at 1-, 2-, 3-, or 5-week timepoints following injection (n = 4 animals at each timepoint). ***B,*** Averaged IOP measurements for C57 animals for all days post-injection (Days ≥1). *, $p \leq 0.05$.

Microbead:saline ratios of retinal *Trpv1* transcript levels collected at 1, 2, 3, and 5 weeks indicated no significant changes from unity at these timepoints (Figure 3.2). Although no significant changes were discovered in whole tissue, a trend toward reduced *Trpv1* expression at later timepoints may indicate a delayed downregulation of *Trpv1* transcript following pressure elevation.

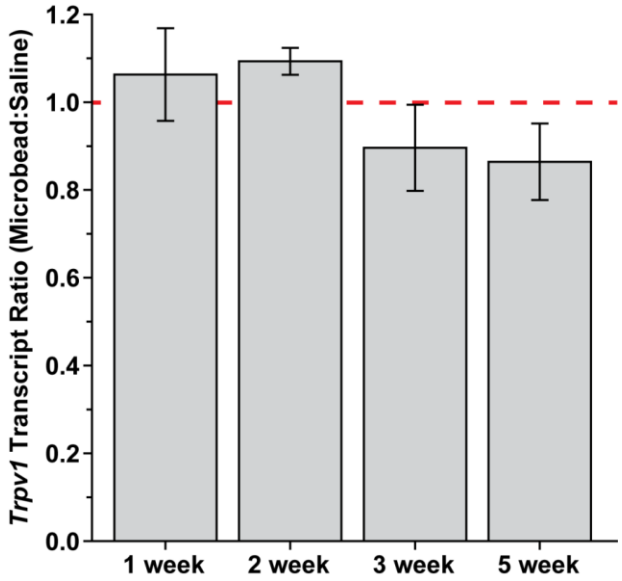

Figure 3.2. *Trpv1* transcript levels following microbead-induced pressure elevation. C57 mice were injected with microbeads to elevate intraocular pressure. At 1, 2, 3, and 5 weeks following injection, whole-retinal qPCR was conducted to measure *Trpv1* transcript levels by $2^{\Delta\Delta Ct}$ analysis. Microbead eye:saline eye *Trpv1* transcript level ratios were calculated for each group (*n* = 4 animals per timepoint). All groups non-significant when compared to unity (red line).

TRPV1 protein levels increase transiently in response to IOP elevation

Significant changes in *Trpv1* transcript levels may have been excluded by our choice of timepoints for qPCR quantification (Figure 3.2), so we looked at protein expression using both earlier and later timepoints. Microbead injection was used to elevate IOP in C57 mice, which were sacrificed for histological tissue preparation at 4-day, 1-, 3-, 5-, and 7-week timepoints (*n* =

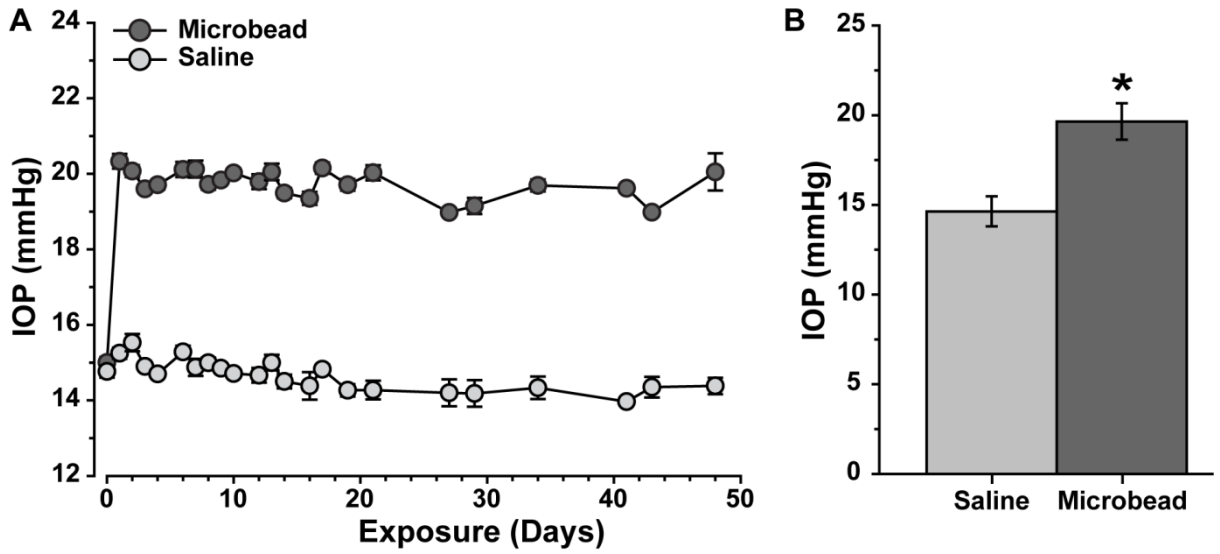

Figure 3.3. Microbead-induced IOP elevation for animals used in histological experiments. ***A,*** Measurements of IOP taken from C57 mice injected with microbeads. Baseline IOPs (Day 0) were measured prior to injection. Each animal received an injection of microbeads in one eye and an equivalent volume of saline in the contralateral eye. IOP was monitored in microbead- and saline-injected mice for 4-day, 1-, 3-, 5-, or 7-week exposures prior to sacrifice (n = 3-5 animals per timepoint). ***B,*** Averaged IOP measurements for C57 animals for all days post-injection (Days ≥1). *, $p \leq 0.001$.

3-5 animals per timepoint, Figure 3.3A). Post-injection IOPs averaged for all animals indicate an approximately 34% elevation in microbead-injected eyes compared to contralateral eyes injected with an equivalent volume of saline. Pressure elevation in microbead-injected eyes was significant when compared to saline-injected eyes ($p \leq 0.001$; Figure 3.3B).

Retinal sections from C57 mice with 4-day, 1-, 3-, 5-, and 7-week IOP elevations demonstrated TRPV1 expression that was apparent in multiple retinal layers (Figure 3.4), as expected (Zimov and Yazulla, 2004, 2007; Sappington and Calkins, 2008; Leonelli et al., 2009; Sappington et al., 2009; Martinez-Garcia et al., 2013). Across most retinal sections from saline-injected eyes, TRPV1 exhibits membranous localization in nuclear layers (GCL, INL, ONL), punctate labeling in synaptic layers (IPL, OPL), and diffuse labeling within the unmyelinated portion of the RGC axons (NFL). At early, 4 day timepoints for both saline- and microbead-

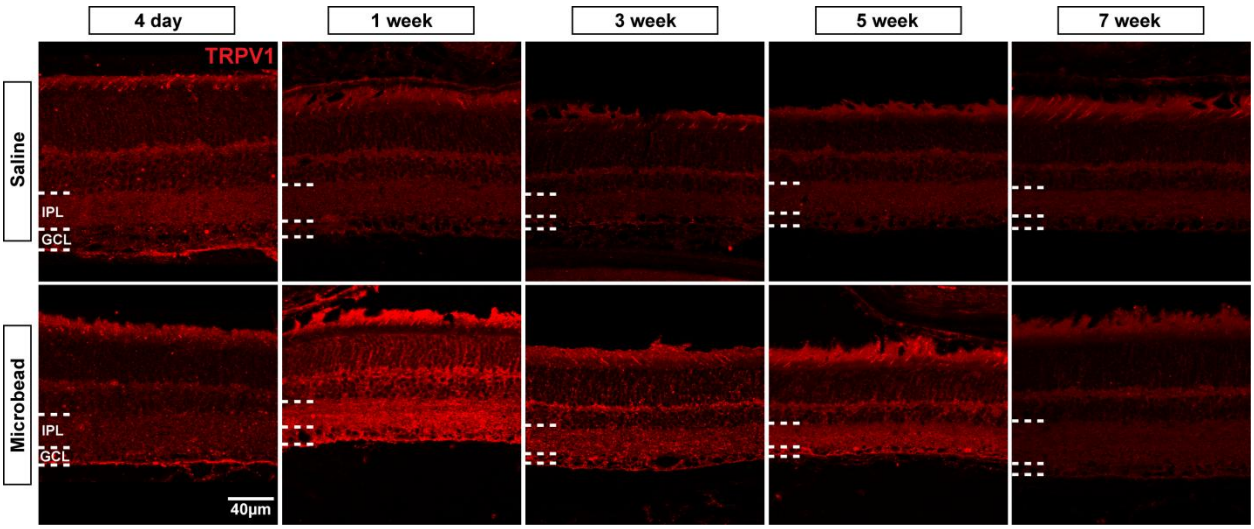

Figure 3.4. TRPV1 protein levels transiently increase following IOP elevation. Vertical sections of C57 mouse retinas immuno-labeled for TRPV1 protein. TRPV1 intensity transiently increases in retinas from microbead-injected eyes, including layers that include the RGC cell body (GCL) and dendrites (IPL). GCL: ganglion cell layer, IPL: inner plexiform layer.

injected eyes, TRPV1 localization within the RGCs in the ganglion cell layer appeared diffuse within the cell soma and membrane. In microbead-injected eyes, qualitative assessment of TRPV1-associated fluorescence levels indicate a transient increase in TRPV1 following 1 week of elevated IOP. At this 1 week timepoint, TRPV1 intensity appears to be increased in layers associated with the RGC membrane and dendrites compared to saline-injected control eyes.

TRPV1 expression was apparent throughout the retina; however, we were interested in RGC-specific expression based on our knowledge of its influence on RGC survival (Ward et al., 2014). Quantification of average fluorescent pixel intensity in each RGC-associated region of the retina was used to determine TRPV1 levels in specific retinal layers. The microbead:saline ratios of TRPV1 expression for each of these layers indicated that there was a significant increase in TRPV1 within the inner plexiform layer at 1 week post-injection (Figure 3.5). Increases in TRPV1 protein levels were transient, and levels exhibited a gradual decrease out to the 7-week timepoint.

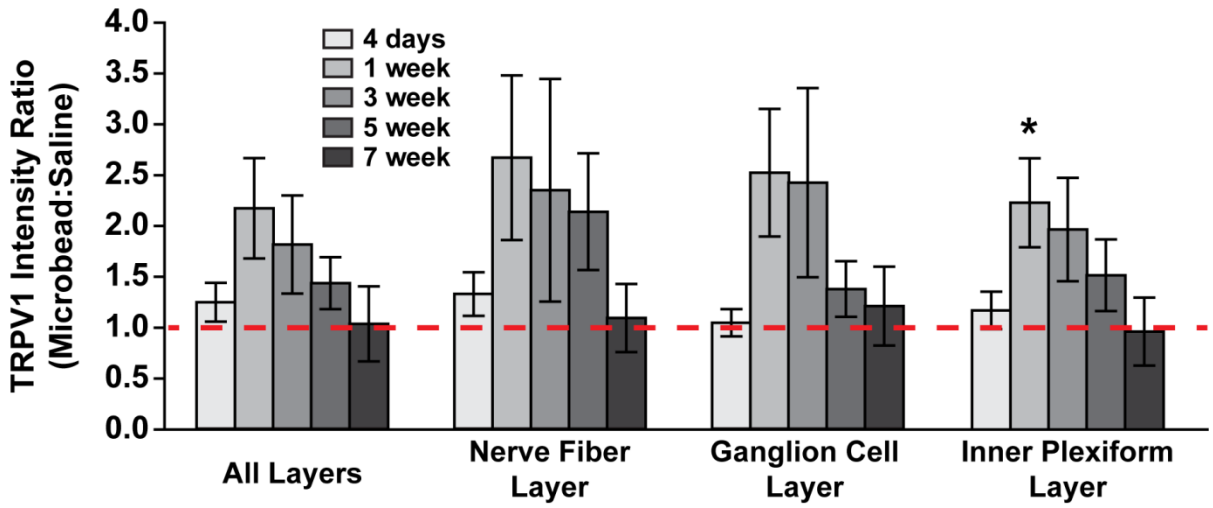

Figure 3.5. Microbead-induced IOP elevation transiently increases TRPV1 protein levels. Ratio of fluorescent intensity (microbead:saline) of immuno-labeled TRPV1 in sections of vertical retinal tissue. All retinal layers exhibited a trend toward transient elevation at 1 week, which was significant for the inner plexiform layer (*, p = 0.037, *n* = 3-5 animals per timepoint).

Modulation of dendritic and synaptic protein levels by elevated IOP

Based on immunohistochemical detection of TRPV1 in the inner plexiform layer (IPL; Figure 3.4), which includes dendrites of RGCs, we wanted to examine if changes in TRPV1 coincided with changes in dendritic and synaptic protein levels in the IPL. To determine if changes observed for TRPV1, MAP2, and PSD-95 expression were not due to tissue quality, non-specific binding of antibodies, or technical issues, we performed negative and positive controls using tissue from our time course animals. For negative control slides, I used the 1week timepoint, where TRPV1 labeling intensity was the strongest. As a negative control, no primary antibody was used in the staining protocol, and no non-specific binding of secondary antibody was observed in our tissue (Figure 3.6A). As a positive control, an antibody against choline acetyltransferase (ChAT) protein was used to show that our immunolabeling protocol yields specific binding. ChAT labeling is enriched at two synaptic layers within which cholinergic

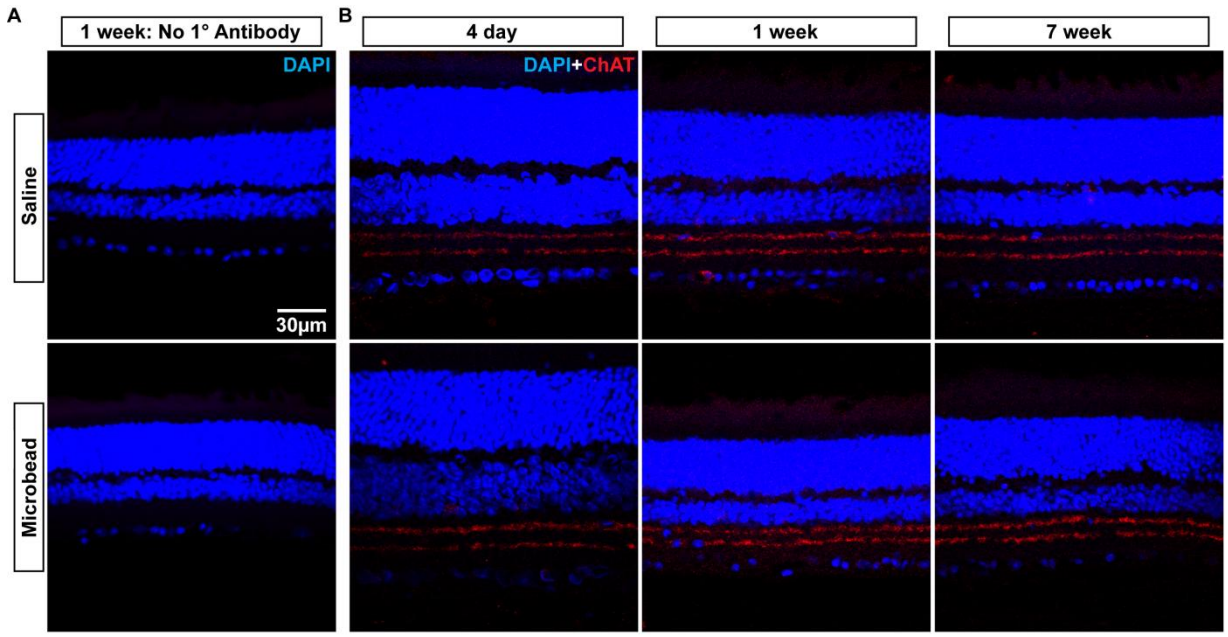

Figure 3.6. Controls for immunohistochemistry protocol. ***A,*** As a negative control, primary antibody was omitted from the immunolabeing protocol to examine potential non-specific binding of secondary antibody to tissue. Sections from the same 1 week tissue that exhibited the strongest immunolabeling for TRPV1 were used for this negative control. ***B,*** As a positive control, choline acetyltransferase (ChAT) protein exhibits specific binding in distinctive layers of the IPL. This marker, associated with cholinergic amacrine cells, exhibits a uniform level of expression across all timepoints and treatments.

amacrine cells form connections with RGCs. Our staining labeled these synaptic layers (Figure 3.6B), as seen in other studies (Kang et al., 2004; Feng et al., 2006; Samuel et al., 2011).

Dendritic MAP2 protein levels exhibited a transient increase in fluorescence in microbead tissue from 4 days to 3 weeks (Figure 3.7). We observed localization of MAP2 protein in the inner plexiform layer of the retina, as seen previously (Okabe et al., 1989; Seki et al., 2003; Vugler et al., 2008). Postsynaptic protein PSD-95 exhibited a similar trend in fluorescence, which also peaked at 3 weeks before decreasing (Figure 3.8). We observed localization of PSD-95 protein in the inner plexiform layer of the retina, as seen previously (Grunert et al., 2002; Stevens et al., 2007). Fluorescent intensity was quantified and averaged across IPL tissue area for both MAP2 and PSD-95 (Figure 3.9).

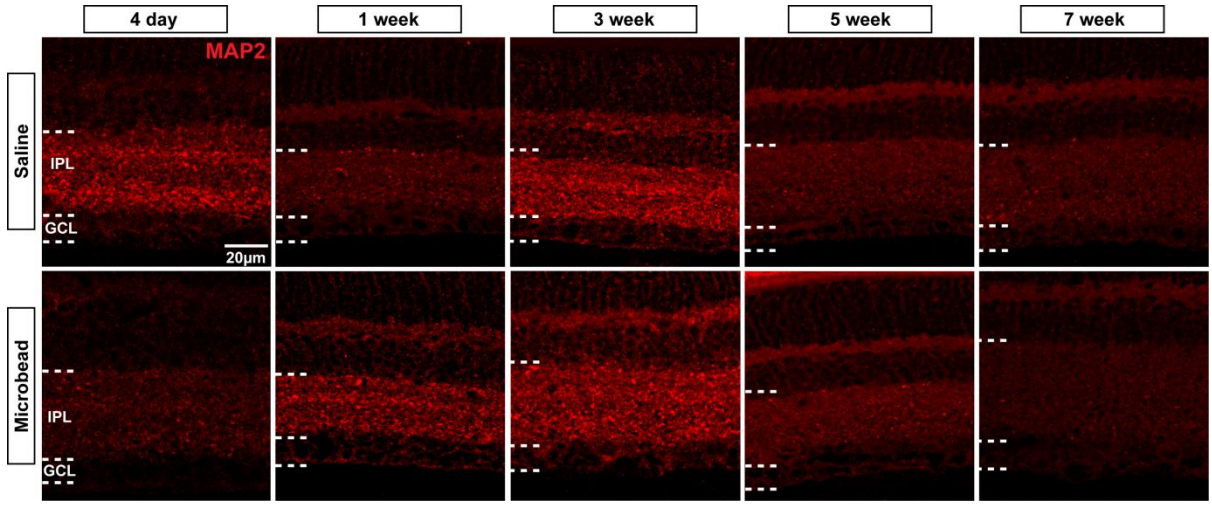

Figure 3.7. Dendritic MAP2 protein levels transiently increase following IOP elevation. Vertical sections of C57 mouse retinas immuno-labeled for dendritic MAP2 protein. MAP2 intensity transiently increases in retinas from microbead-injected eyes, especially in the IPL synaptic layer containing the dendrites of RGCs. IPL: inner plexiform layer.

The MAP2 microbead:saline fluorescent intensity ratio was significantly increased at the 1-week timepoint ($p = 0.012$; Figure 3.9A). This ratio remained elevated at 3 weeks, though this timepoint was not significantly elevated. At 5 and 7 weeks, the MAP2 ratio decreased and was not significantly different from unity. Similarly, the PSD-95 microbead:saline fluorescent intensity ratio increased from 4 days to 1-week and 3-week timepoints (Figure 3.9B). This ratio returned to levels near unity at 5- and 7-week timepoints. Similar to MAP2, the 1-week timepoint was significantly elevated above unity ($p = 0.05$). In the case of both MAP2 and PSD-95, elevation of protein expression in the IPL was transient. This transient nature matches well with the changes seen in TRPV1 expression in tissue from the same animals (Figures 3.4 and 3.5).

Colocalization of TRPV1 with postsynaptic protein PSD-95

TRPV1 and postsynaptic protein PSD-95 both exhibit transient increases in intensity levels (Figures 3.5 and 3.9B). This transient increase coincides, as is apparent in co-labeling of the two proteins in sections (Figure 3.10). Using orthogonal views across several serial optical sections of this co-labeled tissue, it appears that TRPV1 protein exhibits an increase in colocalization with PSD-95 after 1 week of IOP elevation (Figure 3.11). This increase in colocalization was diminished at 5 weeks, though some examples of overlapping TRPV1 and PSD-95 puncta are still apparent (Figure 3.11, arrows).

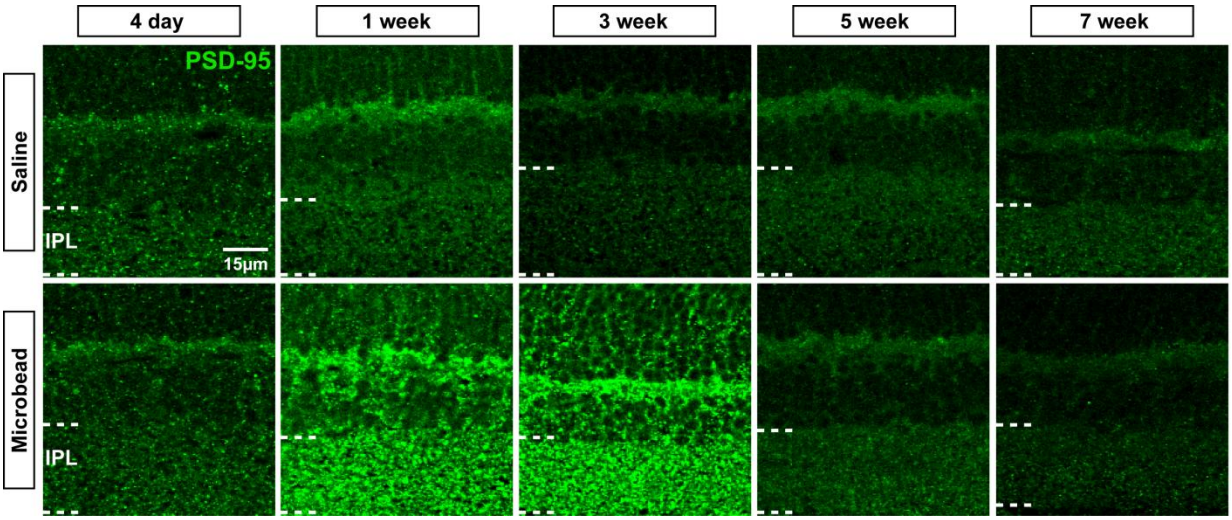

Figure 3.8. Postsynaptic PSD-95 protein levels transiently increase following IOP elevation. Vertical sections of C57 mouse retinas immuno-labeled for postsynaptic PSD-95 protein. PSD-95 intensity transiently increases in retinas from microbead-injected eyes, especially in the IPL synaptic layer containing the dendrites of RGCs. IPL: inner plexiform layer.

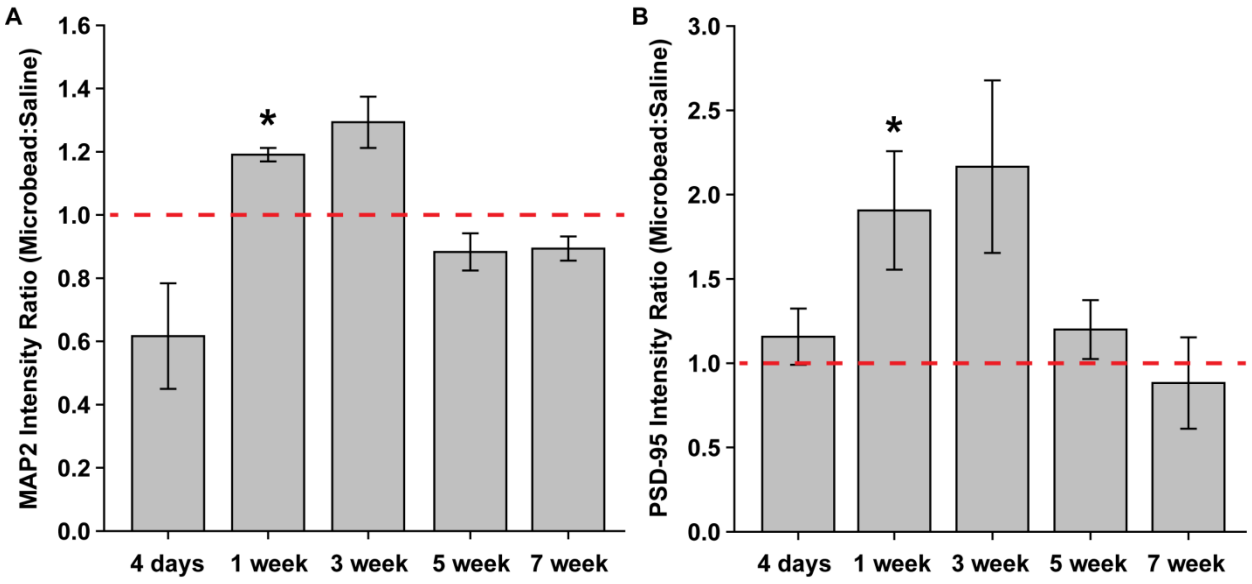

Figure 3.9. Quantification of PSD-95 and MAP2 protein levels in the inner plexiform layer. Red dashed line indicates equal levels of protein expression between eyes, where microbead:saline ratio equals one. ***A,*** Ratio of fluorescent intensity (microbead:saline) of immunolabeled MAP2 in sections of vertical retinal tissue. * = 0.012, *n* = 3-5 animals per group. ***B,*** Ratio of fluorescent intensity (microbead:saline) of immunolabeled PSD-95 in sections of vertical retinal tissue. * = 0.05, *n* = 3-5 animals per timepoint.

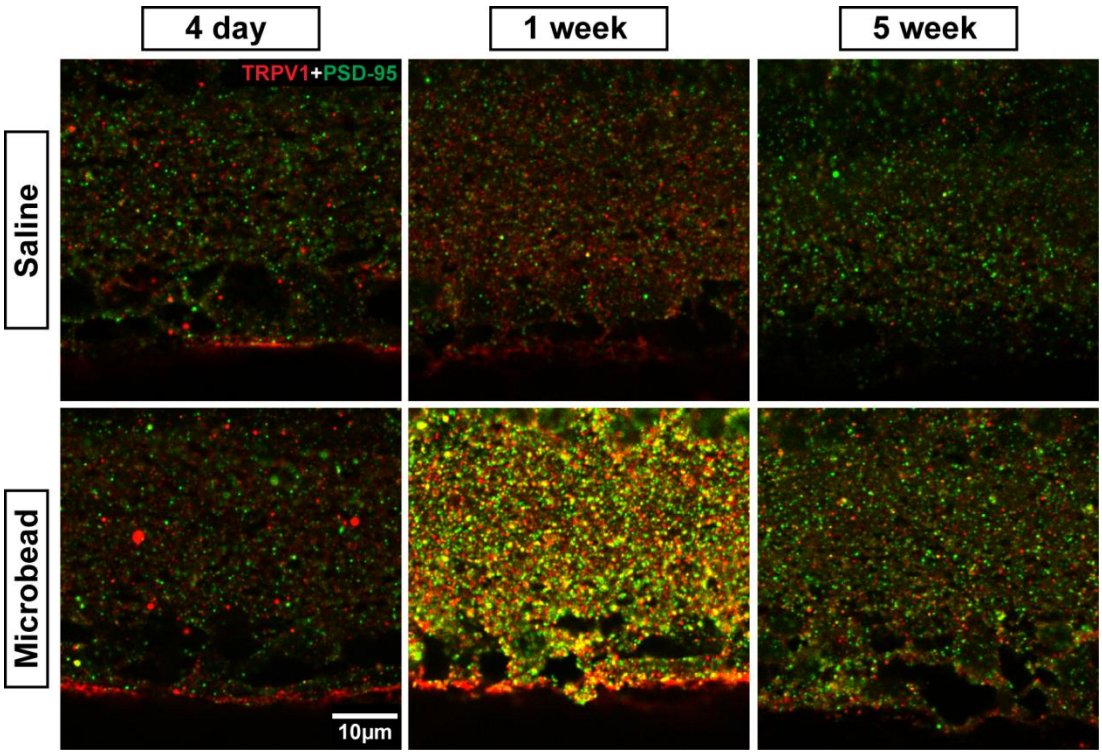

Figure 3.10. Ocular hypertension transiently increases TRPV1 and PSD-95 protein in inner plexiform layer. Vertical retinal sections from C57 mouse eyes labeled for TRPV1 (red) and postsynaptic protein PSD-95 (green). Eyes were injected with microbeads (bottom row) to elevate IOP or saline (top row) as a control.

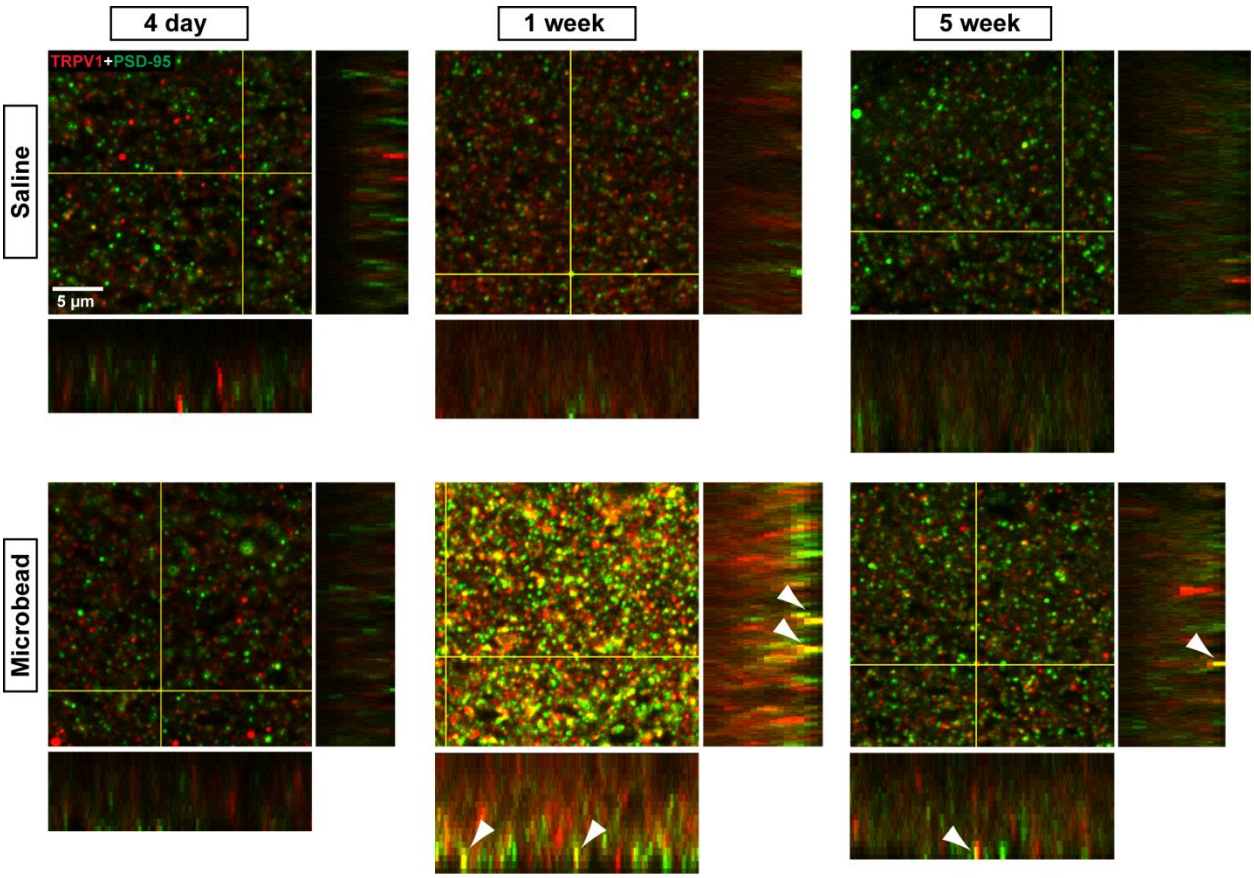

Figure 3.11. Ocular hypertension transiently increases proximity of TRPV1 and PSD-95 proteins. Micrographs of inner plexiform layer from vertical sections through C57 mouse retina. Eyes were injected with microbeads (bottom row) to elevate IOP or saline (top row) as a control. Orthogonal views (at side and bottom of each micrograph) represent serial stacks compiled across tissue depth at each yellow line. *X*-axis line represents orthogonal image below microgaph and *Y*-axis line represents orthogonal image at side of micrograph. Arrowheads represent TRPV1 (red) and PSD-95 (green) puncta in close apposition with each other (yellow).

Discussion

Within the CNS, it is apparent that TRPV1 expression in neurons is affected by injurious stressors and pathology. Increases in TRPV1 protein were observed in lingual nerve injury (Biggs et al., 2007), chronic constriction injury (Kanai et al., 2005), and gentamicin-induced ototoxicity (Ishibashi et al., 2009). In human tissue, increases in TRPV1 protein levels were found in aged and photoaged skin and its associated nerve fibers (Lee et al., 2009), as well as in tissue collected from patients with traumatic and diabetic neuropathy (Facer et al., 2007).

Within the retina, changes in TRPV1 protein levels have been observed accompanying elevated IOP *in vivo*. DBA/2 mice often exhibit gradual IOP elevation with age, which is followed by progressive degeneration of RGCs (John et al., 1998; Inman et al., 2006). In aged DBA/2 mice with elevated pressure, qualitative analysis of retinal immunolabeling indicated an apparent increase in TRPV1 localization to the inner plexiform layer (Sappington et al., 2009). In contrast, a model of retinal ischemia induced by high intraocular pressure saw whole retinal levels of TRPV1 decrease (Nucci et al., 2007b). This study used a transient, nonphysiological IOP (120 mmHg for 45 minutes), which is a much more robust insult than the gradual elevations (pressures of 17.7 and 21.8 mmHg) seen in the DBA/2 study (Nucci et al. 2007; Sappington et al. 2009). Though these studies affect TRPV1 protein levels in opposite directions, they both indicate that IOP likely influences TRPV1 protein levels in the retina.

Using our model of microbead-induced IOP elevation, we were able to determine how increased pressure affected TRPV1 levels and localization. Our studies of *Trpv1* mRNA levels indicated no significant changes in the ratio between microbead- and saline-injected eyes. We did, however, see TRPV1 protein levels increase transiently at 1 week following microbead injection, and this effect was significant within the inner plexiform layer upon quantification.

Although not statistically significant, qualitative assessment indicates that TRPV1 protein levels transiently increased across most layers of the retina. It therefore may be the case that this transient increase is biologically, but not statistically, significant. This discrepancy between mRNA and protein expression could be due to when mRNA levels were measured (10 days versus 7 days for protein) and that any increase in *Trpv1* mRNA had already returned to baseline. Our *Trpv1* qPCR results are consistent with an early and transient increase in TRPV1 protein after injury. To confirm this, future studies should focus on earlier timepoints to determine how soon after microbead injection *Trpv1* mRNA increases. The pressure elevation for this cohort of animals was also lower and less consistent than it was for cohorts used in other experiments, so this study could be improved with earlier timepoints and with mice exhibiting robust, consistent IOP elevation following microbead injection.

Following IOP elevation, we also observed a transient increase in postsynaptic protein PSD-95 in the inner plexiform layer at 1 week post-injection. Other studies in the rodent retina have seen similar transient increases in PSD-95 following injury. In rat retina following optic nerve injury, an initial reduction in PSD-95 levels was observed 1 day after injury, followed by a transient increase (above control levels) that peaked at 7 days (Li et al., 2012). This pattern was observed in both mRNA and protein levels from whole retinal tissue. In another study using a model of rat sciatic nerve injury, an initial decrease in PSD-95 protein was also observed 6 hours after crush, which was sustained before levels rebounded at 1 week and increased above basal levels at 2 and 4 weeks (Gao et al., 2008). Similar to these injury studies, our results seem to indicate a transient increase in PSD-95 expression in response to IOP-induced stress. It is known that PSD-95 is required for activity-dependent synapse stabilization (Ehrlich et al., 2007), so

upregulation of the protein at synaptic sites may help stabilize syanpses that are in the process of being compromised.

Similar to TRPV1 and PSD-95 expression, we observed a significant elevation in MAP2 levels in the inner plexiform layer 1 week after microbead injection. The initial decrease in MAP2 expression at 4 days post-injection may coincide with compromised RGC activity due to the stressor of IOP elevation, as loss of MAP2 is an early indicator of neuronal injury (Akulinin and Dahlstrom, 2003; Huh et al., 2003). In a rodent model of focal cerebral ischemia, it was observed that most neurons progressively lost MAP2 immostaining, however some neurons in the central ischemic core exhibited increased MAP2 staining (Dawson and Hallenbeck, 1996). Maintenance of dendrites is activity-dependent (Lin and Koleske, 2010), and neuronal depolarization is known to increase dendritic MAP2 levels and association with microtubules (Roberts et al., 1998; Vaillant et al., 2002). We hypothesize that RGCs may respond to stressors by boosting activity (Ward et al., 2014), which may explain the rebound and increase in MAP2 levels observed at our 1 week timepoint. Evidence of dendritic remodeling has been observed in neurodegenerative diseases including ALS, AD, and glaucoma (Karpati et al., 1988; Arendt et al., 1995; Baloyannis, 2009; Liu et al., 2011). Likewise, in studies examining cortical tissue damaged by ischemia, increased MAP2 staining observed in peri-lesional areas is thought to indicate compensatory restructuring in neurons that survive the insult (Bidmon et al., 1998; Li et al., 1998; Adkins-Muir and Jones, 2003).

Our co-labeling studies with TRPV1 and PSD-95 indicated that levels of both proteins increased transiently following IOP elevation. Based on studies of pre-embedding immunogold labeling of TRPV1 in hippocampus and extended amygdala, it appears that TRPV1 may exhibit perisynaptic expression rather than labeling associated directly with the postsynaptic density

(Puente et al., 2011; Puente et al., 2014). Qualitatively, our co-labeling data indicate that at 1 week post-injection, TRPV1 and PSD-95 appear to be more closely associated with each other. Though we would have liked to pursue similar studies with MAP2, species cross-reactivity between our primary antibodies prevented us from colabeling our sections with both TRPV1 and MAP2. Despite this experimental limitation, we are able to conclude that TRPV1, MAP2, and PSD-95 all exhibit a transient increase in protein level within the IPL following 1 week of IOP elevation. It is important to note that these are simply changes in protein level, and our MAP2 and PSD-95 results do not necessarily provide information about what is happening to the dendritic structures themselves.

Our working hypothesis is that TRPV1 functions as an intrinsic stress responder that slows down RGC degeneration by increasing excitatory activity at RGC synapses. In the DBA/2 mouse model of glaucoma, RGCs experiencing degeneration regularly exhibit dendrites with decreased complexity that lack higher-order branching, an indication of dendritic pruning (Jakobs et al., 2005). Likewise, it is known that synaptic activity is a crucial factor in long-term synapse maintenance (Lin and Koleske, 2010). Increased TRPV1 activity at RGC synapses may counter the dendritic pruning seen in glaucoma, as retention of synapses requires maintenance of synaptic activity. Our study and others have shown that eyes with elevated IOP exhibit increased levels of TRPV1 in the inner plexiform layer of the retina (Sappington et al., 2009), supporting the idea of increased synapse potentiation in response to stress. The inner plexiform layer includes extensive synaptic connections between RGC dendrites and bipolar cells, so the increases in TRPV1, PSD-95, and MAP2 that we observed in this layer may be part of a stress response to stabilize dendritic and synaptic structures in response to elevated IOP.

CHAPTER 4

TRPV1 INFLUENCES RETINAL GANGLION CELL DENDRITIC COMPLEXITY

Introduction

Within the CNS, it is well understood that TRPV1 modulates synaptic transmission in a multitude of neuronal systems (Marsch et al., 2007; Gibson et al., 2008; Li et al., 2008; Chavez et al., 2010; Grueter et al., 2010; Bennion et al., 2011). Previous studies have used subcellular localization techniques to show that TRPV1 may exert such modulatory effects in dendritic and perisynaptic structures (Puente et al., 2011; Puente et al., 2014). *In vitro* cultures of RGCs indicate an expression of TRPV1 throughout neurites (Sappington et al., 2009), and our studies in Chapter 3 demonstrate that TRPV1 may localize to RGC dendrites *in vivo* (Figures 3.3, 3.9, 3.10). Intriguingly, following microbead-induced IOP elevation, temporal changes in TRPV1 and in dendritic and synaptic protein levels within the inner plexiform layer exhibited similar dynamics (Figures 3.4 and 3.8), consistent with a synaptic modulatory role of TRPV1.

We have demonstrated in Chapter 2 that TRPV1 promotes RGC survival following IOP elevation *in vivo* (Ward et al., 2014), so it is important to consider how our knowledge of TRPV1 expression and localization pairs with this function. Having observed a putative increase in dendritic TRPV1 expression, it is possible that TRPV1 exerts its effects at the synapse to help RGCs respond to stress and survive. It is worthwhile to examine prospective mechanisms such as this one because previous work has demonstrated that merely preventing RGC apoptosis does not also prevent degenerative progression. For example, deleting the *Bax* pro-apoptosis gene does not prevent glaucomatous axonopathy despite successfully protecting the RGC soma from

death (Libby et al., 2005). It is apparent from this result that the response of the RGC to insult will involve signal integration between dendrites, soma, and axon, as well as interactions with the cell's synaptic contacts (Morquette and Di Polo, 2008).

Our hypothesis is that TRPV1 in the dendrites may influence overall RGC survival by modulating synaptic activity of RGCs in the retina. If TRPV1 can help prevent dendritic retraction, loss of synaptic connections, and reduction in synaptic activity in response to stress, RGCs would stand a better chance of surviving. In line with this hypothesis, it is believed that many CNS neurons have an intrinsic tuning ability with respect to their firing rates, and that they use this tuning as a method for homeostatic synaptic plasticity. Neurons involved in excitatory synapses are known to monitor their own activity, and in turn modify synaptic strength at their dendrites (Ibata et al., 2008; Turrigiano, 2008; Lee, 2012). This process appears to involve trafficking of glutamatergic receptors to or from synaptic sites (Turrigiano, 2008). Such mechanisms have already been demonstrated to involve Ca^{2+}-permeable AMPA and NMDA receptors, and may be partially regulated by Ca^{2+} signaling in dendrites (Yu and Goda, 2009; Lee, 2012).

It has already been hypothesized that this homeostatic synaptic plasticity is used in periods of elevated plasticity, such as recovery of neuronal function following injury (Lee, 2012). In support of this hypothesis, it is known that Ca^{2+}-permeable AMPA receptors are upregulated in neurons and their synaptic sites in models of neuronal insult and injury (Liu et al., 2006; Spaethling et al., 2008). TRPV1 may similarly be upregulated in dendritic and perisynaptic sites following injury, making it a prime candidate for regulating homeostatic plasticity like other Ca^{2+}-permeable channels.

Given the potential for TRPV1 to influence synapse survival following injury, we examined whether *Trpv1*-/- influenced dendritic morphology following microbead-induced IOP elevation. If TRPV1 influences synaptic homeostasis as part of an RGC survival mechanism, then we would predict that *Trpv1*-/- mice will exhibit accelerated dendritic retraction following IOP elevation. We examined this by quantifying RGC morphometric data and conducting Sholl analyses of dendrite complexity in C57 and *Trpv1*-/- mice after 2 and 4 weeks of IOP elevation.

Materials and Methods

Intracellular labeling of RGCs

Young C57 and *Trpv1*-/- mice (1 month) received injections of microbeads to elevate IOP for either ~2 or ~4 weeks (durations ranged from 12-15 days and 25-28 days, respectively) as described previously (Sappington et al., 2010). All procedures and IOP measurement methods followed those described in Chapter 2 Methods. In preparation for intracellular labeling of RGCs, mice were sacrificed by cervical dislocation followed by decapitation. Eyes were enucleated and dissected in oxygenated AMES media (Sigma) to remove the retina, which was then manually cleared of vitreous. Retinas were hemisected and transferred to a 0.5 mL enzyme solution containing hyaluronidase (300 units) and collagenase (120 units) to remove any remaining vitreous (Schmidt and Kofuji, 2011). This solution was placed in a dark oxygenated chamber and gently rocked for 10 minutes. Retinal halves were transferred to a holding chamber containing oxygenated AMES media for a minimum of 15 minutes. Retinal halves were placed RGC-side up in a recording chamber mounted on the stage of an Olympus BX50W1 upright fluorescent microscope (Olympus America) enclosed by a Faraday cage. The recording chamber was perfused with fresh oxygenated AMES at a rate of 2 mL/min.

Borosilicate glass microelectrodes with a resistance of 5-10 MOhms were pulled on a p-97 Flaming/Brown puller (Sutter Instruments, Sarasota, FL) and filled with a solution containing (in mM) K-gluconate (130), KCl (10), HEPES (10), $MgCl_2$ (2), EGTA (1), Na_2ATP (2), and NaGTP (0.3). For intracellular labeling, 1% Lucifer Yellow (LY, lithium salt; Life Technologies, Grand Island, NY) was also included in the internal solution. These microelectrodes were placed against select RGC somas using light positive pressure to clear the inner limiting membrane found on the surface of the retina. Gentle suction was then applied to form a gigaohm seal with

the RGC. Next, stronger bursts of rapid suction were applied to rupture the plasma membrane and gain access to the cell while keeping the cell intact. The result was a whole-cell patch clamp configuration. Cells were then labeled with LY via simple diffusion. Following a period of no less than 15 minutes, the microelectrode was gently removed, allowing the plasma membrane to reseal. This resulted in individual fluorescently-labeled RGCs. Within the retinal halves, multiple RGCs with non-overlapping dendritic trees were filled with LY. After labeling, retinal halves were transferred to 4% paraformaldehyde (PFA, Sigma) and incubated at 4ºC for a minimum of 1 day. Retinas were rinsed in PBS, whole-mounted on a glass slide, and cover slipped for confocal imaging.

Morphometric quantification of RGC dendrites

Confocal images of LY-filled RGCs from whole-mounted retinal halves were imaged using an Olympus FV-1000 inverted confocal microscope. Only cells within the ganglion cell layer with obvious axons were imaged and analyzed in order to distinguish between RGCs and displaced amacrine cells. Using confocal images (0.101 mm^2 per image), RGC somas and dendrites were traced manually using Adobe Illustrator CS5 (version 15.0.0, Adobe Systems Incorporated, San Jose, CA).

Somal area was measured using the ImageJ software (National Institutes of Health, Bethesda, MD) area quantification measurement tool (Figure 4.1A, yellow). Similarly, dendritic area was measured as the area bounded by a line connecting the outermost points of the dendrites around the edge of the dendritic tree (Figure 4.1A, cyan). Total dendritic length was measured in Image-Pro Plus (version 5.1.0.20, Media Cybernetics, Rockville, MD) using the dendrite length measurement routine (Figure 4.1A, black). Dendritic density was calculated by dividing a cell's

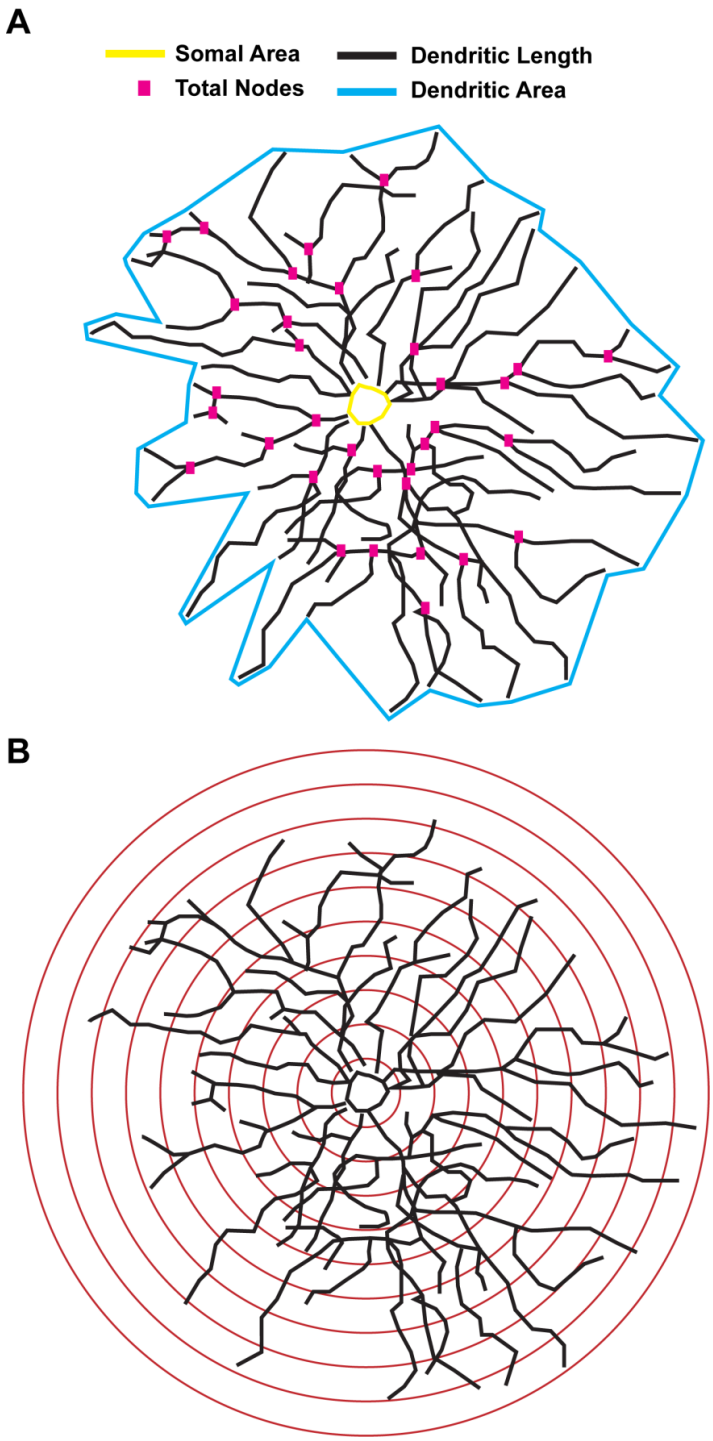

Figure 4.1. Quantification of RGC dendritic morphometry. ***A,*** Confocal micrographs of Lucifer Yellow-filled RGCs were traced to measure several morphometric features, such as somal area (yellow), dendritic length (black), dendritic area (cyan), and total dendritic nodes (magenta). ***B,*** Dendritic morphology and complexity was examined by conducting Sholl analysis on RGC tracings. Concentric circles of increasing radius were centered about the RGC soma, and we quantified the number of dendritic intersections with each circle.

total dendritic length by its dendritic area. Nodes, or regions where dendrites branch, were manually quantified in Photoshop using the count tool (Figure 4.1A, magenta). Nodal density was calculated by dividing the number of nodes in the cell's dendritic tree by the dendritic area.

Sholl analysis of RGC dendrites

Sholl analysis of dendrites was conducted on images of traced dendrites using ImageJ software. Before analysis, the software was calibrated to the resolution of our original confocal images (1.614 pixels/µm) to guarantee correct measurements. Running the Sholl analysis routine in ImageJ, we drew a line from the center of the RGC soma to the farthest dendrite tip. Concentric circles were drawn around the soma, with a radius step size of 10 µm. This routine sampled the number of dendritic branches that intersected the circular rings drawn around the soma (Figure 4.1B).

Statistical methods

Group averages were calculated and compared in SigmaPlot (version 11.1, SYSTAT) using two-sided *t*-tests for all data passing Shapiro-Wilk normality tests. For data that did not pass Shapiro-Wilk normality, non-parametric Mann-Whitney Rank Sum tests were used. Error as reported in text and on bar graphs represents mean ± SEM.

Results

Microbead-induced IOP elevation in C57 and *Trpv1*-/- mice

To examine whether IOP elevation induces differential morphological changes between C57 and *Trpv1*-/- mice, we injected C57 and *Trpv1*-/- mouse eyes with microbeads (Sappington et al., 2010; Chen et al., 2011). A single microbead injection was used to elevate IOP in these mice for either 2 weeks or 4 weeks (Figure 4.2A). Cohorts of 2 week and 4 week mice were examined in both C57 and *Trpv1*-/- groups.

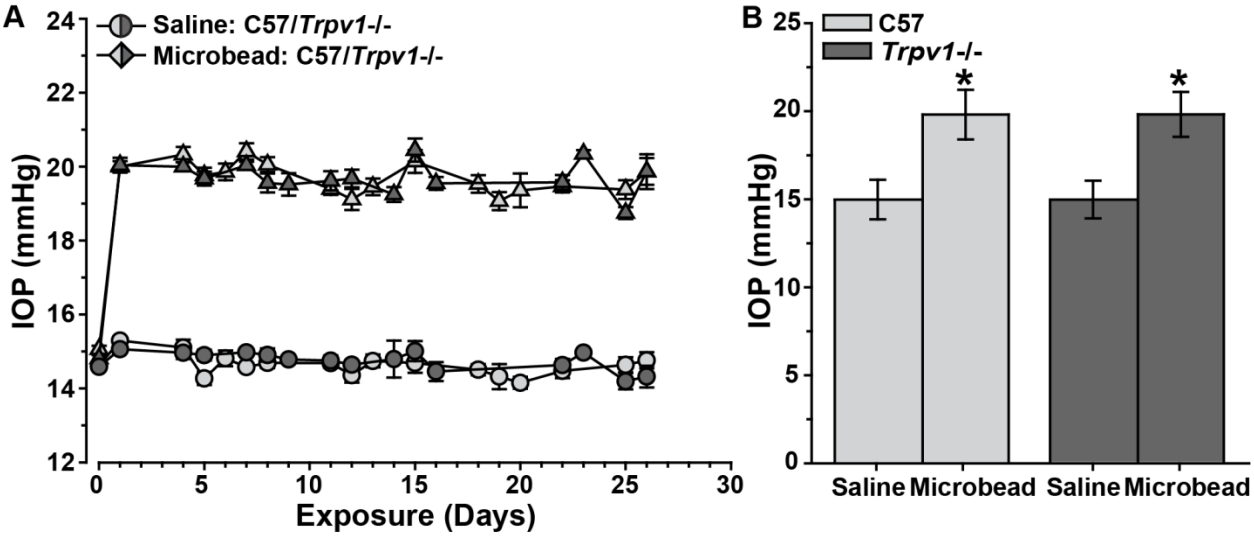

Figure 4.2. Microbead-induced IOP elevation for animals used in morphological studies. ***A,*** Measurements of IOP taken from C57 and *Trpv1*-/- mice injected with microbeads. Baseline IOPs (Day 0) were measured prior to injection. Each animal received an injection of microbeads in one eye and an equivalent volume of saline in the contralateral eye. Each line represents IOPs of animals from cohorts sacrificed at either 2-week or 4-week timepoints following injection. ***B,*** Averaged IOP measurements for C57 and *Trpv1*-/- animals for all days post-injection (Days ≥1). *, $p \leq 0.009$.

Post-injection IOPs were averaged separately for C57 and *Trpv1*-/- mice (Figure 4.2B). For C57 mice, post-injection IOPs indicate an approximately 32% elevation in microbead-injected eyes compared to contralateral eyes injected with an equivalent volume of saline.

Likewise, *Trpv1*-/- mice also exhibited an approximately 32% elevation in microbead-injected eyes compared to saline-injected eyes. This IOP elevation was statistically significant for both C57 ($p = 0.009$) and *Trpv1*-/- mice ($p = 0.007$). No difference in IOP was observed between genotypes for microbead- or saline-injected eyes ($p > 0.998$).

Morphometric analysis of RGCs from C57 and *Trpv1*-/- mice

Following either 2 or 4 weeks of IOP elevation, retinas were collected from C57 and *Trpv1*-/- mouse eyes to conduct morphometric analysis of RGCs. Micrographs were created for Lucifer Yellow-filled RGCs, and tracings of cell somas and dendrites were produced. Micrographs and tracings were gathered for filled cells from C57 (Figures 4.3 and 4.4, respectively) and *Trpv1*-/- mice (Figures 4.5 and 4.6, respectively). Both C57 and *Trpv1*-/- mice exhibited a variety of morphological subtypes with respect to dendritic structure, consistent with the known diversity of RGC subtypes (Coombs et al., 2006). At least 20 filled RGCs were used in analysis from each cohort studied (n = 20-39 RGCs per cohort).

RGC somal area ranged from 148.42 ± 11.75 to 178.95 ± 25.94 μm^2 across all groups, which matches with data previously published from mouse studies (Coombs et al., 2006). For comparisons made within each genotype (C57 vs. *Trpv1*-/-) and within treatment group (microbead injected vs. saline injected), no significant differences were observed in RGC somal area (Figure 4.7A). RGC dendritic area ranged from 33,197 ± 3,171 to 51,594 ± 8,167 μm^2 across all groups, which was similar to measurements reported previously (Coombs et al., 2006; Mazzoni et al., 2008). No significant differences in area were observed due to genotype or microbead injection (Figure 4.7B). Total RGC dendritic length ranged from 2,015.7 ± 159.8 to 2,557.6 ± 272.8 μm across all groups, indicating a wide variety across RGC subtypes, as has

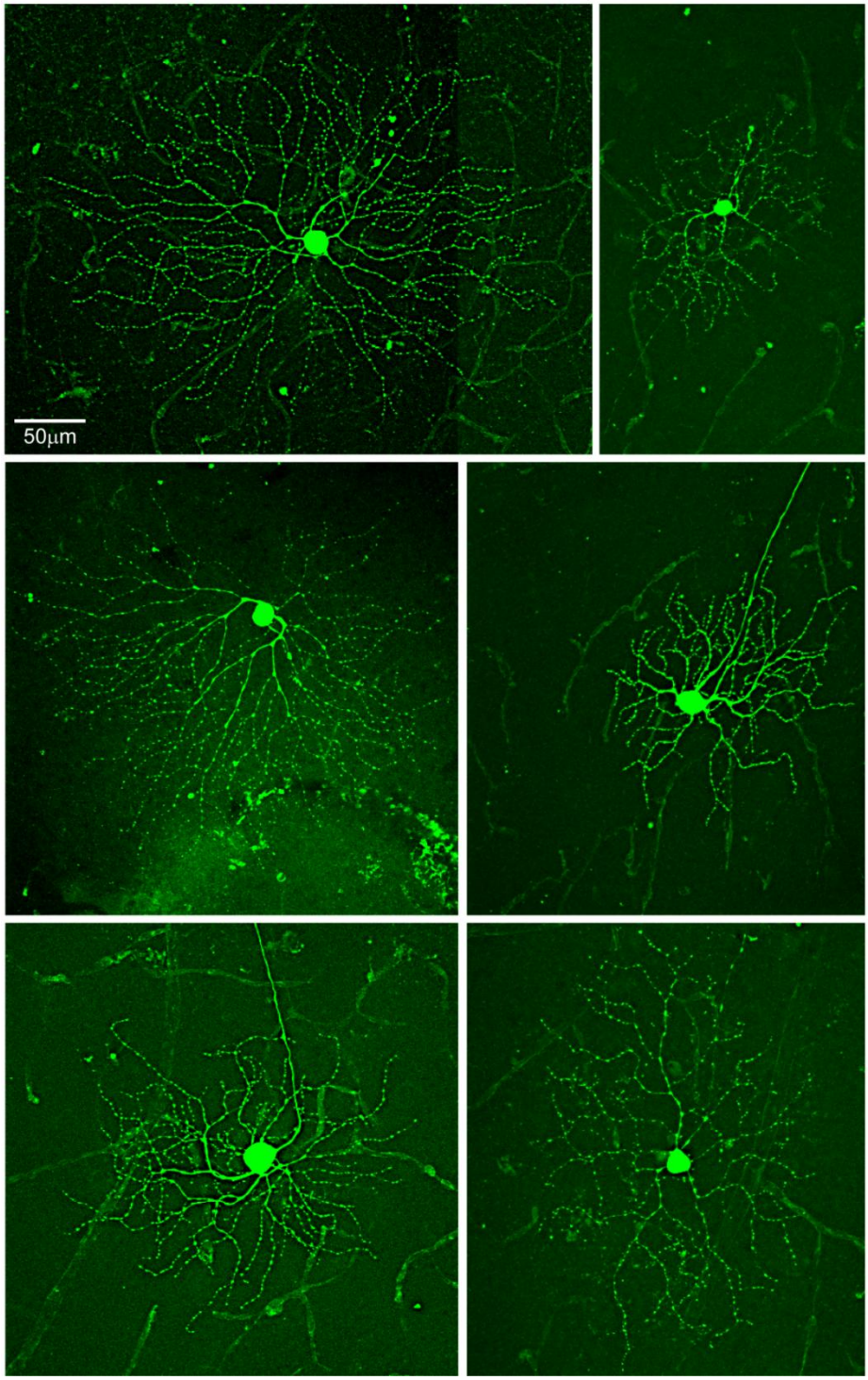

Figure 4.3. Lucifer Yellow-filled RGCs from C57 mice. Confocal micrographs from C57 mouse retinas of RGCs filled with Lucifer Yellow exhibit a variety of morphological subtypes. Micrographs were obtained from C57 mice following either 2 or 4 weeks of microbead-induced pressure elevation and were used for measurements and calculations of morphometric data.

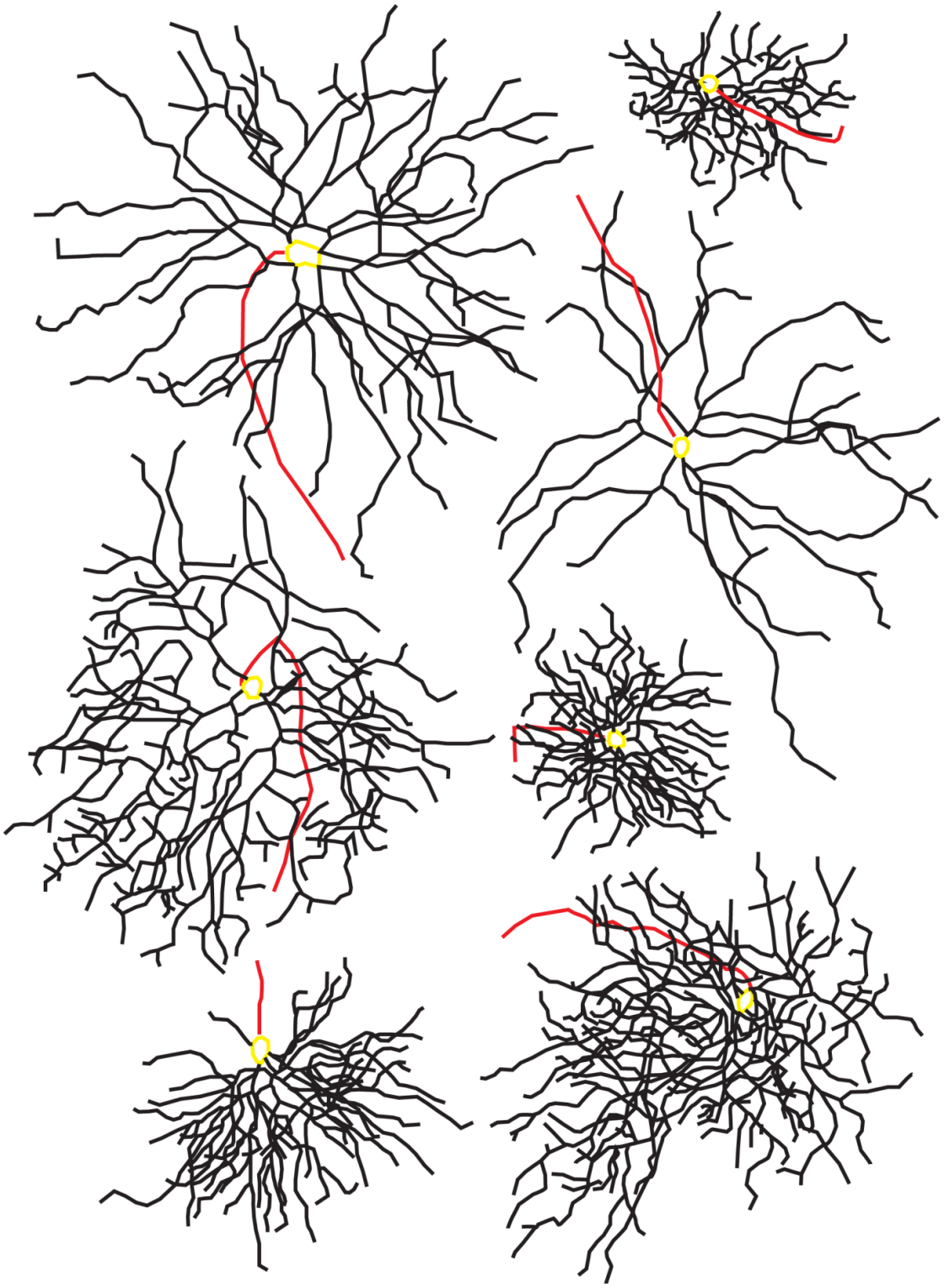

Figure 4.4. Traced C57 mouse RGCs used for morphometric measurements. Examples of tracings generated from Lucifer Yellow-filled RGCs from C57 mice. Tracings indicate RGC dendrites (black), soma (yellow), and axon (red). Measurements of soma area, dendritic area, dendritic length, and dendritic nodes were derived from these tracings.

been observed previously (Coombs et al., 2006; Mazzoni et al., 2008). Significant differences in total dendritic length were observed between 4-week saline-injected mice from C57 and *Trpv1*-/- cohorts ($p = 0.042$, Figure 4.7C). These comparisons were no longer significant when dendritic length was normalized to dendritic area to calculate dendritic density, which ranged from 57.6 ± 2.9 to 66.1 ± 4.3 nm^{-1} (Figure 4.7D).

Total dendritic nodes, which are points where dendrites branch, ranged in number from 31.4 ± 2.2 to 48.5 ± 5.2 nodes across all groups, similar to counts reported previously (Mazzoni et al., 2008). Significant differences in total dendritic nodes were observed between 4-week saline-injected mice from C57 and *Trpv1*-/- cohorts ($p = 0.008$, Figure 4.7E). These comparisons were no longer significant when total dendritic node counts were normalized to dendritic area to calculate dendritic nodal density, which ranged from $9.46 \times 10^{-4} \pm 9.1 \times 10^{-5}$ to $1.27 \times 10^{-3} \pm 1.5 \times 10^{-4}$ nodes/μm^2 (Figure 4.7F).

Sholl analysis of RGCs from C57 and *Trpv1*-/- mice

All RGCs used in morphometric analyses were used for subsequent Sholl analysis to examine branching complexity at consecutive 10 µm distance increments from the RGC soma. RGCs from mice sacrificed 2 weeks post-injection exhibited peak dendritic complexity approximately 70 µm away from their somas (Figure 4.8A). *Trpv1*-/- mice appeared to exhibit decreased complexity compared to C57 mice at this distance. For both C57 and *Trpv1*-/- animals, it did not appear that there was an effect of microbead injection on dendritic branching. RGCs from mice sacrificed 4 weeks post-injection all exhibited a peak dendritic complexity approximately 70-80 µm from their somas (Figure 4.8B). *Trpv1*-/- mice again appeared to

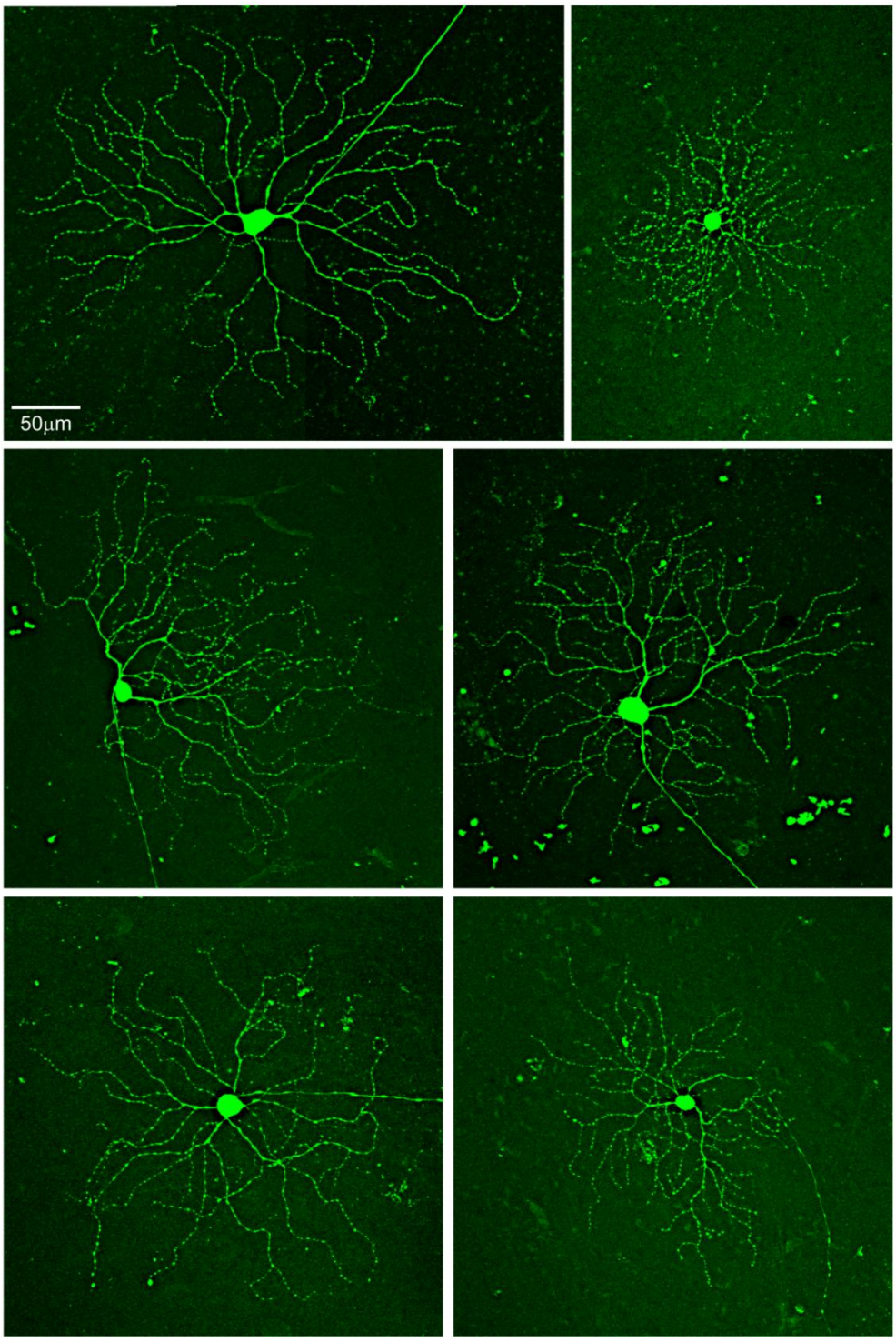

Figure 4.5. Lucifer Yellow-filled RGCs from *Trpv1*-/- mice. Confocal micrographs from *Trpv1*-/- mouse retinas of RGCs filled with Lucifer Yellow exhibit a variety of morphological subtypes. Micrographs were obtained from *Trpv1*-/- mice following either 2 or 4 weeks of microbead-induced pressure elevation and were used for measurements and calculations of morphometric data.

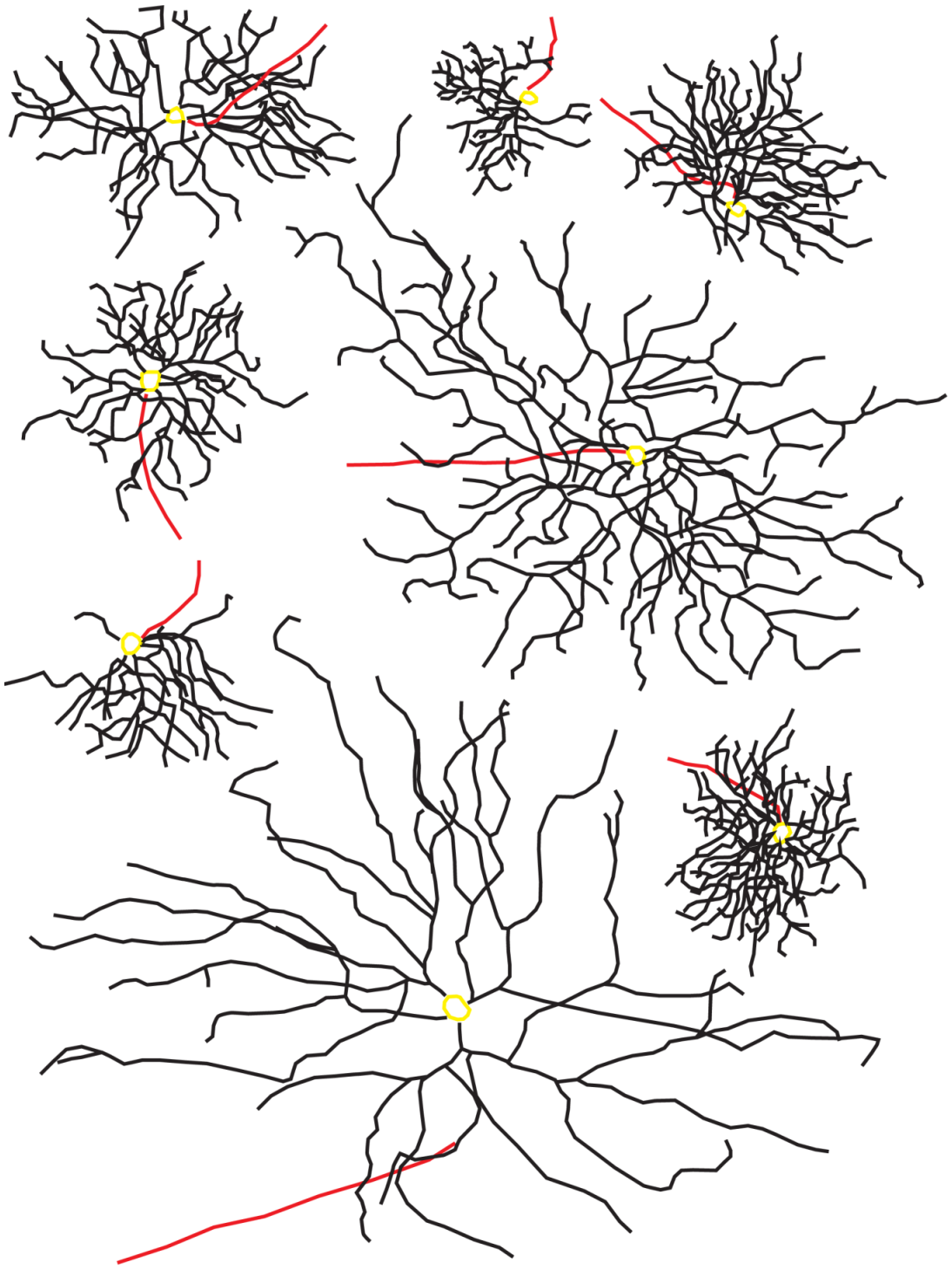

Figure 4.6. Traced *Trpv1*-/- mouse RGCs used for morphometric measurements. Examples of tracings generated from Lucifer Yellow-filled RGCs from *Trpv1*-/- mice. Tracings indicate RGC dendrites (black), soma (yellow), and axon (red). Measurements of soma area, dendritic area, dendritic length, and dendritic nodes were derived from these tracings.

exhibit decreased complexity compared to C57 mice at this radius. These animals also did not appear to exhibit an effect of microbead injection on dendritic branching.

Comparisons between groups (Figure 4.9) indicated that all significant comparisons arose from genotype (C57 versus *Trpv1*-/-) and not from treatment (saline-injected eye vs. microbead-injected eye). At 2 weeks post-injection (Figure 4.9A), significant differences ($p \leq 0.05$, $n \leq 40$ RGCs for each group compared) existed between RGCs from microbead-injected C57 and microbead-injected *Trpv1*-/- mice. At both 40 and 60 µm away from the RGC soma, the number of dendritic intersections for *Trpv1*-/- was reduced by 16% compared to C57. At 4 weeks post-injection (Figure 4.9B), significant differences existed between RGCs ($n \leq 28$ for each group compared) from microbead-injected C57 and microbead-injected *Trpv1*-/- mice at 50 µm ($p \leq 0.05$), 60 µm ($p \leq 0.01$), 70 µm ($p \leq 0.001$), 80 µm ($p \leq 0.05$). Compared to C57, the number of intersections of *Trpv1*-/- RGCs in these groups was reduced by 24% at 50 µm, 27% at 60 µm, 29% at 70 µm, and 28% at 80 µm. Only one 4 week saline-injected C57 and saline-injected *Trpv1*-/- comparison was significant, and this was at a distance of 90 µm from the soma (Figure 4.9B). Compared to C57, the number of intersections of *Trpv1*-/- RGCs in this group were reduced by 31% ($p \leq 0.05$, $n \leq 28$ RGCs for each group compared).

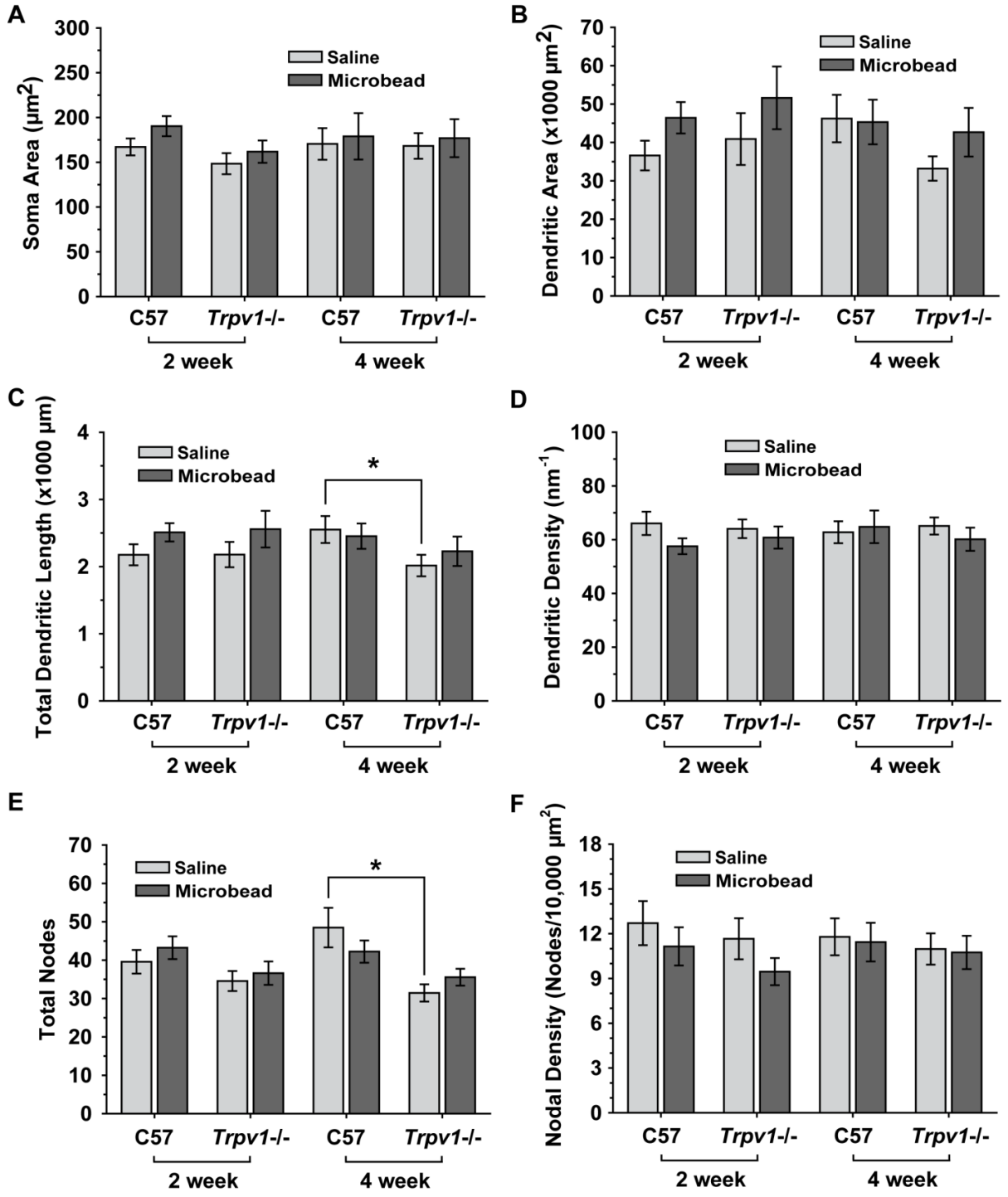

Figure 4.7. Quantification of RGC morphometry. Morphometric measurements of Lucifer Yellow-filled RGCs were conducted following either 2 or 4 weeks of microbead-induced IOP elevation. Changes in morphology were examined by quantifying the following metrics: ***A,*** soma area; ***B,*** dendritic area; ***C,*** total dendritic length, * $p \leq 0.05$; ***D,*** dendritic density (dendritic length normalized to dendritic area); ***E,*** total dendritic nodes, * $p \leq 0.05$; ***F,*** dendritic nodal density (total dendritic nodes normalized to dendritic area).

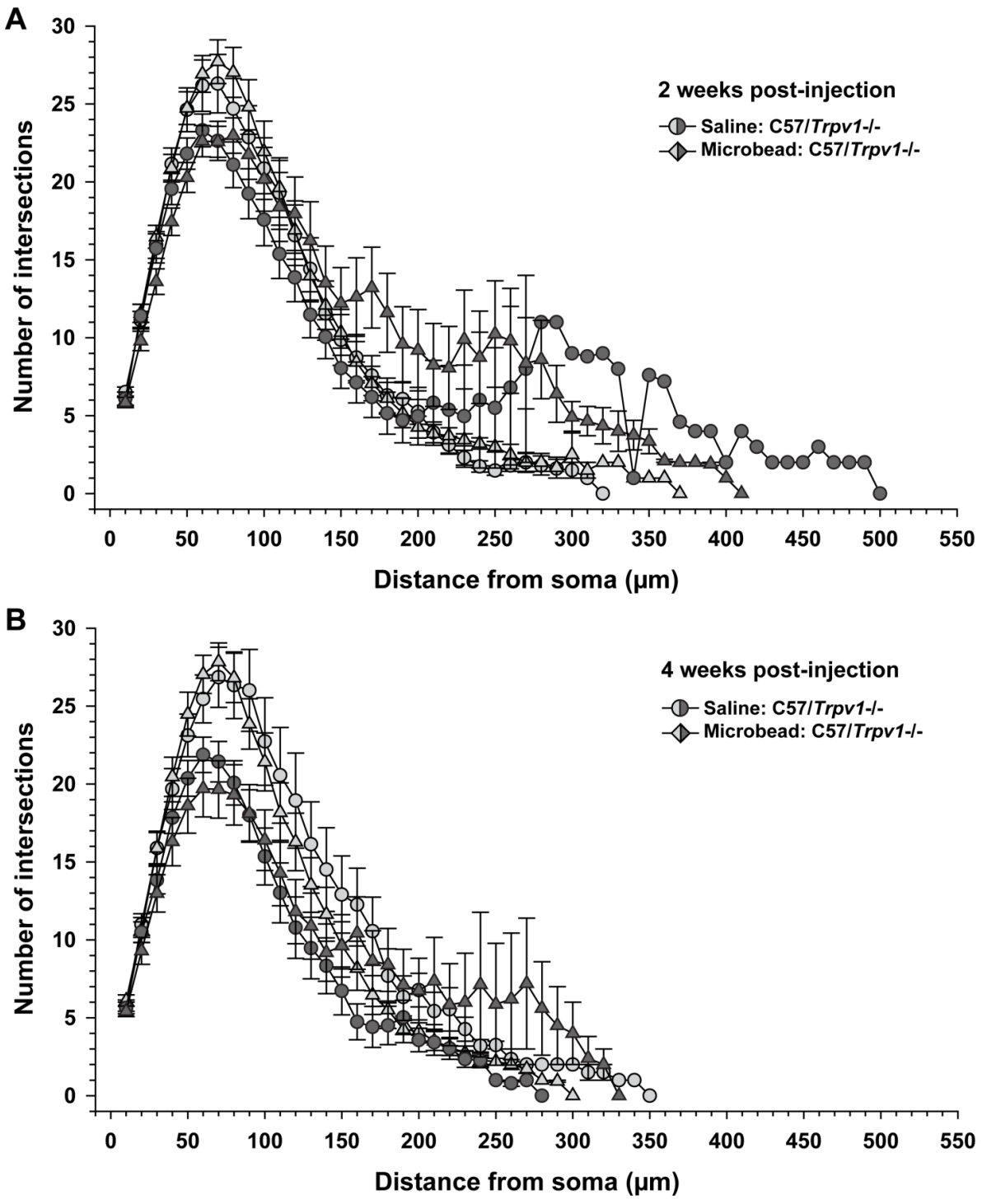

Figure 4.8. Sholl analysis of C57 and *Trpv1*-/- RGC dendrites. Number of intersections of Lucifer Yellow-filled RGC dendrites with concentric rings drawn about the cell soma (see Figure 4.1 for schematic). Quantifications were conducted for C57 and *Trpv1*-/- animals following either ***A,*** 2 weeks or ***B,*** 4 weeks of microbead-induced IOP elevation.

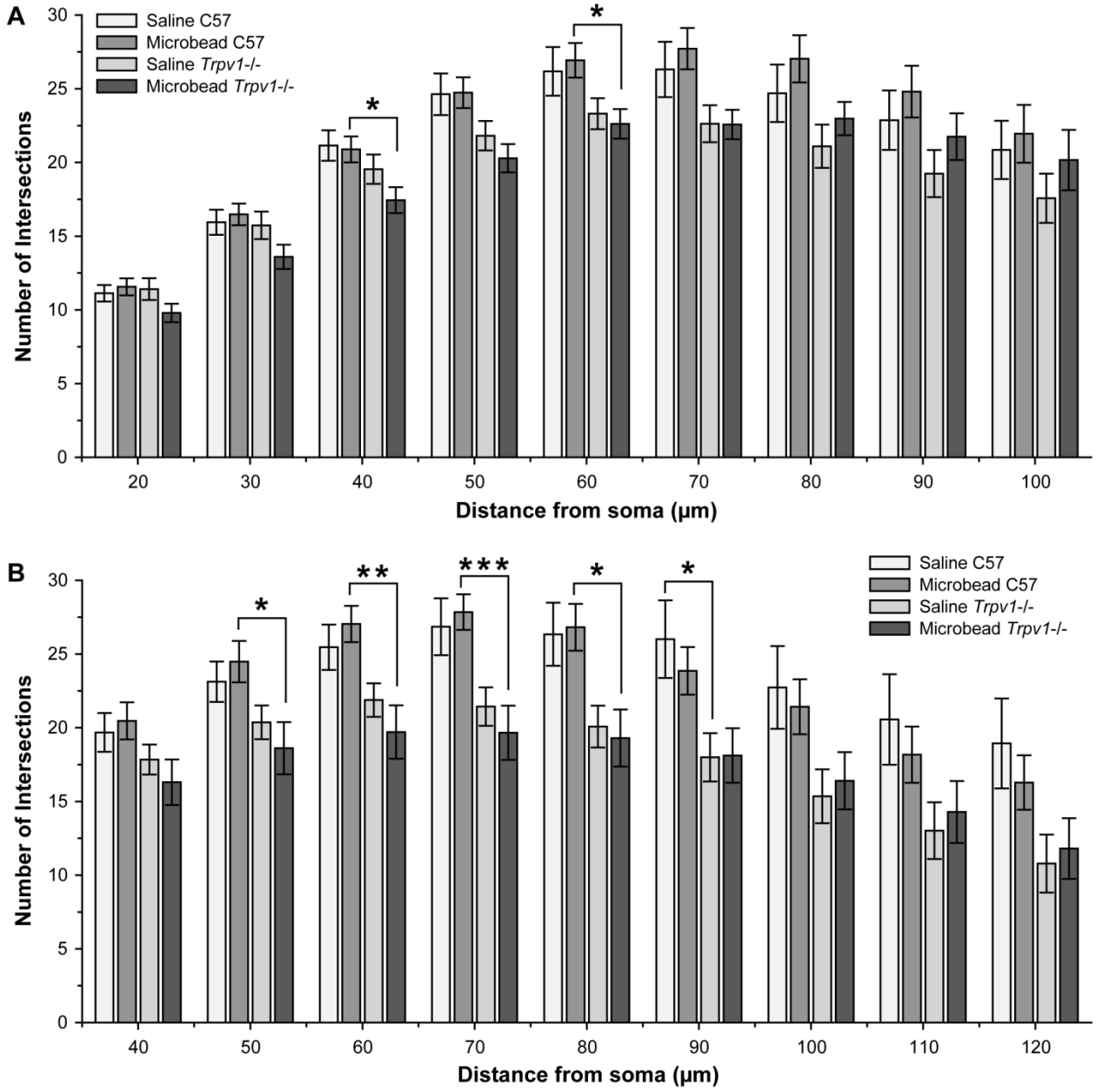

Figure 4.9. *Trpv1*-/- affects dendritic complexity as determined by Sholl analysis. Number of intersections of Lucifer Yellow-filled RGCs were quantified for Figure 4.8 and presented as averages for 9 consecutive radii that encompassed the greatest number of intersections. Averaged number of intersections were determined for cohorts of C57 and *Trpv1*-/- mice exposed to elevated pressure for ***A***, 2 weeks or ***B,*** 4 weeks. *, $p \leq 0.05$; **, $p \leq 0.01$; ***, $p \leq 0.001$.

Discussion

Reduced synaptic connectivity as well as dendritic retraction and abnormalities are common features of neurodegenerative diseases (Lin and Koleske, 2010). These degenerative alterations are observed in neurons from patients or models of Parkinson's disease (Solis et al., 2007), Alzheimer's disease (Flood, 1991; Hanks and Flood, 1991; Moolman et al., 2004), and Huntington's disease (Spires et al., 2004). These changes are also a feature in glaucomatous degeneration, as determined in a variety of species: human (Pavlidis et al., 2003), primate (Weber et al., 1998), feline (Shou et al., 2003), and mouse (Jakobs et al., 2005). Understanding how and when dendritic retraction fits into the pathophysiology of glaucoma is an active area of research that is informed by our knowledge from other neurodegenerative diseases (Morquette and Di Polo, 2008). Knowledge of synaptic dynamics during disease will aid in determining therapeutic windows to rescue challenged neurons. For example, in Alzheimer's disease, it is known that decline in memory and cognition is strongly correlated with synapse and dendrite loss, a degenerative feature that precedes actual cell death (Terry et al., 1991; Falke et al., 2003; Lin and Koleske, 2010). Therefore, in diseases like glaucoma, it may be important to focus on preservation of RGC synapses if dysfunctioning cells are to be rescued. Given the importance of TRPV1 in RGC survival, we hypothesized that TRPV1 may be imporant in slowing retraction of RGC dendrites following IOP elevation.

Our studies addressed this hypothesis by conducting morphometric analyses of C57 and *Trpv1*-/- mouse RGCs after 2 and 4 weeks of IOP elevation. These analyses indicated no changesbetween RGCs from saline- and microbead-injected eyes as measured by somal area, dendritic area, total dendritic length, dendritic density, total dendritic nodes, and dendritic nodal density (Figure 4.7). When considering only saline-injected retinas from 4 week cohorts, RGCs

from *Trpv1*-/- mice exhibited a significant reduction in total dendritic length and total dendritic nodes (Figure 4.7C,E) when compared to those from C57 mice. We did not expect to see such an alteration between this groups, which indicates that genotype may affect RGC dendritic morphometry. It is possible that *Trpv1*-/- animals simply possess RGCs with different morphometric properties; however, we would expect to see a difference in the 2 week animals as well, which we do not. Although unlikely, it cannot be ruled out that the act of injection itself causes alterations in RGC dendrites. To completely rule this possibility out, we would need to supplement these studies with C57 and *Trpv1*-/- animals that are naïve with respect to injection.

Another consideration is that between all groups compared, the number of cells measured for each group ranged from 20-39 RGCs. Although several different methods of classifying RGC subtypes have been proposed (Sun et al., 2002; Badea and Nathans, 2004; Kong et al., 2005), it is estimated that at minimum 14 distinct subtypes of RGCs exist in the mouse retina (Coombs et al., 2006). Morphometric data collected from each of these subtypes indicate an appreciable variety in size, shape, and complexity of dendritic trees across all subtypes. Although RGCs were chosen for Lucifer Yellow filling with no prior knowledge of subtype, it is possible that certain subtypes were over- or underrepresented in our data. This seems especially possible given our relatively low sample size (n = 20-39 RGCs) compared to the number of RGC subtypes (a minimum of 14 proposed). In an effort to account for some of this variability, we normalized total dendritic length and total dendritic node counts to the dendritic area of each cell to calculate dendritic density and dendritic node density, respectively. When comparing the same groups using this normalized data, we discovered no statistically significant differences (Figure 4.7D,F).

To examine dendritic complexity, we conducted Sholl analysis (Sholl, 1953) on the same RGCs from which we collected morphometric data. This analytical method simply provides

information regarding the number of dendritic branches relative to distance from a neuron's soma (Milosevic and Ristanovic, 2007). At both 2 (Figure 4.8A) and 4 weeks (Figure 4.8B), it appears that there is a genotypic difference in complexity as determined by the peak point of the curve. These curves seem to suggest that *Trpv1*-/- animals possess RGCs that are less complex regardless of their exposure to elevated IOP. Curves from *Trpv1*-/- mice 2 weeks after treatment indicate instances of RGCs with relatively long dendrites (extending beyond 400 µm from the RGC soma). Of note, these lengthy dendrites exist in *Trpv1*-/- retinas from both saline- and microbead-injected eyes, indicating that this is not an effect of treatment. Few RGCs actually contributed to these extended components of the *Trpv1*-/- curves, as can be observed by the associated error bars for those data points. Data points from the furthest locations on the curves have no error bars, as they represent measurements from a singular RGC. Although the tail end of these *Trpv1*-/- curves are influenced by a few RGCs, it is possible that this is a real effect and not simply due to an insufficient sampling of RGCs subtypes across all experimental groups. These extensive dendrites are only seen in *Trpv1*-/- animals regardless of treatment, so the absence of TRPV1 may disrupt regulation of proper dendritic structure in RGCs.

It is known that TRPV1 activation can result in neuronal growth cone retraction, so it is possible that *Trpv1*-/- animals are unable to properly regulate necessary dendritic retraction (Goswami et al., 2007). This disruption of retraction may then result in a set of RGCs that exhibit more expansive dendritic trees. This effect is more apparent in the 2-week *Trpv1*-/- animals (both saline and microbead), and is only marginally apparent in 4-week *Trpv1*-/- animals (microbead only). It is possible that this could be a short-lived effect seen as an injury response to the injection, which would explain why it occurs in both saline and microbead groups. To see if this is the case, dendrites of RGCs from mice naïve to injection would need to be examined as well.

Statistically significant differences were observed only between phenotypes (C57 versus *Trpv1*-/-), and occurred at multiple distances in both 2- (Figure 4.9A) and 4-week (Figure 4.9B) groups of RGCs. The common feature between our morphometric data (Figure 4.8) and Sholl analysis (Figure 4.9) is that *Trpv1*-/- dendrite elaboration is reduced compared to C57 dendrites, regardless of whether they were exposed to IOP elevation. Without consideration of potential effects of genotype, our analyses indicate no significant differences between RGCs from saline- and microbead-injected eyes at either 2 or 4 weeks post-injection. Currently, only one study has systematically, but not exhaustively characterized RGC dendritic morphology using a microbead occlusion model similar to ours (Della Santina et al., 2013). This study used similar durations of IOP elevation (15 and 30 days compared to our 12-15 and 25-28 days, respectively), and these elevations were of a comparable magnitude. Their analyses indicated no significant retraction at 2 weeks. At 4 weeks, they note that a subset of OFF transient RGCs exhibited significant dendritic retraction, whereas OFF sustained and ON sustained cells did not. This study is not exhaustive, as these were the only RGC subtypes examined, but it does suggest a context for our data.

First, we may benefit from examining RGCs from longer durations of IOP elevation. Second, it appears that not all subtypes of RGCs exhibit retraction at early timepoints, a possibility that has been supported by work in a laser-induced model of ocular hypertension (Feng et al., 2013). Currently, we do not have enough data to analyze changes by subtype, so we may consider either collecting more measurements at 2 and 4 weeks or extending the duration of IOP elevation to cause a more robust effect. Due to these limitations, we are unable to presently determine whether TRPV1 aids in the preservation of RGC synapses and dendrites exposed to elevated IOP.

CHAPTER 5

SUMMARY

Purpose of studies

The objective of these studies was to examine how cation channel TRPV1 (transient receptor potential vanilloid-1) modulates neurodegeneration of RGCs in glaucoma. From prior studies *in vitro*, we knew that TRPV1 activity influences RGC survival in response to pressure (Sappington et al., 2009). Using this knowledge, we decided to examine the influence of TRPV1 in glaucomatous degeneration of RGCs in an *in vivo* model of glaucoma. We hypothesized that TRPV1 functions to counteract RGC dysfunction through enhancing synaptic activity at RGC dendrites. This hypothesis was addressed using three specific aims:

Aim 1. Determine influence of TRPV1 on RGC degenerative outcomes.

Aim 2. Determine compartmental nature of TRPV1 response in RGCs.

Aim 3. Establish relevance of TRPV1 in survival of RGC dendrites.

Determining the influence of TRPV1 on RGC degenerative outcomes

Examining the responses of C57 and *Trpv1*-/- animals to microbead-induced IOP elevation allowed us to better understand the function of TRPV1 during glaucomatous pathology. As expected, microbead injection reduced transport of CTB to the LGN and SC in C57 mice; however, deficits in transport were significantly worse in *Trpv1*-/- mice. As expected, examination of RGC axons in sections of the optic nerve revealed that microbead injection caused a reduction in axon counts and density. This reduction was significantly worse in *Trpv1*-/-

mice than in C57 mice. When looking at the retina, RGC soma counts were not significantly reduced for C57 mice as a result of microbead injection. *Trpv1*-/- mice, however, did exhibit a reduction in RGC somas in the retina, but this reduction was limited to the nasal quadrant of the retina, as has been seen in previous studies (Lambert et al., 2011). Examination of phosphorylated neurofilaments in these retinas revealed somatodendritic accumulations in RGCs that reflected dysfunction in transport along their axons. In terms of phosphorylated neurofilaments (pNF), *Trpv1*-/- mice exhibited more RGCs with pNF accumulation than did C57 mice.

Future directions for this part of the project could entail trying to examine if these changes occur in a progressive model of disease that exhibits gradual IOP elevation. For instance, this might involve backcrossing *Trpv1*-/- mice onto a DBA/2 genetic background. The same outcome measures could be used in terms of assessing pathology. Unfortunately, conducting the backcrossing would take a long time and the development of a large colony would be necessary to assess several ages of animals. It is also possible that the inherent variability of the DBA/2 progression might make results difficult to interpret. We saw variability in progression across all mice used in our microbead-induced study (see data distributions in Figures 2.10A, 2.12A), so it is likely the variability would be even greater using animals on the DBA/2 background.

Determining the compartmental nature of the TRPV1 response in RGCs

To determine if elevated IOP changes TRPV1 levels at both the mRNA and protein level, we conducted qPCR and immunohistochemistry experiments. These experiments were conducted using C57 mice injected with microbeads, which were sacrificed at several different

timepoints. We did not observe a significant change in *Trpv1* transcript levels following IOP elevation; however, it is possible that we missed the window of time in which levels of this transcript would be increased. This possibility is especially informed by our immunolabeling data, in which we saw early increases in TRPV1. By quantifying fluorescent intensity within cellular and synaptic layers of the retina, we were able to determine that TRPV1 protein levels are increased in the inner plexiform layer following one week of pressure elevation. This increase was transient and was not significant for later timepoints. The inner plexiform layer includes the dendrites of RGCs, so it is possible that this increase in protein in the inner plexiform layer was due to increased expression of TRPV1 in the RGC dendrites.

Our immunolabeling data also indicated increased protein levels of synaptic protein PSD-95 and dendritic protein MAP2 following 1 week of pressure elevation. Similar to our immunolabeling data for TRPV1, these increases were transient. It is possible that the upregulation of these proteins is a compensatory response following the stressor of increased IOP. In our examination of TRPV1 and PSD-95 expression together in the inner plexiform layer, we observed that both proteins exhibited increased levels after 1 week of IOP elevation, and that they also appeared to become more closely associated with each other. This increased colocalization was transient, and decreased again after the 1 week timepoint.

Future directions for this part of the project would entail conducting high resolution imaging of RGC dendritic synapses and dendritic structures. Confocal microscopy does not possess the resolving power to determine if TRPV1 is truly localized within dendritic and synaptic structures, so we would have to use other imaging techniques. Based on studies that demonstrated perisynaptic localization of TRPV1 (Puente et al., 2011; Puente et al., 2014), it would be worth seeing if TRPV1 might modulate RGC synaptic activity in a similar location.

These studies would require using pre-embedding immunogold labeling for TRPV1 and imaging by high resolution electron microscopy. While those studies might take longer to develop, a quicker, but less sensitive method to examine this would involve collecting synaptosomes from retinal tissue and conducting Western blots for TRPV1. Although this technique provides no spatial or cell-type specific information, it could implicate TRPV1 as a synaptic protein in the mouse retina.

Establishing the relevance of TRPV1 in survival of RGC dendrites

Based on our knowledge that knockout of *Trpv1* makes microbead-induced pathology worse, and that TRPV1 protein levels increase in the inner plexiform layer after IOP elevation, we wanted to examine if TRPV1 might exhibit a stress response role within the dendrites. If TRPV1 is important in maintenance of dendrites during stress, we would expect to see that, in comparison to C57 mice, *Trpv1*-/- mice exhibit an accelerated retraction of dendrites following microbead injection. To examine this, we elevated pressure in C57 and *Trpv1*-/- mice by microbead injection, which was sustained for either 2 weeks or 4 weeks. After collecting retinas from these mice, we used Lucifer Yellow to fill randomly-selected RGCs for our analyses. This allowed for imaging of RGCs for morphometric analysis of dendritic structures.

It seems that we used timepoints that may have been too early to detect dendritic changes, as we saw no difference in any measure when comparing between saline and microbead eyes. However, when we compared RGCs from C57 to those from *Trpv1*-/-, we saw that there may be a difference in dendritic elaboration based on genotype. These differences were most noticeable by Sholl analysis, in which we could see differences in peak dendritic complexity between C57 and *Trpv1*-/- animals at both 2 and 4 week timepoints. It is intriguing to consider the idea that

during development, TRPV1 may play a role in determining the branching complexity profile of RGCs.

Future directions for this part of the project would entail collecting morphological information from many more RGCs. This would allow for a more complete analysis that could be broken down based on RGC subtype. This may be an important approach, as other studies indicate that RGC subtype plays a role in determining vulnerability of specific RGCs to progression of dendritic retraction (Della Santina et al., 2013; Feng et al., 2013). In a study that used timepoints similar to ours, it was observed that only one of the three RGC subtypes they examined actually exhibited dendritic retraction in response to microbead-induced IOP elevation (Della Santina et al., 2013). This issue of subtype specificity may not be as prominent if we elected to consider longer periods of pressure elevation. Considering that we have chosen timepoints at which we see no difference between saline and microbead groups, we will need to consider using longer durations of IOP elevation.

Potential mechanisms of TRPV1 in RGC survival

Based on our results, we speculate that TRPV1 is involved in signaling and synaptic plasticity mechanisms that may be responsible for helping RGCs survive in response to stress. Future studies will need to focus upon how this occurs, and there are numerous possibilities for investigation. In order to understand the mechanism of TRPV1 in RGC survival, it will be important to understand what is activating TRPV1 *in vivo* during glaucomatous stress. Upstream of the receptor itself, we must understand what in the disease environment is activating TRPV1, and whether or not levels of this activator change during the course of the disease. TRPV1 can be activated by endogenous ligands, including various endocannabinoids, which can additionally

influence neuronal survival due to their activity at cannabinoid receptors. An important study would examine how TRPV1-activating endocannabinoid levels change within the retina following elevation of IOP by microbead injection.

To understand TRPV1-related mechanisms central to this set of studies, it will also be important to understand what is occurring subsequent to TRPV1 activation. We have proposed that TRPV1 activation helps maintain synaptic activity in response to elevated stress. Using electrophysiology, we have already determined that in C57 mice, RGCs exhibit increased spontaneous firing rates following IOP elevation (Ward et al., 2014). This increase in firing rate was not present in RGCs from *Trpv1*-/- animals. These electrophysiology results seem to indicate that *Trpv1*-/- causes RGCs to lose an intrinsic mechanism that increases RGC excitation in response to glaucomatous stress.

Currently, we are unsure what could cause this increase in RGC excitation, but it could potentially be mediated by alterations in endocannabinoid levels. Previous studies have indicated that enhancing synaptic activity, even in injured or degenerating neurons, helps these neurons survive (Corredor and Goldberg, 2009). Even following optic nerve axotomy in rats, stimulating retinal neurons using a trans-corneal electrode increased RGC survival *in vivo* (Morimoto et al., 2005). If we apply this knowledge to the data presented here as well as from our *Trpv1*-/- electrophysiology, we may begin to understand mechanistically how TRPV1 influences RGC survival. To tie this activity to neuronal survival, it would be interesting to see if pro-survival signaling, such as CREB signaling, is increased as a result of this TRPV1 activation (Brunet et al., 2001). It is possible that TRPV1-mediated enhancement of RGC activity could lead to both maintenance of synaptic structures, as well as changes in pro-survival signaling downstream of

channel activation. It will be important to further explore the mechanism of how TRPV1 influences RGC survival, as this may help in developing treatment strategies for glaucoma.

TRPV1-based interventions for neurodegeneration in glaucoma

In the past, glaucoma treatment has been focused on preventing progression, but recently, research has focused on targeting mechanisms that may allow for early interventions and preventative measures. One of the mechanisms that has garnered much attention is cannabinoid signaling, which can exhibit overlap with TRPV1 signaling due to common ligands (Pertwee, 2006). It has been demonstrated that the cannabinoid system is at least one component of the response to toxic and traumatic insults within the CNS (Mechoulam and Shohami, 2007; Fowler et al., 2010). Using the knowledge that both TRPV1 and cannabinoid signaling can enhance survival in response to neuronal stress, it seems practical to develop interventions that exploit both mechanisms.

The cannabinoid system is perhaps best known because the active component of marijuana, Δ^9-tetrahydrocannabinol (THC), activates cannabinoid receptors CB1 and CB2 (Pertwee, 2008). However, these receptors can also be activated by endocannabinoids, which are cannabinoid receptor ligands that are produced endogenously. This means that, aside from their activation by exogenous compounds like THC, these receptors and their endogenous ligands must constitute a system used for particular purposes by cells. Within the CNS, we know that endocannabinoids can mediate aspects of synaptic plasticity and neuroprotection (Yazulla, 2008). These mechanisms involve retrograde suppression of neurotransmitter release from presynaptic terminals. From a mechanistic standpoint, this suppression occurs when dendrites of a postsynaptic neuron become depolarized, leading to a Ca^{2+}-dependent release of

endocannabinoid, which then diffuses to CB1 receptors on the presynaptic neuron to reduce neurotransmitter release (Ohno-Shosaku et al., 2001; Wilson and Nicoll, 2001). This suppression of neurotransmitter release can be neuroprotective, as in the case of injurious situations in which excessive glutamate release can cause excitotoxicity (van der Stelt et al., 2002).

Neuroprotective potential is not the only factor that makes cannabinoids an interesting focus for future glaucoma therapeutics—cannabinoids have long been linked to reduction in IOP (Green, 1979). It is apparent that cannabinoids are responsible for IOP reduction by locally acting upon CB1 receptors in the eye (Song and Slowey, 2000). Exogenous cannabinoids can influence IOP; however, endocannabinoids known to exist within human ocular tissue as well (Chen et al., 2005; Matias et al., 2006), and the cannabinoid receptors at which they act are also found there (Porcella et al., 2000; Stamer et al., 2001), indicating potential mechanisms for endogenous regulation of IOP. In glaucoma, IOP is the leading modifiable risk factor (Sommer, 1989; Gordon et al., 2002), and lowering IOP is the most common form of treatment thus far (Heijl et al., 2002). Therapeutic interventions that target the endocannabinoid system are therefore encouraging because they may influence neuroprotective mechanisms in two different ways: directly by affecting endocannabinoid signaling related to neuronal survival and indirectly by lowering IOP.

Such neuroprotective intervention should also consider the knowledge of TRPV1 presented here. Our studies indicate that in response to elevated IOP, TRPV1 helps counter degenerative progression in a mouse model of glaucoma. Therefore, in considering therapeutic mechanisms, it would make sense to use compounds that modulate both endocannabinoid and TRPV1 signaling. This idea has been supported by *in vivo* work in the rat retina, which suggests

that by activating cannabinoid and TRPV1 receptors, anandamide protects against RGC death by high IOP (Nucci et al., 2007b).

One difficulty in targeting the endocannabinoid system is that endocannabinoids are hydrolyzed *in vivo*, and thus their bioavailability may be a concern during treatment. For example, anandamide is hydrolyzed by fatty acid amide hydrolase (FAAH), which breaks the amide bond and produces arachidonic acid and ethanolamine (Cravatt et al., 1996; Giang and Cravatt, 1997; McKinney and Cravatt, 2005). This degradation by FAAH occurs within cells, thus a controversial hypothesis has been asserted that there exists an undiscovered anandamide membrane transporter (AMT) which clears anandamide from the extracellular space (Bari et al., 2006; Nucci et al., 2008). An AMT may exist, as various compounds have been demonstrated to function as anandamide uptake inhibitors (Beltramo et al., 1997; Melck et al., 1999; Rakhshan et al., 2000; Di Marzo et al., 2002). Interestingly, some of these compounds that block anandamide uptake can also interact with FAAH, cannabinoid receptors, or TRPV1. One intriguing anandamide inhibitor is olvanil, which is formed as the condensation product of the polar head of capsaicin and oleic acid (Melck et al., 1999). In one study, olvanil in propylene glycol was applied to the eye via topical administration, causing significant IOP reduction in rabbits (Laine et al., 2001). In addition to inhibiting anandamide uptake, olvanil activates both TRPV1 and cannabinoid receptors (Di Marzo et al., 1998; Appendino et al., 2005). Olvanil may therefore have potential in glaucoma treatment due to several reasons: (1) inhibiting anandamide uptake allows for longer activation of cannabinoid receptors by anandamide, (2) olvanil itself can activate both cannabinoid receptors and TRPV1, and (3) olvanil has been demonstrated to reduce IOP. By both reducing IOP and targeting endogenous TRPV1- and CB1 receptor-mediated

neuroprotective signaling, olvanil and similar compounds may offer a more comprehensive way of addressing glaucoma.

Tailoring new and more effective intervention strategies for glaucoma patients is crucial. Currently, intervention strategies are focused on later stages of the disease; however, during these stages, vision loss is occurring and many RGCs have already died (Figure 5.1, red box). This is not an ideal stage for intervention, as RGCs cannot be restored following apoptosis; therefore, interventions at this stage can only hope to preserve what vision is left. For interventions to be most effective, they must work to preempt vision loss by protecting RGCs during earlier stages of dysfunction (Figure 5.1, green bracket). In these studies, we have demonstrated that TRPV1 is a component of an early response to glaucomatous stress, and that it is important for RGC survival in response to this stress. Based on these results, it would make sense to develop treatments for use at an early stage and that would, at least in part, target TRPV1 signaling.

In developing early intervention, more animal studies would need to be conducted using compounds such as olvanil. It would be important to see what the bioavailability of this drug would be within ocular tissue following topical administration to the eye, as this is a concern (Jarvinen et al., 2002). If the drug cannot act on TRPV1 and cannabinoid receptors within the retina, then it will be no more effective than current eye drop therapies that simply lower IOP. However, if in addition to lowering IOP, olvanil is also able to act on TRPV1 and cannabinoid receptors in the retina, this drug may provide a more comprehensive protection to RGCs under stress.

Should animal models demonstrate that olvanil or similar drugs are more effective than drugs that simply lower IOP, developing interventions for human patients could be a possibility.

Such intervention will likely need to be developed with a subset of patients who haven't demonstrated vision loss, but are at risk for glaucoma due to elevated pressure. These patients

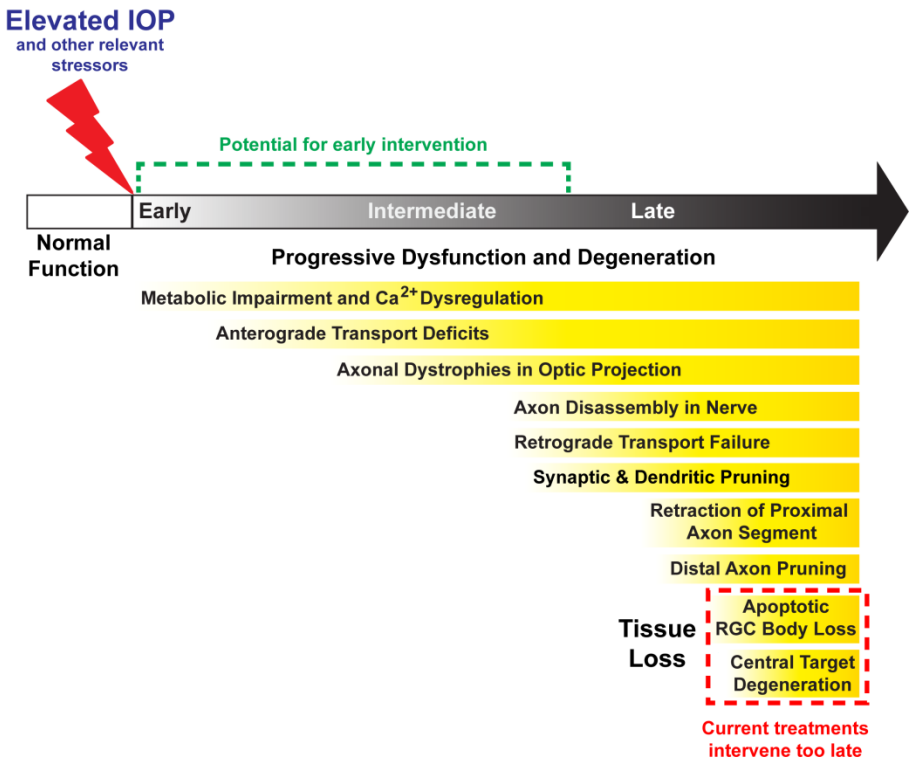

Figure 5.1. Timeline of degeneration and potential for intervention. Using results from animal models of glaucoma, a timeline for pathological features of disease progression can be approximated. In glaucoma, loss of vision is due to death of RGCs, which cannot be replaced; therefore, interventions that occur later in disease progression can only focus upon preventing further RGC death. Unfortunately, current interventions usually occur once disease progression is in later stages (red box). Our work with TRPV1 indicates that modulating early protective responses to disease-related stressors may prolong RGC survival. This timeline from animal models suggests that there is a window of time (green bracket) in which early intervention would be beneficial, allowing RGCs to maintain function instead of progressing to apoptosis.

Figure altered and used with permission from DJ Calkins. Timeline events adapted from Calkins (2012).

would be able to benefit from TRPV1- and cannabinoid receptor-mediated mechanisms of neuroprotection that may rely upon retention of synapses in the retina. Patients who are at later stages of disease would already exhibit retraction and loss of synapses in the retina, and thus

would not be able to benefit as robustly from such mechanisms of intervention (Figure 5.1, red box). It is important to realize that the success of any TRPV1-mediated treatment strategy would likely need to be early in disease progression, and thus continued research to identify early-stage disease biomarkers will be especially crucial for identifying patients who might benefit from such treatment. This knowledge, combined with screening for elevated IOP, would help identify at-risk patients who might benefit from early-stage intervention that, in part, would take advantage of TRPV1-mediated signaling.

Conclusions

Altogether, these studies indicate that TRPV1 helps counter degenerative progression in an *in vivo* mouse model of glaucoma. In our microbead model, *Trpv1*-/- animals exhibited accelerated pathology across all of our degenerative outcome measures when compared to C57 animals. In examining C57 retinas exposed to various durations of elevated IOP, we observed transient increases of TRPV1 in a synaptic layer of the retina associated with RGC dendritic structures. This may suggest that these channels modulate synaptic activity soon after insult from elevated IOP. Although we were not able to determine if *Trpv1*-/- animals exhibited accelerated dendritic pathology in our morphometric analyses, we did observe an interesting genotypic effect on RGC dendritic complexity, regardless of IOP exposure. As a whole, these results suggest that TRPV1, and TRP channels in general, may be relevant for modulation of neurodegenerative disease progression, and that these channels may be useful therapeutic targets.

REFERENCES

Aarts MM, Tymianski M (2005) TRPMs and neuronal cell death. Pflugers Arch 451:243-249.

Abramov AY, Scorziello A, Duchen MR (2007) Three distinct mechanisms generate oxygen free radicals in neurons and contribute to cell death during anoxia and reoxygenation. J Neurosci 27:1129-1138.

Adkins-Muir DL, Jones TA (2003) Cortical electrical stimulation combined with rehabilitative training: enhanced functional recovery and dendritic plasticity following focal cortical ischemia in rats. Neurol Res 25:780-788.

Agopyan N, Head J, Yu S, Simon SA (2004) TRPV1 receptors mediate particulate matter-induced apoptosis. Am J Physiol Lung Cell Mol Physiol 286:L563-572.

Akulinin VA, Dahlstrom A (2003) Quantitative analysis of MAP2 immunoreactivity in human neocortex of three patients surviving after brain ischemia. Neurochem Res 28:373-378.

Alexianu ME, Ho BK, Mohamed AH, La Bella V, Smith RG, Appel SH (1994) The role of calcium-binding proteins in selective motoneuron vulnerability in amyotrophic lateral sclerosis. Ann Neurol 36:846-858.

Amantini C, Mosca M, Nabissi M, Lucciarini R, Caprodossi S, Arcella A, Giangaspero F, Santoni G (2007) Capsaicin-induced apoptosis of glioma cells is mediated by TRPV1 vanilloid receptor and requires p38 MAPK activation. J Neurochem 102:977-990.

Ames A, 3rd, Nesbett FB (1981) In vitro retina as an experimental model of the central nervous system. J Neurochem 37:867-877.

Anderson DR, Hendrickson A (1974) Effect of intraocular pressure on rapid axoplasmic transport in monkey optic nerve. Invest Ophthalmol Vis Sci 13:771-783.

Anderson MG, Smith RS, Hawes NL, Zabaleta A, Chang B, Wiggs JL, John SW (2002) Mutations in genes encoding melanosomal proteins cause pigmentary glaucoma in DBA/2J mice. Nat Genet 30:81-85.

Appendino G, De Petrocellis L, Trevisani M, Minassi A, Daddario N, Moriello AS, Gazzieri D, Ligresti A, Campi B, Fontana G, Pinna C, Geppetti P, Di Marzo V (2005) Development of the first ultra-potent "capsaicinoid" agonist at transient receptor potential vanilloid type 1 (TRPV1) channels and its therapeutic potential. J Pharmacol Exp Ther 312:561-570.

Arendt T, Bruckner MK, Bigl V, Marcova L (1995) Dendritic reorganisation in the basal forebrain under degenerative conditions and its defects in Alzheimer's disease. III. The basal forebrain compared with other subcortical areas. J Comp Neurol 351:223-246.

Arundine M, Tymianski M (2003) Molecular mechanisms of calcium-dependent neurodegeneration in excitotoxicity. Cell Calcium 34:325-337.

Badea TC, Nathans J (2004) Quantitative analysis of neuronal morphologies in the mouse retina visualized by using a genetically directed reporter. J Comp Neurol 480:331-351.

Baloyannis SJ (2009) Dendritic pathology in Alzheimer's disease. J Neurol Sci 283:153-157.

Bari M, Battista N, Fezza F, Gasperi V, Maccarrone M (2006) New insights into endocannabinoid degradation and its therapeutic potential. Mini Rev Med Chem 6:257-268.

Beltramo M, Stella N, Calignano A, Lin SY, Makriyannis A, Piomelli D (1997) Functional role of high-affinity anandamide transport, as revealed by selective inhibition. Science 277:1094-1097.

Bennion D, Jensen T, Walther C, Hamblin J, Wallmann A, Couch J, Blickenstaff J, Castle M, Dean L, Beckstead S, Merrill C, Muir C, St Pierre T, Williams B, Daniel S, Edwards JG (2011) Transient receptor potential vanilloid 1 agonists modulate hippocampal CA1 LTP via the GABAergic system. Neuropharmacology 61:730-738.

Berridge MJ (1998) Neuronal calcium signaling. Neuron 21:13-26.

Berridge MJ, Lipp P, Bootman MD (2000) The versatility and universality of calcium signalling. Nat Rev Mol Cell Biol 1:11-21.

Bhave G, Zhu W, Wang H, Brasier DJ, Oxford GS, Gereau RWt (2002) cAMP-dependent protein kinase regulates desensitization of the capsaicin receptor (VR1) by direct phosphorylation. Neuron 35:721-731.

Bidmon HJ, Jancsik V, Schleicher A, Hagemann G, Witte OW, Woodhams P, Zilles K (1998) Structural alterations and changes in cytoskeletal proteins and proteoglycans after focal cortical ischemia. Neuroscience 82:397-420.

Biggs JE, Yates JM, Loescher AR, Clayton NM, Boissonade FM, Robinson PP (2007) Changes in vanilloid receptor 1 (TRPV1) expression following lingual nerve injury. Eur J Pain 11:192-201.

Biggs JE, Yates JM, Loescher AR, Clayton NM, Robinson PP, Boissonade FM (2008) Effect of SB-750364, a specific TRPV1 receptor antagonist, on injury-induced ectopic discharge in the lingual nerve. Neurosci Lett 443:41-45.

Brunet A, Datta SR, Greenberg ME (2001) Transcription-dependent and -independent control of neuronal survival by the PI3K-Akt signaling pathway. Curr Opin Neurobiol 11:297-305.

Brustovetsky N, Brustovetsky T, Jemmerson R, Dubinsky JM (2002) Calcium-induced cytochrome c release from CNS mitochondria is associated with the permeability transition and rupture of the outer membrane. J Neurochem 80:207-218.

Buckingham BP, Inman DM, Lambert W, Oglesby E, Calkins DJ, Steele MR, Vetter ML, Marsh-Armstrong N, Horner PJ (2008) Progressive ganglion cell degeneration precedes neuronal loss in a mouse model of glaucoma. J Neurosci 28:2735-2744.

Buki A, Okonkwo DO, Wang KK, Povlishock JT (2000) Cytochrome c release and caspase activation in traumatic axonal injury. J Neurosci 20:2825-2834.

Bunt AH, Hendrickson AE, Lund JS, Lund RD, Fuchs AF (1975) Monkey retinal ganglion cells: morphometric analysis and tracing of axonal projections, with a consideration of the peroxidase technique. J Comp Neurol 164:265-285.

Burgoyne CF, Downs JC, Bellezza AJ, Suh JK, Hart RT (2005) The optic nerve head as a biomechanical structure: a new paradigm for understanding the role of IOP-related stress and strain in the pathophysiology of glaucomatous optic nerve head damage. Prog Retin Eye Res 24:39-73.

Calkins DJ (2012) Critical pathogenic events underlying progression of neurodegeneration in glaucoma. Prog Retin Eye Res 31:702-719.

Calkins DJ, Horner PJ, Roberts R, Gradianu M, Berkowitz BA (2008) Manganese-enhanced MRI of the DBA/2J mouse model of hereditary glaucoma. Invest Ophthalmol Vis Sci 49:5083-5088.

Campbell IC, Coudrillier B, Ethier CR (2013) Biomechanics of the posterior eye: A critical role in health and disease. J Biomech Eng 136.

Carriedo SG, Yin HZ, Weiss JH (1996) Motor neurons are selectively vulnerable to AMPA/kainate receptor-mediated injury in vitro. J Neurosci 16:4069-4079.

Carter-Dawson L, Crawford ML, Harwerth RS, Smith EL, 3rd, Feldman R, Shen FF, Mitchell CK, Whitetree A (2002) Vitreal glutamate concentration in monkeys with experimental glaucoma. Invest Ophthalmol Vis Sci 43:2633-2637.

Casson RJ (2006) Possible role of excitotoxicity in the pathogenesis of glaucoma. Clin Exp Ophthalmol 34:54-63.

Caterina MJ, Leffler A, Malmberg AB, Martin WJ, Trafton J, Petersen-Zeitz KR, Koltzenburg M, Basbaum AI, Julius D (2000) Impaired nociception and pain sensation in mice lacking the capsaicin receptor. Science 288:306-313.

Cavanaugh DJ, Chesler AT, Jackson AC, Sigal YM, Yamanaka H, Grant R, O'Donnell D, Nicoll RA, Shah NM, Julius D, Basbaum AI (2011) Trpv1 reporter mice reveal highly restricted brain distribution and functional expression in arteriolar smooth muscle cells. J Neurosci 31:5067-5077.

Chan SL, Mattson MP (1999) Caspase and calpain substrates: roles in synaptic plasticity and cell death. J Neurosci Res 58:167-190.

Chaudhary P, Ahmed F, Sharma SC (1998) MK801-a neuroprotectant in rat hypertensive eyes. Brain Res 792:154-158.

Chavez AE, Chiu CQ, Castillo PE (2010) TRPV1 activation by endogenous anandamide triggers postsynaptic long-term depression in dentate gyrus. Nat Neurosci 13:1511-1518.

Chen H, Wei X, Cho KS, Chen G, Sappington R, Calkins DJ, Chen DF (2011) Optic neuropathy due to microbead-induced elevated intraocular pressure in the mouse. Invest Ophthalmol Vis Sci 52:36-44.

Chen J, Matias I, Dinh T, Lu T, Venezia S, Nieves A, Woodward DF, Di Marzo V (2005) Finding of endocannabinoids in human eye tissues: implications for glaucoma. Biochemical and biophysical research communications 330:1062-1067.

Chklovskii DB, Koulakov AA (2004) Maps in the brain: what can we learn from them? Annu Rev Neurosci 27:369-392.

Choi WS, Lee EH, Chung CW, Jung YK, Jin BK, Kim SU, Oh TH, Saido TC, Oh YJ (2001) Cleavage of Bax is mediated by caspase-dependent or -independent calpain activation in dopaminergic neuronal cells: protective role of Bcl-2. J Neurochem 77:1531-1541.

Choo YS, Johnson GV, MacDonald M, Detloff PJ, Lesort M (2004) Mutant huntingtin directly increases susceptibility of mitochondria to the calcium-induced permeability transition and cytochrome c release. Hum Mol Genet 13:1407-1420.

Chung MK, Guler AD, Caterina MJ (2008) TRPV1 shows dynamic ionic selectivity during agonist stimulation. Nat Neurosci 11:555-564.

Ciura S, Bourque CW (2006) Transient receptor potential vanilloid 1 is required for intrinsic osmoreception in organum vasculosum lamina terminalis neurons and for normal thirst responses to systemic hyperosmolality. J Neurosci 26:9069-9075.

Coombs J, van der List D, Wang GY, Chalupa LM (2006) Morphological properties of mouse retinal ganglion cells. Neuroscience 140:123-136.

Corredor RG, Goldberg JL (2009) Electrical activity enhances neuronal survival and regeneration. J Neural Eng 6:055001.

Cravatt BF, Giang DK, Mayfield SP, Boger DL, Lerner RA, Gilula NB (1996) Molecular characterization of an enzyme that degrades neuromodulatory fatty-acid amides. Nature 384:83-87.

Crish SD, Calkins DJ (2011) Neurodegeneration in glaucoma: progression and calcium-dependent intracellular mechanisms. Neuroscience 176:1-11.

Crish SD, Sappington RM, Inman DM, Horner PJ, Calkins DJ (2010) Distal axonopathy with structural persistence in glaucomatous neurodegeneration. Proc Natl Acad Sci U S A 107:5196-5201.

Crish SD, Dapper JD, MacNamee SE, Balaram P, Sidorova TN, Lambert WS, Calkins DJ (2013) Failure of axonal transport induces a spatially coincident increase in astrocyte BDNF prior to synapse loss in a central target. Neuroscience 229:55-70.

Daly D, Rong W, Chess-Williams R, Chapple C, Grundy D (2007) Bladder afferent sensitivity in wild-type and TRPV1 knockout mice. J Physiol 583:663-674.

Dapper JD, Crish SD, Pang IH, Calkins DJ (2013) Proximal inhibition of p38 MAPK stress signaling prevents distal axonopathy. Neurobiol Dis 59C:26-37.

Davis JB, Gray J, Gunthorpe MJ, Hatcher JP, Davey PT, Overend P, Harries MH, Latcham J, Clapham C, Atkinson K, Hughes SA, Rance K, Grau E, Harper AJ, Pugh PL, Rogers DC, Bingham S, Randall A, Sheardown SA (2000) Vanilloid receptor-1 is essential for inflammatory thermal hyperalgesia. Nature 405:183-187.

Dawson DA, Hallenbeck JM (1996) Acute focal ischemia-induced alterations in MAP2 immunostaining: description of temporal changes and utilization as a marker for volumetric assessment of acute brain injury. J Cereb Blood Flow Metab 16:170-174.

Della Santina L, Inman DM, Lupien CB, Horner PJ, Wong RO (2013) Differential progression of structural and functional alterations in distinct retinal ganglion cell types in a mouse model of glaucoma. J Neurosci 33:17444-17457.

Di Marzo V, Lastres-Becker I, Bisogno T, De Petrocellis L, Milone A, Davis JB, Fernandez-Ruiz JJ (2001) Hypolocomotor effects in rats of capsaicin and two long chain capsaicin homologues. Eur J Pharmacol 420:123-131.

Di Marzo V, Bisogno T, Melck D, Ross R, Brockie H, Stevenson L, Pertwee R, De Petrocellis L (1998) Interactions between synthetic vanilloids and the endogenous cannabinoid system. FEBS Lett 436:449-454.

Di Marzo V, Griffin G, De Petrocellis L, Brandi I, Bisogno T, Williams W, Grier MC, Kulasegram S, Mahadevan A, Razdan RK, Martin BR (2002) A structure/activity relationship study on arvanil, an endocannabinoid and vanilloid hybrid. J Pharmacol Exp Ther 300:984-991.

DiStefano PS, Friedman B, Radziejewski C, Alexander C, Boland P, Schick CM, Lindsay RM, Wiegand SJ (1992) The neurotrophins BDNF, NT-3, and NGF display distinct patterns of retrograde axonal transport in peripheral and central neurons. Neuron 8:983-993.

Doly S, Fischer J, Salio C, Conrath M (2004) The vanilloid receptor-1 is expressed in rat spinal dorsal horn astrocytes. Neurosci Lett 357:123-126.

Doyle MW, Bailey TW, Jin YH, Andresen MC (2002) Vanilloid receptors presynaptically modulate cranial visceral afferent synaptic transmission in nucleus tractus solitarius. J Neurosci 22:8222-8229.

Drager UC, Hubel DH (1976) Topography of visual and somatosensory projections to mouse superior colliculus. J Neurophysiol 39:91-101.

Drager UC, Olsen JF (1980) Origins of crossed and uncrossed retinal projections in pigmented and albino mice. J Comp Neurol 191:383-412.

Dreher B, Sefton AJ, Ni SY, Nisbett G (1985) The morphology, number, distribution and central projections of Class I retinal ganglion cells in albino and hooded rats. Brain Behav Evol 26:10-48.

Ehrlich I, Klein M, Rumpel S, Malinow R (2007) PSD-95 is required for activity-driven synapse stabilization. Proc Natl Acad Sci U S A 104:4176-4181.

El-Husseini AE, Schnell E, Chetkovich DM, Nicoll RA, Bredt DS (2000) PSD-95 involvement in maturation of excitatory synapses. Science 290:1364-1368.

El Andaloussi-Lilja J, Lundqvist J, Forsby A (2009) TRPV1 expression and activity during retinoic acid-induced neuronal differentiation. Neurochem Int 55:768-774.

Facer P, Casula MA, Smith GD, Benham CD, Chessell IP, Bountra C, Sinisi M, Birch R, Anand P (2007) Differential expression of the capsaicin receptor TRPV1 and related novel receptors TRPV3, TRPV4 and TRPM8 in normal human tissues and changes in traumatic and diabetic neuropathy. BMC Neurol 7:11.

Falke E, Nissanov J, Mitchell TW, Bennett DA, Trojanowski JQ, Arnold SE (2003) Subicular dendritic arborization in Alzheimer's disease correlates with neurofibrillary tangle density. Am J Pathol 163:1615-1621.

Farkas RH, Chowers I, Hackam AS, Kageyama M, Nickells RW, Otteson DC, Duh EJ, Wang C, Valenta DF, Gunatilaka TL, Pease ME, Quigley HA, Zack DJ (2004) Increased expression of iron-regulating genes in monkey and human glaucoma. Invest Ophthalmol Vis Sci 45:1410-1417.

Feng L, Xie X, Joshi PS, Yang Z, Shibasaki K, Chow RL, Gan L (2006) Requirement for Bhlhb5 in the specification of amacrine and cone bipolar subtypes in mouse retina. Development 133:4815-4825.

Feng L, Zhao Y, Yoshida M, Chen H, Yang JF, Kim TS, Cang J, Troy JB, Liu X (2013) Sustained ocular hypertension induces dendritic degeneration of mouse retinal ganglion cells that depends on cell type and location. Invest Ophthalmol Vis Sci 54:1106-1117.

Ferreira SM, Lerner SF, Brunzini R, Evelson PA, Llesuy SF (2004) Oxidative stress markers in aqueous humor of glaucoma patients. Am J Ophthalmol 137:62-69.

Flammer J, Orgul S, Costa VP, Orzalesi N, Krieglstein GK, Serra LM, Renard JP, Stefansson E (2002) The impact of ocular blood flow in glaucoma. Prog Retin Eye Res 21:359-393.

Flood DG (1991) Region-specific stability of dendritic extent in normal human aging and regression in Alzheimer's disease. II. Subiculum. Brain Res 540:83-95.

Fowler CJ, Rojo ML, Rodriguez-Gaztelumendi A (2010) Modulation of the endocannabinoid system: neuroprotection or neurotoxicity? Exp Neurol 224:37-47.

Furutani R, Kibayashi K (2012) Morphological alteration and reduction of MAP2-immunoreactivity in pyramidal neurons of cerebral cortex in a rat model of focal cortical compression. J Neurotrauma 29:1266-1276.

Gao S, Fei M, Cheng C, Yu X, Chen M, Shi S, Qin J, Guo Z, Shen A (2008) Spatiotemporal expression of PSD-95 and nNOS after rat sciatic nerve injury. Neurochem Res 33:1090-1100.

Garcia-Sanz N, Fernandez-Carvajal A, Morenilla-Palao C, Planells-Cases R, Fajardo-Sanchez E, Fernandez-Ballester G, Ferrer-Montiel A (2004) Identification of a tetramerization domain in the C terminus of the vanilloid receptor. J Neurosci 24:5307-5314.

Garcia-Valenzuela E, Shareef S, Walsh J, Sharma SC (1995) Programmed cell death of retinal ganglion cells during experimental glaucoma. Exp Eye Res 61:33-44.

Gasparini L, Crowther RA, Martin KR, Berg N, Coleman M, Goedert M, Spillantini MG (2011) Tau inclusions in retinal ganglion cells of human P301S tau transgenic mice: effects on axonal viability. Neurobiol Aging 32:419-433.

Gazzieri D, Trevisani M, Springer J, Harrison S, Cottrell GS, Andre E, Nicoletti P, Massi D, Zecchi S, Nosi D, Santucci M, Gerard NP, Lucattelli M, Lungarella G, Fischer A, Grady EF, Bunnett NW, Geppetti P (2007) Substance P released by TRPV1-expressing neurons produces reactive oxygen species that mediate ethanol-induced gastric injury. Free Radic Biol Med 43:581-589.

Ghanem AA, Arafa LF, El-Baz A (2010) Oxidative stress markers in patients with primary open-angle glaucoma. Curr Eye Res 35:295-301.

Ghezzi A, Martinelli V, Torri V, Zaffaroni M, Rodegher M, Comi G, Zibetti A, Canal N (1999) Long-term follow-up of isolated optic neuritis: the risk of developing multiple sclerosis, its outcome, and the prognostic role of paraclinical tests. J Neurol 246:770-775.

Giang DK, Cravatt BF (1997) Molecular characterization of human and mouse fatty acid amide hydrolases. Proc Natl Acad Sci U S A 94:2238-2242.

Gibson HE, Edwards JG, Page RS, Van Hook MJ, Kauer JA (2008) TRPV1 channels mediate long-term depression at synapses on hippocampal interneurons. Neuron 57:746-759.

Gleichmann M, Mattson MP (2011) Neuronal calcium homeostasis and dysregulation. Antioxid Redox Signal 14:1261-1273.

Goldblum D, Mittag T (2002) Prospects for relevant glaucoma models with retinal ganglion cell damage in the rodent eye. Vision Res 42:471-478.

Goni-Oliver P, Lucas JJ, Avila J, Hernandez F (2007) N-terminal cleavage of GSK-3 by calpain: a new form of GSK-3 regulation. J Biol Chem 282:22406-22413.

Gordon MO, Beiser JA, Brandt JD, Heuer DK, Higginbotham EJ, Johnson CA, Keltner JL, Miller JP, Parrish RK, 2nd, Wilson MR, Kass MA (2002) The Ocular Hypertension Treatment Study: baseline factors that predict the onset of primary open-angle glaucoma. Archives of ophthalmology 120:714-720.

Goswami C, Schmidt H, Hucho F (2007) TRPV1 at nerve endings regulates growth cone morphology and movement through cytoskeleton reorganization. FEBS J 274:760-772.

Goswami C, Rademacher N, Smalla KH, Kalscheuer V, Ropers HH, Gundelfinger ED, Hucho T (2010) TRPV1 acts as a synaptic protein and regulates vesicle recycling. J Cell Sci 123:2045-2057.

Green DR, Reed JC (1998) Mitochondria and apoptosis. Science 281:1309-1312.

Green K (1979) The ocular effects of cannabinoids. Curr Top Eye Res 1:175-215.

Grueter BA, Brasnjo G, Malenka RC (2010) Postsynaptic TRPV1 triggers cell type-specific long-term depression in the nucleus accumbens. Nat Neurosci 13:1519-1525.

Grunert U, Haverkamp S, Fletcher EL, Wassle H (2002) Synaptic distribution of ionotropic glutamate receptors in the inner plexiform layer of the primate retina. J Comp Neurol 447:138-151.

Hanks SD, Flood DG (1991) Region-specific stability of dendritic extent in normal human aging and regression in Alzheimer's disease. I. CA1 of hippocampus. Brain Res 540:63-82.

Hanna MC, Calkins DJ (2006) Expression and sequences of genes encoding glutamate receptors and transporters in primate retina determined using 3'-end amplification polymerase chain reaction. Mol Vis 12:961-976.

Hare WA, WoldeMussie E, Lai RK, Ton H, Ruiz G, Chun T, Wheeler L (2004a) Efficacy and safety of memantine treatment for reduction of changes associated with experimental glaucoma in monkey, I: Functional measures. Invest Ophthalmol Vis Sci 45:2625-2639.

Hare WA, WoldeMussie E, Weinreb RN, Ton H, Ruiz G, Wijono M, Feldmann B, Zangwill L, Wheeler L (2004b) Efficacy and safety of memantine treatment for reduction of changes associated with experimental glaucoma in monkey, II: Structural measures. Invest Ophthalmol Vis Sci 45:2640-2651.

Harwerth RS, Crawford ML, Frishman LJ, Viswanathan S, Smith EL, 3rd, Carter-Dawson L (2002) Visual field defects and neural losses from experimental glaucoma. Prog Retin Eye Res 21:91-125.

Heijl A, Leske MC, Bengtsson B, Hyman L, Bengtsson B, Hussein M, Early Manifest Glaucoma Trial G (2002) Reduction of intraocular pressure and glaucoma progression: results from the Early Manifest Glaucoma Trial. Arch Ophthalmol 120:1268-1279.

Hinton DR, Sadun AA, Blanks JC, Miller CA (1986) Optic-nerve degeneration in Alzheimer's disease. N Engl J Med 315:485-487.

Ho KW, Ward NJ, Calkins DJ (2012) TRPV1: a stress response protein in the central nervous system. Am J Neurodegener Dis 1:1-14.

Hollands H, Johnson D, Hollands S, Simel DL, Jinapriya D, Sharma S (2013) Do findings on routine examination identify patients at risk for primary open-angle glaucoma? The rational clinical examination systematic review. JAMA 309:2035-2042.

Hollenbeck PJ, Saxton WM (2005) The axonal transport of mitochondria. J Cell Sci 118:5411-5419.

Howell GR, Soto I, Zhu X, Ryan M, Macalinao DG, Sousa GL, Caddle LB, MacNicoll KH, Barbay JM, Porciatti V, Anderson MG, Smith RS, Clark AF, Libby RT, John SW (2012) Radiation treatment inhibits monocyte entry into the optic nerve head and prevents neuronal damage in a mouse model of glaucoma. J Clin Invest 122:1246-1261.

Hu H, Lu W, Zhang M, Zhang X, Argall AJ, Patel S, Lee GE, Kim YC, Jacobson KA, Laties AM, Mitchell CH (2010) Stimulation of the P2X7 receptor kills rat retinal ganglion cells in vivo. Exp Eye Res 91:425-432.

Huang W, Wang H, Galligan JJ, Wang DH (2008) Transient receptor potential vanilloid subtype 1 channel mediated neuropeptide secretion and depressor effects: role of endoplasmic reticulum associated Ca2+ release receptors in rat dorsal root ganglion neurons. J Hypertens 26:1966-1975.

Huang W, Fileta J, Rawe I, Qu J, Grosskreutz CL (2010) Calpain activation in experimental glaucoma. Invest Ophthalmol Vis Sci 51:3049-3054.

Huh JW, Raghupathi R, Laurer HL, Helfaer MA, Saatman KE (2003) Transient loss of microtubule-associated protein 2 immunoreactivity after moderate brain injury in mice. J Neurotrauma 20:975-984.

Hunter DR, Haworth RA (1979) The Ca2+-induced membrane transition in mitochondria. I. The protective mechanisms. Arch Biochem Biophys 195:453-459.

Hwang SJ, Burette A, Rustioni A, Valtschanoff JG (2004) Vanilloid receptor VR1-positive primary afferents are glutamatergic and contact spinal neurons that co-express neurokinin receptor NK1 and glutamate receptors. J Neurocytol 33:321-329.

Ibata K, Sun Q, Turrigiano GG (2008) Rapid synaptic scaling induced by changes in postsynaptic firing. Neuron 57:819-826.

Ichimiya Y, Emson PC, Mountjoy CQ, Lawson DE, Heizmann CW (1988) Loss of calbindin-28K immunoreactive neurones from the cortex in Alzheimer-type dementia. Brain Res 475:156-159.

Iester M, De Feo F, Douglas GR (2012) Visual field loss morphology in high- and normal-tension glaucoma. J Ophthalmol 2012:327326.

Inman DM, Sappington RM, Horner PJ, Calkins DJ (2006) Quantitative correlation of optic nerve pathology with ocular pressure and corneal thickness in the DBA/2 mouse model of glaucoma. Invest Ophthalmol Vis Sci 47:986-996.

Inman DM, Lambert WS, Calkins DJ, Horner PJ (2013) alpha-Lipoic acid antioxidant treatment limits glaucoma-related retinal ganglion cell death and dysfunction. PLoS One 8:e65389.

Ishibashi T, Takumida M, Akagi N, Hirakawa K, Anniko M (2009) Changes in transient receptor potential vanilloid (TRPV) 1, 2, 3 and 4 expression in mouse inner ear following gentamicin challenge. Acta Otolaryngol 129:116-126.

Jakobs TC, Libby RT, Ben Y, John SW, Masland RH (2005) Retinal ganglion cell degeneration is topological but not cell type specific in DBA/2J mice. J Cell Biol 171:313-325.

Jarvinen T, Pate DW, Laine K (2002) Cannabinoids in the treatment of glaucoma. Pharmacol Ther 95:203-220.

Jeffery G (1984) Retinal ganglion cell death and terminal field retraction in the developing rodent visual system. Brain Res 315:81-96.

Jeon CJ, Strettoi E, Masland RH (1998) The major cell populations of the mouse retina. J Neurosci 18:8936-8946.

Jiang CY, Fujita T, Yue HY, Piao LH, Liu T, Nakatsuka T, Kumamoto E (2009) Effect of resiniferatoxin on glutamatergic spontaneous excitatory synaptic transmission in substantia gelatinosa neurons of the adult rat spinal cord. Neuroscience 164:1833-1844.

John SW, Smith RS, Savinova OV, Hawes NL, Chang B, Turnbull D, Davisson M, Roderick TH, Heckenlively JR (1998) Essential iris atrophy, pigment dispersion, and glaucoma in DBA/2J mice. Invest Ophthalmol Vis Sci 39:951-962.

Jones RC, 3rd, Xu L, Gebhart GF (2005) The mechanosensitivity of mouse colon afferent fibers and their sensitization by inflammatory mediators require transient receptor potential vanilloid 1 and acid-sensing ion channel 3. J Neurosci 25:10981-10989.

Julien JP, Mushynski WE (1998) Neurofilaments in health and disease. Prog Nucleic Acid Res Mol Biol 61:1-23.

Kaas JH, Qi HX, Burish MJ, Gharbawie OA, Onifer SM, Massey JM (2008) Cortical and subcortical plasticity in the brains of humans, primates, and rats after damage to sensory afferents in the dorsal columns of the spinal cord. Exp Neurol 209:407-416.

Kanai Y, Nakazato E, Fujiuchi A, Hara T, Imai A (2005) Involvement of an increased spinal TRPV1 sensitization through its up-regulation in mechanical allodynia of CCI rats. Neuropharmacology 49:977-984.

Kang TH, Ryu YH, Kim IB, Oh GT, Chun MH (2004) Comparative study of cholinergic cells in retinas of various mouse strains. Cell Tissue Res 317:109-115.

Karlsson U, Sundgren-Andersson AK, Johansson S, Krupp JJ (2005) Capsaicin augments synaptic transmission in the rat medial preoptic nucleus. Brain Res 1043:1-11.

Karpati G, Carpenter S, Durham H (1988) A hypothesis for the pathogenesis of amyotrophic lateral sclerosis. Rev Neurol (Paris) 144:672-675.

Kerrigan LA, Zack DJ, Quigley HA, Smith SD, Pease ME (1997) TUNEL-positive ganglion cells in human primary open-angle glaucoma. Arch of Ophthalmol 115:1031-1035.

Kim SR, Kim SU, Oh U, Jin BK (2006) Transient receptor potential vanilloid subtype 1 mediates microglial cell death in vivo and in vitro via Ca2+-mediated mitochondrial damage and cytochrome c release. J Immunol 177:4322-4329.

Kim SR, Lee DY, Chung ES, Oh UT, Kim SU, Jin BK (2005) Transient receptor potential vanilloid subtype 1 mediates cell death of mesencephalic dopaminergic neurons in vivo and in vitro. J Neurosci 25:662-671.

Kim SR, Chung YC, Chung ES, Park KW, Won SY, Bok E, Park ES, Jin BK (2007) Roles of transient receptor potential vanilloid subtype 1 and cannabinoid type 1 receptors in the brain: neuroprotection versus neurotoxicity. Mol Neurobiol 35:245-254.

Kondo Y, Takada M, Honda Y, Mizuno N (1993) Bilateral projections of single retinal ganglion cells to the lateral geniculate nuclei and superior colliculi in the albino rat. Brain Res 608:204-215.

Kong JH, Fish DR, Rockhill RL, Masland RH (2005) Diversity of ganglion cells in the mouse retina: unsupervised morphological classification and its limits. J Comp Neurol 489:293-310.

Koplas PA, Rosenberg RL, Oxford GS (1997) The role of calcium in the desensitization of capsaicin responses in rat dorsal root ganglion neurons. J Neurosci 17:3525-3537.

Koronyo-Hamaoui M, Koronyo Y, Ljubimov AV, Miller CA, Ko MK, Black KL, Schwartz M, Farkas DL (2011) Identification of amyloid plaques in retinas from Alzheimer's patients and noninvasive in vivo optical imaging of retinal plaques in a mouse model. Neuroimage 54 Suppl 1:S204-217.

Laine K, Jarvinen T, Savinainen J, Laitinen JT, Pate DW, Jarvinen K (2001) Effects of topical anandamide-transport inhibitors, AM404 and olvanil, on intraocular pressure in normotensive rabbits. Pharm Res 18:494-499.

Lambert WS, Ruiz L, Crish SD, Wheeler LA, Calkins DJ (2011) Brimonidine prevents axonal and somatic degeneration of retinal ganglion cell neurons. Mol Neurodegener 6:4.

Lappin SC, Randall AD, Gunthorpe MJ, Morisset V (2006) TRPV1 antagonist, SB-366791, inhibits glutamatergic synaptic transmission in rat spinal dorsal horn following peripheral inflammation. Eur J Pharmacol 540:73-81.

Lastres-Becker I, de Miguel R, De Petrocellis L, Makriyannis A, Di Marzo V, Fernandez-Ruiz J (2003) Compounds acting at the endocannabinoid and/or endovanilloid systems reduce hyperkinesia in a rat model of Huntington's disease. J Neurochem 84:1097-1109.

Lee HK (2012) Ca-permeable AMPA receptors in homeostatic synaptic plasticity. Front Mol Neurosci 5:17.

Lee MS, Kwon YT, Li M, Peng J, Friedlander RM, Tsai LH (2000) Neurotoxicity induces cleavage of p35 to p25 by calpain. Nature 405:360-364.

Lee YM, Kim YK, Chung JH (2009) Increased expression of TRPV1 channel in intrinsically aged and photoaged human skin in vivo. Exp Dermatol 18:431-436.

Leonelli M, Martins DO, Britto LR (2013) Retinal cell death induced by TRPV1 activation involves NMDA signaling and upregulation of nitric oxide synthases. Cell Mol Neurobiol 33:379-392.

Leonelli M, Martins DO, Kihara AH, Britto LR (2009) Ontogenetic expression of the vanilloid receptors TRPV1 and TRPV2 in the rat retina. Int J Dev Neurosci 27:709-718.

Levin LA (2001) Relevance of the site of injury of glaucoma to neuroprotective strategies. Surv Ophthalmol 45 Suppl 3:S243-249.

Levkovitch-Verbin H, Martin KR, Quigley HA, Baumrind LA, Pease ME, Valenta D (2002) Measurement of amino acid levels in the vitreous humor of rats after chronic intraocular pressure elevation or optic nerve transection. J Glaucoma 11:396-405.

Levkovitch-Verbin H, Dardik R, Vander S, Nisgav Y, Kalev-Landoy M, Melamed S (2006) Experimental glaucoma and optic nerve transection induce simultaneous upregulation of proapoptotic and prosurvival genes. Invest Ophthalmol Vis Sci 47:2491-2497.

Li C, Zhou Y, Liu Z, Tuo J, Hu N, Guan H (2012) Spatiotemporal expression of postsynaptic density 95 in rat retina after optic nerve injury. J Mol Neurosci 46:595-605.

Li HB, Mao RR, Zhang JC, Yang Y, Cao J, Xu L (2008) Antistress effect of TRPV1 channel on synaptic plasticity and spatial memory. Biol Psychiatry 64:286-292.

Li Y, Jiang N, Powers C, Chopp M (1998) Neuronal damage and plasticity identified by microtubule-associated protein 2, growth-associated protein 43, and cyclin D1 immunoreactivity after focal cerebral ischemia in rats. Stroke 29:1972-1980.

Libby RT, Li Y, Savinova OV, Barter J, Smith RS, Nickells RW, John SW (2005) Susceptibility to neurodegeneration in a glaucoma is modified by Bax gene dosage. PLoS Genet 1:17-26.

Liedtke W (2006) Transient receptor potential vanilloid channels functioning in transduction of osmotic stimuli. J Endocrinol 191:515-523.

Lin MT, Beal MF (2006) Mitochondrial dysfunction and oxidative stress in neurodegenerative diseases. Nature 443:787-795.

Lin S-Y, Corey DP (2005) TRP channels in mechanosensation. Curr Opin Neurobiol 15:350-357.

Lin YC, Koleske AJ (2010) Mechanisms of synapse and dendrite maintenance and their disruption in psychiatric and neurodegenerative disorders. Annu Rev Neurosci 33:349-378.

Lishko PV, Procko E, Jin X, Phelps CB, Gaudet R (2007) The ankyrin repeats of TRPV1 bind multiple ligands and modulate channel sensitivity. Neuron 54:905-918.

Liu B, Liao M, Mielke JG, Ning K, Chen Y, Li L, El-Hayek YH, Gomez E, Zukin RS, Fehlings MG, Wan Q (2006) Ischemic insults direct glutamate receptor subunit 2-lacking AMPA receptors to synaptic sites. J Neurosci 26:5309-5319.

Liu M, Duggan J, Salt TE, Cordeiro MF (2011) Dendritic changes in visual pathways in glaucoma and other neurodegenerative conditions. Exp Eye Res 92:244-250.

Liu M, Liu MC, Magoulas C, Priestley JV, Willmott NJ (2003) Versatile regulation of cytosolic Ca2+ by vanilloid receptor I in rat dorsal root ganglion neurons. J Biol Chem 278:5462-5472.

Livak KJ, Schmittgen TD (2001) Analysis of relative gene expression data using real-time quantitative PCR and the 2(-Delta Delta C(T)) Method. Methods 25:402-408.

London A, Benhar I, Schwartz M (2013) The retina as a window to the brain-from eye research to CNS disorders. Nat Rev Neurol 9:44-53.

Lu X, Rong Y, Baudry M (2000) Calpain-mediated degradation of PSD-95 in developing and adult rat brain. Neurosci Lett 286:149-153.

Luetjens CM, Bui NT, Sengpiel B, Munstermann G, Poppe M, Krohn AJ, Bauerbach E, Krieglstein J, Prehn JH (2000) Delayed mitochondrial dysfunction in excitotoxic neuron death: cytochrome c release and a secondary increase in superoxide production. J Neurosci 20:5715-5723.

Ma W, Zhang Y, Bantel C, Eisenach JC (2005) Medium and large injured dorsal root ganglion cells increase TRPV-1, accompanied by increased alpha2C-adrenoceptor co-expression and functional inhibition by clonidine. Pain 113:386-394.

Maione S, Cristino L, Migliozzi AL, Georgiou AL, Starowicz K, Salt TE, Di Marzo V (2009) TRPV1 channels control synaptic plasticity in the developing superior colliculus. J Physiol 587:2521-2535.

Malenka RC, Bear MF (2004) LTP and LTD: an embarrassment of riches. Neuron 44:5-21.

Mandadi S, Tominaga T, Numazaki M, Murayama N, Saito N, Armati PJ, Roufogalis BD, Tominaga M (2006) Increased sensitivity of desensitized TRPV1 by PMA occurs through PKCepsilon-mediated phosphorylation at S800. Pain 123:106-116.

Marambaud P, Dreses-Werringloer U, Vingtdeux V (2009) Calcium signaling in neurodegeneration. Mol Neurodegener 4:20.

Marinelli S, Pascucci T, Bernardi G, Puglisi-Allegra S, Mercuri NB (2005) Activation of TRPV1 in the VTA excites dopaminergic neurons and increases chemical- and noxious-induced dopamine release in the nucleus accumbens. Neuropsychopharmacology 30:864-870.

Marinelli S, Di Marzo V, Berretta N, Matias I, Maccarrone M, Bernardi G, Mercuri NB (2003) Presynaptic facilitation of glutamatergic synapses to dopaminergic neurons of the rat substantia nigra by endogenous stimulation of vanilloid receptors. J Neurosci 23:3136-3144.

Marsch R, Foeller E, Rammes G, Bunck M, Kossl M, Holsboer F, Zieglgansberger W, Landgraf R, Lutz B, Wotjak CT (2007) Reduced anxiety, conditioned fear, and hippocampal long-term potentiation in transient receptor potential vanilloid type 1 receptor-deficient mice. J Neurosci 27:832-839.

Marshall IC, Owen DE, Cripps TV, Davis JB, McNulty S, Smart D (2003) Activation of vanilloid receptor 1 by resiniferatoxin mobilizes calcium from inositol 1,4,5-trisphosphate-sensitive stores. Br J Pharmacol 138:172-176.

Martinez-Garcia MC, Martinez T, Paneda C, Gallego P, Jimenez AI, Merayo J (2013) Differential expression and localization of transient receptor potential vanilloid 1 in rabbit and human eyes. Histol Histopathol 28:1507-1516.

Matias I, Wang JW, Moriello AS, Nieves A, Woodward DF, Di Marzo V (2006) Changes in endocannabinoid and palmitoylethanolamide levels in eye tissues of patients with diabetic retinopathy and age-related macular degeneration. Prostaglandins Leukot Essent Fatty Acids 75:413-418.

Mattson MP (1998) Modification of ion homeostasis by lipid peroxidation: roles in neuronal degeneration and adaptive plasticity. Trends Neurosci 21:53-57.

Mattson MP (2004) Pathways towards and away from Alzheimer's disease. Nature 430:631-639.

Mattson MP (2007) Calcium and neurodegeneration. Aging Cell 6:337-350.

Mazzoni F, Novelli E, Strettoi E (2008) Retinal ganglion cells survive and maintain normal dendritic morphology in a mouse model of inherited photoreceptor degeneration. J Neurosci 28:14282-14292.

McKinney MK, Cravatt BF (2005) Structure and function of fatty acid amide hydrolase. Annu Rev Biochem 74:411-432.

McKinnon SJ, Schlamp CL, Nickells RW (2009) Mouse models of retinal ganglion cell death and glaucoma. Exp Eye Res 88:816-824.

McLachlan DR, Wong L, Bergeron C, Baimbridge KG (1987) Calmodulin and calbindin D28K in Alzheimer disease. Alzheimer Dis Assoc Disord 1:171-179.

Mechoulam R, Shohami E (2007) Endocannabinoids and traumatic brain injury. Mol Neurobiol 36:68-74.

Medvedeva YV, Kim MS, Usachev YM (2008) Mechanisms of prolonged presynaptic Ca2+ signaling and glutamate release induced by TRPV1 activation in rat sensory neurons. J Neurosci 28:5295-5311.

Melck D, Bisogno T, De Petrocellis L, Chuang H, Julius D, Bifulco M, Di Marzo V (1999) Unsaturated long-chain N-acyl-vanillyl-amides (N-AVAMs): vanilloid receptor ligands that inhibit anandamide-facilitated transport and bind to CB1 cannabinoid receptors. Biochem Biophys Res Commun 262:275-284.

Meriaux C, Arafah K, Tasiemski A, Wisztorski M, Bruand J, Boidin-Wichlacz C, Desmons A, Debois D, Laprevote O, Brunelle A, Gaasterland T, Macagno E, Fournier I, Salzet M (2011) Multiple changes in peptide and lipid expression associated with regeneration in the nervous system of the medicinal leech. PLoS One 6:e18359.

Miller BA (2006) The role of TRP channels in oxidative stress-induced cell death. J Membr Biol 209:31-41.

Milosevic NT, Ristanovic D (2007) The Sholl analysis of neuronal cell images: semi-log or log-log method? J Theor Biol 245:130-140.

Mohapatra DP, Nau C (2005) Regulation of Ca2+-dependent desensitization in the vanilloid receptor TRPV1 by calcineurin and cAMP-dependent protein kinase. J Biol Chem 280:13424-13432.

Moiseenkova-Bell VY, Stanciu LA, Serysheva, II, Tobe BJ, Wensel TG (2008) Structure of TRPV1 channel revealed by electron cryomicroscopy. Proc Natl Acad Sci U S A 105:7451-7455.

Moolman DL, Vitolo OV, Vonsattel JP, Shelanski ML (2004) Dendrite and dendritic spine alterations in Alzheimer models. J Neurocytol 33:377-387.

Moore CI, Stern CE, Dunbar C, Kostyk SK, Gehi A, Corkin S (2000) Referred phantom sensations and cortical reorganization after spinal cord injury in humans. Proc Natl Acad Sci U S A 97:14703-14708.

Morenilla-Palao C, Planells-Cases R, Garcia-Sanz N, Ferrer-Montiel A (2004) Regulated exocytosis contributes to protein kinase C potentiation of vanilloid receptor activity. J Biol Chem 279:25665-25672.

Morfini GA, You YM, Pollema SL, Kaminska A, Liu K, Yoshioka K, Bjorkblom B, Coffey ET, Bagnato C, Han D, Huang CF, Banker G, Pigino G, Brady ST (2009a) Pathogenic huntingtin inhibits fast axonal transport by activating JNK3 and phosphorylating kinesin. Nat Neurosci 12:864-871.

Morfini GA, Burns M, Binder LI, Kanaan NM, LaPointe N, Bosco DA, Brown RH, Jr., Brown H, Tiwari A, Hayward L, Edgar J, Nave KA, Garberrn J, Atagi Y, Song Y, Pigino G, Brady ST (2009b) Axonal transport defects in neurodegenerative diseases. J Neurosci 29:12776-12786.

Morimoto T, Miyoshi T, Matsuda S, Tano Y, Fujikado T, Fukuda Y (2005) Transcorneal electrical stimulation rescues axotomized retinal ganglion cells by activating endogenous retinal IGF-1 system. Invest Ophthalmol Vis Sci 46:2147-2155.

Morquette JB, Di Polo A (2008) Dendritic and synaptic protection: is it enough to save the retinal ganglion cell body and axon? J Neuroophthalmol 28:144-154.

Morrison JC, Moore CG, Deppmeier LM, Gold BG, Meshul CK, Johnson EC (1997) A rat model of chronic pressure-induced optic nerve damage. Exp Eye Res 64:85-96.

Motil J, Chan WK, Dubey M, Chaudhury P, Pimenta A, Chylinski TM, Ortiz DT, Shea TB (2006) Dynein mediates retrograde neurofilament transport within axons and anterograde delivery of NFs from perikarya into axons: regulation by multiple phosphorylation events. Cell Motil Cytoskeleton 63:266-286.

Musella A, De Chiara V, Rossi S, Prosperetti C, Bernardi G, Maccarrone M, Centonze D (2009) TRPV1 channels facilitate glutamate transmission in the striatum. Mol Cell Neurosci 40:89-97.

Mutai H, Heller S (2003) Vertebrate and invertebrate TRPV-like mechanoreceptors. Cell Calcium 33:471-478.

Neufeld AH, Liu B (2003) Glaucomatous optic neuropathy: when glia misbehave. Neuroscientist 9:485-495.

Ning A, Cui J, To E, Ashe KH, Matsubara J (2008) Amyloid-beta deposits lead to retinal degeneration in a mouse model of Alzheimer disease. Invest Ophthalmol Vis Sci 49:5136-5143.

Nongpiur ME, Ku JY, Aung T (2011) Angle closure glaucoma: a mechanistic review. Curr Opin Ophthalmol 22:96-101.

Nowak JZ (1987) The retina as a model neural tissue: comparative studies on retinal and brain aminergic mechanisms. Pol J Pharmacol Pharm 39:451-482.

Nucci C, Bari M, Spano A, Corasaniti M, Bagetta G, Maccarrone M, Morrone LA (2008) Potential roles of (endo)cannabinoids in the treatment of glaucoma: from intraocular pressure control to neuroprotection. Prog Brain Res 173:451-464.

Nucci C, Tartaglione R, Cerulli A, Mancino R, Spano A, Cavaliere F, Rombola L, Bagetta G, Corasaniti MT, Morrone LA (2007a) Retinal damage caused by high intraocular pressure-induced transient ischemia is prevented by coenzyme Q10 in rat. Int Rev Neurobiol 82:397-406.

Nucci C, Gasperi V, Tartaglione R, Cerulli A, Terrinoni A, Bari M, De Simone C, Agro AF, Morrone LA, Corasaniti MT, Bagetta G, Maccarrone M (2007b) Involvement of the endocannabinoid system in retinal damage after high intraocular pressure-induced ischemia in rats. Invest Ophthalmol Vis Sci 48:2997-3004.

Numazaki M, Tominaga T, Takeuchi K, Murayama N, Toyooka H, Tominaga M (2003) Structural determinant of TRPV1 desensitization interacts with calmodulin. Proc Natl Acad Sci U S A 100:8002-8006.

Oesch NW, Kothmann WW, Diamond JS (2011) Illuminating synapses and circuitry in the retina. Curr Opin Neurobiol 21:238-244.

Ohno-Shosaku T, Maejima T, Kano M (2001) Endogenous cannabinoids mediate retrograde signals from depolarized postsynaptic neurons to presynaptic terminals. Neuron 29:729-738.

Okabe S, Shiomura Y, Hirokawa N (1989) Immunocytochemical localization of microtubule-associated proteins 1A and 2 in the rat retina. Brain Res 483:335-346.

Osborne NN (2009) Recent clinical findings with memantine should not mean that the idea of neuroprotection in glaucoma is abandoned. Acta Ophthalmol 87:450-454.

Osborne NN, Ugarte M, Chao M, Chidlow G, Bae JH, Wood JP, Nash MS (1999) Neuroprotection in relation to retinal ischemia and relevance to glaucoma. Surv Ophthalmol 43 Suppl 1:S102-128.

Pang IH, Clark AF (2007) Rodent models for glaucoma retinopathy and optic neuropathy. J Glaucoma 16:483-505.

Panov AV, Burke JR, Strittmatter WJ, Greenamyre JT (2003) In vitro effects of polyglutamine tracts on Ca2+-dependent depolarization of rat and human mitochondria: relevance to Huntington's disease. Arch Biochem Biophys 410:1-6.

Panov AV, Gutekunst CA, Leavitt BR, Hayden MR, Burke JR, Strittmatter WJ, Greenamyre JT (2002) Early mitochondrial calcium defects in Huntington's disease are a direct effect of polyglutamines. Nat Neurosci 5:731-736.

Pavlidis M, Stupp T, Naskar R, Cengiz C, Thanos S (2003) Retinal ganglion cells resistant to advanced glaucoma: a postmortem study of human retinas with the carbocyanine dye DiI. Invest Ophthalmol Vis Sci 44:5196-5205.

Pegorini S, Zani A, Braida D, Guerini-Rocco C, Sala M (2006) Vanilloid VR1 receptor is involved in rimonabant-induced neuroprotection. Br J Pharmacol 147:552-559.

Pegorini S, Braida D, Verzoni C, Guerini-Rocco C, Consalez GG, Croci L, Sala M (2005) Capsaicin exhibits neuroprotective effects in a model of transient global cerebral ischemia in Mongolian gerbils. Br J Pharmacol 144:727-735.

Perry VH, Oehler R, Cowey A (1984) Retinal ganglion cells that project to the dorsal lateral geniculate nucleus in the macaque monkey. Neuroscience 12:1101-1123.

Pertwee RG (2006) The pharmacology of cannabinoid receptors and their ligands: an overview. Int J Obes (Lond) 30 Suppl 1:S13-18.

Pertwee RG (2008) The diverse CB1 and CB2 receptor pharmacology of three plant cannabinoids: delta9-tetrahydrocannabinol, cannabidiol and delta9-tetrahydrocannabivarin. Br J Pharmacol 153:199-215.

Peters JH, McDougall SJ, Fawley JA, Smith SM, Andresen MC (2010) Primary afferent activation of thermosensitive TRPV1 triggers asynchronous glutamate release at central neurons. Neuron 65:657-669.

Petzold A, Gveric D, Groves M, Schmierer K, Grant D, Chapman M, Keir G, Cuzner L, Thompson EJ (2008) Phosphorylation and compactness of neurofilaments in multiple sclerosis: indicators of axonal pathology. Exp Neurol 213:326-335.

Pigino G, Pelsman A, Mori H, Busciglio J (2001) Presenilin-1 mutations reduce cytoskeletal association, deregulate neurite growth, and potentiate neuronal dystrophy and tau phosphorylation. J Neurosci 21:834-842.

Pigino G, Morfini G, Atagi Y, Deshpande A, Yu C, Jungbauer L, LaDu M, Busciglio J, Brady S (2009) Disruption of fast axonal transport is a pathogenic mechanism for intraneuronal amyloid beta. Proc Natl Acad Sci U S A 106:5907-5912.

Pingle SC, Matta JA, Ahern GP (2007) Capsaicin receptor: TRPV1 a promiscuous TRP channel. Handb Exp Pharmacol 179:155-171.

Plant TD, Zollner C, Mousa SA, Oksche A (2006) Endothelin-1 potentiates capsaicin-induced TRPV1 currents via the endothelin A receptor. Exp Biol Med (Maywood) 231:1161-1164.

Porcella A, Maxia C, Gessa GL, Pani L (2000) The human eye expresses high levels of CB1 cannabinoid receptor mRNA and protein. Eur J Neurosci 12:1123-1127.

Posmantur RM, Kampfl A, Taft WC, Bhattacharjee M, Dixon CE, Bao J, Hayes RL (1996) Diminished microtubule-associated protein 2 (MAP2) immunoreactivity following cortical impact brain injury. J Neurotrauma 13:125-137.

Puente N, Cui Y, Lassalle O, Lafourcade M, Georges F, Venance L, Grandes P, Manzoni OJ (2011) Polymodal activation of the endocannabinoid system in the extended amygdala. Nat Neurosci 14:1542-1547.

Puente N, Reguero L, Elezgarai I, Canduela MJ, Mendizabal-Zubiaga J, Ramos-Uriarte A, Fernandez-Espejo E, Grandes P (2014) The transient receptor potential vanilloid-1 is localized at excitatory synapses in the mouse dentate gyrus. Brain Struct Funct.

Puntambekar P, Mukherjea D, Jajoo S, Ramkumar V (2005) Essential role of Rac1/NADPH oxidase in nerve growth factor induction of TRPV1 expression. J Neurochem 95:1689-1703.

Qiu M, Bulfone A, Martinez S, Meneses JJ, Shimamura K, Pedersen RA, Rubenstein JL (1995) Null mutation of Dlx-2 results in abnormal morphogenesis of proximal first and second branchial arch derivatives and abnormal differentiation in the forebrain. Genes Dev 9:2523-2538.

Qu J, Wang D, Grosskreutz CL (2010) Mechanisms of retinal ganglion cell injury and defense in glaucoma. Exp Eye Res 91:48-53.

Quigley HA (1993) Open-angle glaucoma. N Engl J Med 328:1097-1106.

Quigley HA, Broman AT (2006) The number of people with glaucoma worldwide in 2010 and 2020. Br J Ophthalmol 90:262-267.

Rakhshan F, Day TA, Blakely RD, Barker EL (2000) Carrier-mediated uptake of the endogenous cannabinoid anandamide in RBL-2H3 cells. J Pharmacol Exp Ther 292:960-967.

Reddy PH, Beal MF (2008) Amyloid beta, mitochondrial dysfunction and synaptic damage: implications for cognitive decline in aging and Alzheimer's disease. Trends Mol Med 14:45-53.

Reichstein D, Ren L, Filippopoulos T, Mittag T, Danias J (2007) Apoptotic retinal ganglion cell death in the DBA/2 mouse model of glaucoma. Exp Eye Res 84:13-21.

Reilly CA, Johansen ME, Lanza DL, Lee J, Lim JO, Yost GS (2005) Calcium-dependent and independent mechanisms of capsaicin receptor (TRPV1)-mediated cytokine production and cell death in human bronchial epithelial cells. J Biochem Mol Toxicol 19:266-275.

Roberts JC, Davis JB, Benham CD (2004) [3H]Resiniferatoxin autoradiography in the CNS of wild-type and TRPV1 null mice defines TRPV1 (VR-1) protein distribution. Brain Res 995:176-183.

Roberts LA, Large CH, Higgins MJ, Stone TW, O'Shaughnessy CT, Morris BJ (1998) Increased expression of dendritic mRNA following the induction of long-term potentiation. Brain Res Mol Brain Res 56:38-44.

Rong W, Hillsley K, Davis JB, Hicks G, Winchester WJ, Grundy D (2004) Jejunal afferent nerve sensitivity in wild-type and TRPV1 knockout mice. J Physiol 560:867-881.

Ross RA (2003) Anandamide and vanilloid TRPV1 receptors. Br J Pharmacol 140:790-801.

Roy S, Zhang B, Lee VM, Trojanowski JQ (2005) Axonal transport defects: a common theme in neurodegenerative diseases. Acta Neuropathol 109:5-13.

Ryskamp DA, Witkovsky P, Barabas P, Huang W, Koehler C, Akimov NP, Lee SH, Chauhan S, Xing W, Renteria RC, Liedtke W, Krizaj D (2011) The polymodal ion channel transient receptor potential vanilloid 4 modulates calcium flux, spiking rate, and apoptosis of mouse retinal ganglion cells. J Neurosci 31:7089-7101.

Sadun AA, Bassi CJ (1990) Optic nerve damage in Alzheimer's disease. Ophthalmology 97:9-17.

Sakamoto K, Kuroki T, Okuno Y, Sekiya H, Watanabe A, Sagawa T, Ito H, Mizuta A, Mori A, Nakahara T, Ishii K (2014) Activation of the TRPV1 channel attenuates N-methyl-d-aspartic acid-induced neuronal injury in the rat retina. Eur J Pharmacol.

Salmon JF (1999) Predisposing factors for chronic angle-closure glaucoma. Prog Retin Eye Res 18:121-132.

Samuel MA, Zhang Y, Meister M, Sanes JR (2011) Age-related alterations in neurons of the mouse retina. J Neurosci 31:16033-16044.

Samways DS, Khakh BS, Egan TM (2008) Tunable calcium current through TRPV1 receptor channels. J Biol Chem 283:31274-31278.

Sanchez JF, Krause JE, Cortright DN (2001) The distribution and regulation of vanilloid receptor VR1 and VR1 5' splice variant RNA expression in rat. Neuroscience 107:373-381.

Sappington RM, Calkins DJ (2008) Contribution of TRPV1 to microglia-derived IL-6 and NFkappaB translocation with elevated hydrostatic pressure. Invest Ophthalmol Vis Sci 49:3004-3017.

Sappington RM, Chan M, Calkins DJ (2006) Interleukin-6 protects retinal ganglion cells from pressure-induced death. Invest Ophthalmol Vis Sci 47:2932-2942.

Sappington RM, Sidorova T, Long DJ, Calkins DJ (2009) TRPV1: contribution to retinal ganglion cell apoptosis and increased intracellular Ca2+ with exposure to hydrostatic pressure. Invest Ophthalmol Vis Sci 50:717-728.

Sappington RM, Carlson BJ, Crish SD, Calkins DJ (2010) The microbead occlusion model: a paradigm for induced ocular hypertension in rats and mice. Invest Ophthalmol Vis Sci 51:207-216.

Sasamura T, Sasaki M, Tohda C, Kuraishi Y (1998) Existence of capsaicin-sensitive glutamatergic terminals in rat hypothalamus. Neuroreport 9:2045-2048.

Schmidt TM, Kofuji P (2011) An isolated retinal preparation to record light response from genetically labeled retinal ganglion cells. J Vis Exp.

Schumacher MA, Eilers H (2010) TRPV1 splice variants: structure and function. Front Biosci (Landmark Ed) 15:872-882.

Schwartz M, Yoles E (2000) Self-destructive and self-protective processes in the damaged optic nerve: implications for glaucoma. Invest Ophthalmol Vis Sci 41:349-351.

Scotland RS, Chauhan S, Davis C, De Felipe C, Hunt S, Kabir J, Kotsonis P, Oh U, Ahluwalia A (2004) Vanilloid receptor TRPV1, sensory C-fibers, and vascular autoregulation: a novel mechanism involved in myogenic constriction. Circ Res 95:1027-1034.

Seki M, Nawa H, Fukuchi T, Abe H, Takei N (2003) BDNF is upregulated by postnatal development and visual experience: quantitative and immunohistochemical analyses of BDNF in the rat retina. Invest Ophthalmol Vis Sci 44:3211-3218.

Shankar GM, Bloodgood BL, Townsend M, Walsh DM, Selkoe DJ, Sabatini BL (2007) Natural oligomers of the Alzheimer amyloid-beta protein induce reversible synapse loss by modulating an NMDA-type glutamate receptor-dependent signaling pathway. J Neurosci 27:2866-2875.

Sharif Naeini R, Witty MF, Seguela P, Bourque CW (2006) An N-terminal variant of Trpv1 channel is required for osmosensory transduction. Nat Neurosci 9:93-98.

Shea TB, Chan WK (2008) Regulation of neurofilament dynamics by phosphorylation. Eur J Neurosci 27:1893-1901.

Shea TB, Yabe JT, Ortiz D, Pimenta A, Loomis P, Goldman RD, Amin N, Pant HC (2004) Cdk5 regulates axonal transport and phosphorylation of neurofilaments in cultured neurons. J Cell Sci 117:933-941.

Shirakawa H, Yamaoka T, Sanpei K, Sasaoka H, Nakagawa T, Kaneko S (2008) TRPV1 stimulation triggers apoptotic cell death of rat cortical neurons. Biochem Biophys Res Commun 377:1211-1215.

Sholl DA (1953) Dendritic organization in the neurons of the visual and motor cortices of the cat. J Anat 87:387-406.

Shou T, Liu J, Wang W, Zhou Y, Zhao K (2003) Differential dendritic shrinkage of alpha and beta retinal ganglion cells in cats with chronic glaucoma. Invest Ophthalmol Vis Sci 44:3005-3010.

Sieradzan KA, Mann DM (2001) The selective vulnerability of nerve cells in Huntington's disease. Neuropathol Appl Neurobiol 27:1-21.

Sikand P, Premkumar LS (2007) Potentiation of glutamatergic synaptic transmission by protein kinase C-mediated sensitization of TRPV1 at the first sensory synapse. J Physiol 581:631-647.

Siminoff R, Schwassmann HO, Kruger L (1966) An electrophysiological study of the visual projection to the superior colliculus of the rat. J Comp Neurol 127:435-444.

Sims SM, Holmgren L, Cathcart HM, Sappington RM (2012) Spatial regulation of interleukin-6 signaling in response to neurodegenerative stressors in the retina. Am J Neurodegener Dis 1:168-179.

Smith GD, Gunthorpe MJ, Kelsell RE, Hayes PD, Reilly P, Facer P, Wright JE, Jerman JC, Walhin JP, Ooi L, Egerton J, Charles KJ, Smart D, Randall AD, Anand P, Davis JB (2002) TRPV3 is a temperature-sensitive vanilloid receptor-like protein. Nature 418:186-190.

Smith RG, Henry YK, Mattson MP, Appel SH (1998) Presence of 4-hydroxynonenal in cerebrospinal fluid of patients with sporadic amyotrophic lateral sclerosis. Ann Neurol 44:696-699.

Sobue G, Hashizume Y, Yasuda T, Mukai E, Kumagai T, Mitsuma T, Trojanowski JQ (1990) Phosphorylated high molecular weight neurofilament protein in lower motor neurons in amyotrophic lateral sclerosis and other neurodegenerative diseases involving ventral horn cells. Acta Neuropathol 79:402-408.

Solis O, Limon DI, Flores-Hernandez J, Flores G (2007) Alterations in dendritic morphology of the prefrontal cortical and striatum neurons in the unilateral 6-OHDA-rat model of Parkinson's disease. Synapse 61:450-458.

Sommer A (1989) Intraocular pressure and glaucoma. Am J Ophthalmol 107:186-188.

Sommer A, Tielsch JM, Katz J, Quigley HA, Gottsch JD, Javitt J, Singh K (1991) Relationship between intraocular pressure and primary open angle glaucoma among white and black Americans. The Baltimore Eye Survey. Arch Ophthalmol 109:1090-1095.

Song ZH, Slowey CA (2000) Involvement of cannabinoid receptors in the intraocular pressure-lowering effects of WIN55212-2. J Pharmacol Exp Ther 292:136-139.

Soto I, Oglesby E, Buckingham BP, Son JL, Roberson ED, Steele MR, Inman DM, Vetter ML, Horner PJ, Marsh-Armstrong N (2008) Retinal ganglion cells downregulate gene expression and lose their axons within the optic nerve head in a mouse glaucoma model. J Neurosci 28:548-561.

Spaethling JM, Klein DM, Singh P, Meaney DF (2008) Calcium-permeable AMPA receptors appear in cortical neurons after traumatic mechanical injury and contribute to neuronal fate. J Neurotrauma 25:1207-1216.

Spires TL, Grote HE, Garry S, Cordery PM, Van Dellen A, Blakemore C, Hannan AJ (2004) Dendritic spine pathology and deficits in experience-dependent dendritic plasticity in R6/1 Huntington's disease transgenic mice. The Eur J Neurosci 19:2799-2807.

Stamer WD, Golightly SF, Hosohata Y, Ryan EP, Porter AC, Varga E, Noecker RJ, Felder CC, Yamamura HI (2001) Cannabinoid CB(1) receptor expression, activation and detection of endogenous ligand in trabecular meshwork and ciliary process tissues. Eur J Pharmacol 431:277-286.

Staruschenko A, Jeske NA, Akopian AN (2010) Contribution of TRPV1-TRPA1 interaction to the single channel properties of the TRPA1 channel. J Biol Chem 285:15167-15177.

Stavrovskaya IG, Kristal BS (2005) The powerhouse takes control of the cell: is the mitochondrial permeability transition a viable therapeutic target against neuronal dysfunction and death? Free Radic Biol Med 38:687-697.

Steele MR, Inman DM, Calkins DJ, Horner PJ, Vetter ML (2006) Microarray analysis of retinal gene expression in the DBA/2J model of glaucoma. Invest Ophthalmol Vis Sci 47:977-985.

Stevens B, Allen NJ, Vazquez LE, Howell GR, Christopherson KS, Nouri N, Micheva KD, Mehalow AK, Huberman AD, Stafford B, Sher A, Litke AM, Lambris JD, Smith SJ, John SW, Barres BA (2007) The classical complement cascade mediates CNS synapse elimination. Cell 131:1164-1178.

Stokin GB, Lillo C, Falzone TL, Brusch RG, Rockenstein E, Mount SL, Raman R, Davies P, Masliah E, Williams DS, Goldstein LS (2005) Axonopathy and transport deficits early in the pathogenesis of Alzheimer's disease. Science 307:1282-1288.

Straiker AJ, Maguire G, Mackie K, Lindsey J (1999) Localization of cannabinoid CB1 receptors in the human anterior eye and retina. Invest Ophthalmol Vis Sci 40:2442-2448.

Sugiyama T, Lee SY, Horie T, Oku H, Takai S, Tanioka H, Kuriki Y, Kojima S, Ikeda T (2013) P2X(7) receptor activation may be involved in neuronal loss in the retinal ganglion cell layer after acute elevation of intraocular pressure in rats. Mol Vis 19:2080-2091.

Sun W, Li N, He S (2002) Large-scale morphological survey of mouse retinal ganglion cells. J Comp Neurol 451:115-126.

Sun Y, Savanenin A, Reddy PH, Liu YF (2001) Polyglutamine-expanded huntingtin promotes sensitization of N-methyl-D-aspartate receptors via post-synaptic density 95. J Biol Chem 276:24713-24718.

Takuma H, Kwak S, Yoshizawa T, Kanazawa I (1999) Reduction of GluR2 RNA editing, a molecular change that increases calcium influx through AMPA receptors, selective in the spinal ventral gray of patients with amyotrophic lateral sclerosis. Ann Neurol 46:806-815.

Tan Y, Dourdin N, Wu C, De Veyra T, Elce JS, Greer PA (2006) Ubiquitous calpains promote caspase-12 and JNK activation during endoplasmic reticulum stress-induced apoptosis. J Biol Chem 281:16016-16024.

Terry RD, Masliah E, Salmon DP, Butters N, DeTeresa R, Hill R, Hansen LA, Katzman R (1991) Physical basis of cognitive alterations in Alzheimer's disease: synapse loss is the major correlate of cognitive impairment. Ann Neurol 30:572-580.

Tezel G (2006) Oxidative stress in glaucomatous neurodegeneration: mechanisms and consequences. Prog Retin Eye Res 25:490-513.

Tominaga M, Caterina MJ, Malmberg AB, Rosen TA, Gilbert H, Skinner K, Raumann BE, Basbaum AI, Julius D (1998) The cloned capsaicin receptor integrates multiple pain-producing stimuli. Neuron 21:531-543.

Toth A, Boczan J, Kedei N, Lizanecz E, Bagi Z, Papp Z, Edes I, Csiba L, Blumberg PM (2005) Expression and distribution of vanilloid receptor 1 (TRPV1) in the adult rat brain. Mol Brain Res 135:162-168.

Treesukosol Y, Lyall V, Heck GL, DeSimone JA, Spector AC (2007) A psychophysical and electrophysiological analysis of salt taste in Trpv1 null mice. Am J Physiol Regul Integr Comp Physiol 292:R1799-1809.

Turrigiano GG (2008) The self-tuning neuron: synaptic scaling of excitatory synapses. Cell 135:422-435.

Uboha NV, Flajolet M, Nairn AC, Picciotto MR (2007) A calcium- and calmodulin-dependent kinase Ialpha/microtubule affinity regulating kinase 2 signaling cascade mediates calcium-dependent neurite outgrowth. J Neurosci 27:4413-4423.

Ufret-Vincenty CA, Klein RM, Hua L, Angueyra J, Gordon SE (2011) Localization of the PIP2 sensor of TRPV1 ion channels. J Biol Chem 286:9688-9698.

Vaillant AR, Zanassi P, Walsh GS, Aumont A, Alonso A, Miller FD (2002) Signaling mechanisms underlying reversible, activity-dependent dendrite formation. Neuron 34:985-998.

Van Buren JJ, Bhat S, Rotello R, Pauza ME, Premkumar LS (2005) Sensitization and translocation of TRPV1 by insulin and IGF-I. Mol Pain 1:17.

van der Stelt M, Veldhuis WB, Maccarrone M, Bar PR, Nicolay K, Veldink GA, Di Marzo V, Vliegenthart JF (2002) Acute neuronal injury, excitotoxicity, and the endocannabinoid system. Mol Neurobiol 26:317-346.

Varga A, Bolcskei K, Szoke E, Almasi R, Czeh G, Szolcsanyi J, Petho G (2006) Relative roles of protein kinase A and protein kinase C in modulation of transient receptor potential vanilloid type 1 receptor responsiveness in rat sensory neurons in vitro and peripheral nociceptors in vivo. Neuroscience 140:645-657.

Veldhuis WB, van der Stelt M, Wadman MW, van Zadelhoff G, Maccarrone M, Fezza F, Veldink GA, Vliegenthart JF, Bar PR, Nicolay K, Di Marzo V (2003) Neuroprotection by the endogenous cannabinoid anandamide and arvanil against in vivo excitotoxicity in the rat: role of vanilloid receptors and lipoxygenases. J Neurosci 23:4127-4133.

Vennekens R, Menigoz A, Nilius B (2012) TRPs in the Brain. Rev Physiol Biochem Pharmacol 163:27-64.

Vosler PS, Brennan CS, Chen J (2008) Calpain-mediated signaling mechanisms in neuronal injury and neurodegeneration. Mol Neurobiol 38:78-100.

Vugler AA, Semo M, Joseph A, Jeffery G (2008) Survival and remodeling of melanopsin cells during retinal dystrophy. Vis Neurosci 25:125-138.

Wang JZ, Grundke-Iqbal I, Iqbal K (2007) Kinases and phosphatases and tau sites involved in Alzheimer neurofibrillary degeneration. Eur J Neurosci 25:59-68.

Wang X, Ng YK, Tay SS (2005) Factors contributing to neuronal degeneration in retinas of experimental glaucomatous rats. J Neurosci Res 82:674-689.

Wang X, Teng L, Li A, Ge J, Laties AM, Zhang X (2010) TRPC6 channel protects retinal ganglion cells in a rat model of retinal ischemia/reperfusion-induced cell death. Invest Ophthalmol Vis Sci 51:5751-5758.

Ward NJ, Ho KW, Lambert WS, Weitlauf C, Calkins DJ (2014) Absence of transient receptor potential vanilloid-1 accelerates stress-induced axonopathy in the optic projection. J Neurosci 34:3161-3170.

Wassle H, Boycott BB (1991) Functional architecture of the mammalian retina. Physiol Rev 71:447-480.

Weber AJ, Kaufman PL, Hubbard WC (1998) Morphology of single ganglion cells in the glaucomatous primate retina. Invest Ophthalmol Vis Sci 39:2304-2320.

Wen Z, Guirland C, Ming GL, Zheng JQ (2004) A CaMKII/calcineurin switch controls the direction of Ca(2+)-dependent growth cone guidance. Neuron 43:835-846.

Wenk GL (2003) Neuropathologic changes in Alzheimer's disease. J Clin Psychiatry 64 Suppl 9:7-10.

Whitmore AV, Libby RT, John SW (2005) Glaucoma: thinking in new ways-a role for autonomous axonal self-destruction and other compartmentalised processes? Prog Retin Eye Res 24:639-662.

Williams TL, Day NC, Ince PG, Kamboj RK, Shaw PJ (1997) Calcium-permeable alpha-amino-3-hydroxy-5-methyl-4-isoxazole propionic acid receptors: a molecular determinant of selective vulnerability in amyotrophic lateral sclerosis. Ann Neurol 42:200-207.

Wilson RI, Nicoll RA (2001) Endogenous cannabinoids mediate retrograde signalling at hippocampal synapses. Nature 410:588-592.

WoldeMussie E, Ruiz G, Wijono M, Wheeler LA (2001) Neuroprotection of retinal ganglion cells by brimonidine in rats with laser-induced chronic ocular hypertension. Invest Ophthalmol Vis Sci 42:2849-2855.

Xia J, Lim JC, Lu W, Beckel JM, Macarak EJ, Laties AM, Mitchell CH (2012) Neurons respond directly to mechanical deformation with pannexin-mediated ATP release and autostimulation of P2X7 receptors. J Physiol 590:2285-2304.

Xing J, Li J (2007) TRPV1 receptor mediates glutamatergic synaptic input to dorsolateral periaqueductal gray (dl-PAG) neurons. J Neurophysiol 97:503-511.

Yabe JT, Pimenta A, Shea TB (1999) Kinesin-mediated transport of neurofilament protein oligomers in growing axons. J Cell Sci 112 (Pt 21):3799-3814.

Yazulla S (2008) Endocannabinoids in the retina: from marijuana to neuroprotection. Prog Retin Eye Res 27:501-526.

Yoritaka A, Hattori N, Uchida K, Tanaka M, Stadtman ER, Mizuno Y (1996) Immunohistochemical detection of 4-hydroxynonenal protein adducts in Parkinson disease. Proc Natl Acad Sci U S A 93:2696-2701.

Yu LM, Goda Y (2009) Dendritic signalling and homeostatic adaptation. Curr Opin Neurobiol 19:327-335.

Yuan A, Rao MV, Sasaki T, Chen Y, Kumar A, Veeranna, Liem RK, Eyer J, Peterson AC, Julien JP, Nixon RA (2006) Alpha-internexin is structurally and functionally associated with the neurofilament triplet proteins in the mature CNS. J Neurosci 26:10006-10019.

Zhang X, Huang J, McNaughton PA (2005a) NGF rapidly increases membrane expression of TRPV1 heat-gated ion channels. EMBO J 24:4211-4223.

Zhang X, Zhang M, Laties AM, Mitchell CH (2005b) Stimulation of P2X7 receptors elevates Ca2+ and kills retinal ganglion cells. Invest Ophthalmol Vis Sci 46:2183-2191.

Zheng JQ (2000) Turning of nerve growth cones induced by localized increases in intracellular calcium ions. Nature 403:89-93.

Zimov S, Yazulla S (2004) Localization of vanilloid receptor 1 (TRPV1/VR1)-like immunoreactivity in goldfish and zebrafish retinas: restriction to photoreceptor synaptic ribbons. J Neurocytol 33:441-452.

Zimov S, Yazulla S (2007) Vanilloid receptor 1 (TRPV1/VR1) co-localizes with fatty acid amide hydrolase (FAAH) in retinal amacrine cells. Vis Neurosci 24:581-591.

Zundorf G, Kahlert S, Bunik VI, Reiser G (2009) alpha-Ketoglutarate dehydrogenase contributes to production of reactive oxygen species in glutamate-stimulated hippocampal neurons in situ. Neuroscience 158:610-616.